

AERODYNAMIC DESIGN AND OPTIMIZATION OF HORIZONTAL AXIS WIND
TURBINES BY USING BEM THEORY AND GENETIC ALGORITHM

A THESIS SUBMITTED TO
THE GRADUATE SCHOOL OF NATURAL AND APPLIED SCIENCES
OF
MIDDLE EAST TECHNICAL UNIVERSITY

BY

ÖZLEM CEYHAN

IN PARTIAL FULFILLMENT OF THE REQUIREMENTS
FOR
THE DEGREE OF MASTER OF SCIENCE
IN
AEROSPACE ENGINEERING

SEPTEMBER 2008

Approval of the thesis:

**AERODYNAMIC DESIGN AND OPTIMIZATION OF HORIZONTAL AXIS WIND
TURBINES BY USING BEM THEORY AND GENETIC ALGORITHM**

submitted by **ÖZLEM CEYHAN** in partial fulfillment of the requirements for the degree of
**Master of Science in Aerospace Engineering Department, Middle East Technical Uni-
versity** by,

Prof. Dr. Canan Özgen
Dean, Graduate School of **Natural and Applied Sciences**

Prof. Dr. İsmail H. Tuncer
Head of Department, **Aerospace Engineering**

Prof. Dr. İsmail H. Tuncer
Supervisor, **Aerospace Engineering Dept., METU**

Assist. Prof. Dr. Nilay Sezer Uzol
Co-supervisor, **Mechanical Engineering Dept.,
TOBB University of Economics and Technology**

Examining Committee Members:

Prof. Dr. Cahit Çıray
Aerospace Engineering Dept., METU

Prof. Dr. İsmail H. Tuncer
Aerospace Engineering Dept., METU

Assist. Prof. Dr. Oğuz Uzol
Aerospace Engineering Dept., METU

Assist. Prof. Dr. Güçlü Seber
Aerospace Engineering Dept., METU

MS. Bülent Korkem
Helicopter Flight Sciences Dept.,
TUSAS Aerospace Industries (TAI)

Date:

I hereby declare that all information in this document has been obtained and presented in accordance with academic rules and ethical conduct. I also declare that, as required by these rules and conduct, I have fully cited and referenced all material and results that are not original to this work.

Name, Last Name: ÖZLEM CEYHAN

Signature :

ABSTRACT

AERODYNAMIC DESIGN AND OPTIMIZATION OF HORIZONTAL AXIS WIND TURBINES BY USING BEM THEORY AND GENETIC ALGORITHM

Ceyhan, Özlem

M.S., Department of Aerospace Engineering

Supervisor : Prof. Dr. İsmail H. Tuncer

Co-Supervisor : Assist. Prof. Dr. Nilay Sezer Uzol

September 2008, 101 pages

An aerodynamic design and optimization tool for wind turbines is developed by using both Blade Element Momentum (BEM) Theory and Genetic Algorithm. Turbine blades are optimized for the maximum power production for a given wind speed, a rotational speed, a number of blades and a blade radius. The optimization variables are taken as a fixed number of sectional airfoil profiles, chord lengths, and twist angles along the blade span. The airfoil profiles and their aerodynamic data are taken from an airfoil database for which experimental lift and drag coefficient data are available. The BEM analysis tool developed is first validated with the experimental data for low wind speeds. A 100 kW wind turbine, which is used in the validation, is then optimized. As a result of the optimization, the power production is improved by 40 to 80 percent. The optimization methodology is then employed to design a 1MW wind turbine with a 25m radius.

Keywords: horizontal axis wind turbines, BEM theory, genetic algorithm optimization

ÖZ

YATAY EKSENLİ RÜZGAR TÜRBİNLERİNİN BEM TEORİSİ VE GENETİK ALGORİTMA KULLANILARAK AERODİNAMİK TASARIM VE OPTİMİZASYONU

Ceyhan, Özlem

Yüksek Lisans, Havacılık ve Uzay Mühendisliği Bölümü

Tez Yöneticisi : Prof. Dr. İsmail H. Tuncer

Ortak Tez Yöneticisi : Yard. Doç. Dr. Nilay Sezer Uzol

Eylül 2008, 101 sayfa

Pal Elemanı-Momentum (Blade Element Momentum - BEM) Teorisi ve Genetik Algoritma optimizasyon metodları kullanılarak, yatay eksenli rüzgar türbini tasarım ve optimizasyon aracı geliştirilmiştir. Türbin palleri, verilen rüzgar ve dönme hızı, pal sayısı ve pal uzunluğuna göre, en yüksek gücü üretebilecek şekilde optimize edilmişlerdir. Pal üzerinden alınan belirli sayıdaki airfoil kesitleri, buradaki veter ve burkulma açıları, optimizasyon değişkenleri olarak kullanılmıştır. Airfoil kesitleri ve bunların aerodinamik bilgileri, deneysel kaldırma ve sürüklenme kuvveti katsayılarının bulunduğu bir aerodinamik veritabanından alınmıştır. BEM teorisi analiz programı, düşük rüzgar hızları için deneysel verilerle doğrulanmıştır. Öncelikle, doğrulamalar sırasında da kullanılan 100 kW'lık bir rüzgar türbini optimize edilmiştir. Optimizasyonun sonucunda, yüzde 40'tan yüzde 80'e kadar iyileştirme sağlanmıştır. Daha sonra bu metot, 25 m yarıçaplı, 1MW lık rüzgar türbini tasarım optimizasyonu için kullanılmıştır.

Anahtar Kelimeler: dikey eksenli rüzgar türbinleri, BEM Teorisi, genetik algoritma optimizasyonu

To my family and friends

ACKNOWLEDGMENTS

First of all, I would like to thank to my advisor Ismail H. Tuncer for his guidance, support and helpful discussions that we have made throughout the study. Also, I would like to thank to my co-supervisor Nilay Sezer Uzol for her valuable support and guidance during the thesis work.

I would also like to thank to Yüksel Ortakaya and Bülent Korkem for their endless support and patience during this study. I probably would not finish this thesis without their motivation. Special thanks to Cahit Çıray for his help to develop my vision about aerodynamics.

I am grateful to Deniz Yılmaz and Adnan Ceyhan for their understanding, patience and sharing my whole thesis progress. Many thanks to my colleagues and friends Pınar Şahin, Öznur Yemenici, Güçlü Gözen, Sinem Işık, Miray Demir, Tuğba Ünlü and Gönenç Gürsoy for being on my side during the whole thesis study. Special thanks to Onur Tarımcı for helping me about latex equations. I appreciate the encouragement of my dearest friends Onur Baş, Büşra Akay, Banu Düzgün and Çiğdem Erol during the whole thesis progress.

Finally, I wish to state my gratitude to my family; they always believe in me not only during this thesis study but also during my whole life.

TABLE OF CONTENTS

ABSTRACT	iv
ÖZ	v
DEDICATION	vi
ACKNOWLEDGMENTS	vii
TABLE OF CONTENTS	viii
LIST OF TABLES	xi
LIST OF FIGURES	xiii
LIST OF ABBREVIATIONS	xvii
CHAPTERS	
1 INTRODUCTION	1
1.1 Overview	1
1.2 Wind Turbine Design	6
1.3 Present Study	7
2 BLADE ELEMENT MOMENTUM THEORY	9
2.1 Introduction	9
2.2 Actuator Disc Concept	10
2.3 Angular Momentum	12
2.4 Blade Element Theory	14
2.4.1 Tip Losses	16
2.5 Blade Element Momentum (BEM) Theory	17
2.6 Modifications to BEM Theory	18
2.7 Method Used In the Thesis	20
2.8 Validation of BEM Analysis Tool	24

	2.8.1	NREL Untwisted and Untapered Wind Turbine	24
	2.8.2	NREL Twisted and Untapered Wind Turbine	27
	2.8.3	Risoe Wind Turbine	30
3		AIRFOILS IN WIND TURBINE APPLICATIONS	34
	3.1	Introduction	34
	3.2	Airfoil Terminology and Airfoil Classification	34
	3.3	Aerodynamics of Airfoils	36
	3.4	Airfoil Database	37
	3.5	Airfoil C_l and C_d Data Interpolation and Extrapolation	38
4		GENETIC ALGORITHM AND ITS IMPLEMENTATION	41
	4.1	Introduction	41
	4.2	Genetic Algorithm Overview	41
	4.3	Implementation of GA to Wind Turbine Optimization Problem	43
	4.4	Wind Turbine Optimization	45
	4.4.1	Chord Optimization	46
	4.4.2	Twist Optimization	47
	4.4.3	Airfoils	49
	4.4.4	Operating Conditions	50
5		OPTIMIZATION APPLICATIONS	53
	5.1	Introduction	53
	5.2	Risoe Wind Turbine Optimization	53
	5.2.1	Constraints of Optimization	54
	5.2.2	Generation	56
	5.2.3	Generation Steps	57
	5.2.4	Optimization Results	60
	5.2.5	Performance of Wind Turbines	65
	5.2.6	Thrust Force	70
	5.3	Design Optimization	71
6		CONCLUSION	81
	6.1	Future Work	83

REFERENCES 84

APPENDICES

A AIRFOIL SPECIFICATIONS 87

A.1 AIRFOILS USED IN THE AIRFOIL DATABASE 87

A.2 AIRFOIL FAMILIES USED IN THE OPTIMIZATION 91

A.2.1 NACA 63-2xx Family 91

A.2.2 NACA 63-4xx Family 92

A.2.3 NACA 64-4xx Family 93

A.2.4 NACA 65-4xx Family 94

A.2.5 FX-60 Family 95

A.2.6 FX-61 Family 96

A.2.7 FX-66 Family 97

A.2.8 FX S Family 98

A.2.9 Risoe-A1 Family 99

A.2.10 DU Family 100

A.2.11 FFA Family 101

LIST OF TABLES

TABLES

Table 1.1 International rankings of installed wind power capacity [6].	4
Table 2.1 NREL Phase II wind turbine general characteristics	25
Table 2.2 NREL Phase III wind turbine general characteristics	28
Table 2.3 Risoe wind turbine general characteristics	31
Table 3.1 Airfoil families used in airfoil database	38
Table 5.1 Risoe wind turbine optimization parameters summary	55
Table 5.2 Optimization cases used in Risoe wind turbine optimization.	55
Table 5.3 Competitor study for 1MW wind turbine design optimization	72
Table 5.4 Chosen parameters for optimization	72
Table A.1 Airfoils used in the database.	87
Table A.2 NACA 63-2xx family airfoil distribution along blade span (r/R)	91
Table A.3 NACA 63-4xx family airfoil distribution along blade span (r/R)	92
Table A.4 NACA 64-4xx family airfoil distribution along blade span (r/R)	93
Table A.5 NACA 65-4xx family airfoil distribution along blade span (r/R)	94
Table A.6 FX-60 family airfoil distribution along blade span (r/R)	95
Table A.7 FX-61 family airfoil distribution along blade span (r/R)	96
Table A.8 FX-66 family airfoil distribution along blade span (r/R)	97
Table A.9 FX S family airfoil distribution along blade span (r/R)	98
Table A.10 Risoe-A1 family airfoil distribution along blade span (r/R)	99
Table A.11 DU family airfoil distribution along blade span (r/R)	100

Table A.12FFA family airfoil distribution along blade span (r/R) 101

LIST OF FIGURES

FIGURES

Figure 1.1	Darius type VAWT wind turbine [3].	2
Figure 1.2	Subparts of modern wind turbines (reproduced from [4]).	2
Figure 1.3	An example of off-shore wind farm [3].	3
Figure 1.4	Comparison of power production and size of wind turbines.	4
Figure 1.5	Wind power as a percentage of electricity consumption [8].	5
Figure 1.6	Wind turbine design process (reproduced based on the information given in reference [10]).	6
Figure 2.1	Stream tube generated through wind turbine.	9
Figure 2.2	Actuator disk model of a wind turbine.	10
Figure 2.3	Velocity behind the turbine disc. (Reproduced from [26])	13
Figure 2.4	Definition of blade element used in the theory.	15
Figure 2.5	Velocities and forces acting on a blade element.	16
Figure 2.6	Experimental and predicted C_T values [26].	19
Figure 2.7	Induction factor calculation: Iteration procedure.	23
Figure 2.8	Geometry information of NREL Phase II wind turbine.	25
Figure 2.9	S809 airfoil C_l and C_d coefficients.	26
Figure 2.10	NREL Phase II wind turbine test and analysis comparison.	26
Figure 2.11	Geometry information of NREL Phase III wind turbine.	27
Figure 2.12	NREL Phase III wind turbine test and analysis comparison.	28
Figure 2.13	Local angle of attack and power comparisons of NREL Phase II and Phase III wind turbines for 15 m/s wind speed.	29
Figure 2.14	Geometry information of Risoe wind turbine.	30

Figure 2.15 C_l and C_d coefficients of NACA 63-2xx airfoils.	31
Figure 2.16 Risoe wind turbine test and analysis comparison.	32
Figure 2.17 Blade elements used in Risoe wind turbine analysis.	32
Figure 2.18 Risoe wind turbine BEM analyses with different number of blade elements.	33
Figure 3.1 Basic airfoil properties.	34
Figure 3.2 An example for different thickness distributions in two airfoils.	35
Figure 3.3 DU airfoil family designed for a 55 m diameter wind turbine[31].	36
Figure 3.4 Airfoil data interpolation for angle of attack results compared with originals.	39
Figure 3.5 Airfoil data interpolation for Reynolds number results compared with originals.	39
Figure 3.6 Airfoil data interpolation for Reynolds number results compared with originals.	40
Figure 4.1 Wind turbine genetic algorithm optimization process chart.	44
Figure 4.2 Wind turbine geometrical representation for the optimization process.	45
Figure 4.3 Typical chord distributions of wind turbines [39]	46
Figure 4.4 Twist distribution examples of wind turbines [39].	48
Figure 4.5 Airfoil definition example of blade elements for 63-4xx family	49
Figure 4.6 Thickness distribution of NACA 63-4xx family to 8 blade elements: for optimization problems and real application	50
Figure 4.7 An example of Weibull distribution	51
Figure 5.1 Risoe wind turbine optimization; chord upper and lower limits definitions.	54
Figure 5.2 Risoe wind turbine optimization; twist upper and lower limits definitions.	54
Figure 5.3 Evolution of optimization for each generation.	56
Figure 5.4 Best wind turbine in the population of last generation of various optimization cases Opt1 (a), Opt2 (b) and Opt3 (c)	57
Figure 5.5 Investigated generation steps in Opt3.	58
Figure 5.6 Generation in chord and twist parameters for Opt3.	58
Figure 5.7 Generation in airfoils for Opt3 and 2D C_l and C_d comparisons.	59

Figure 5.8 Chord and twist distribution comparisons of optimization results with Risoe wind turbine.	61
Figure 5.9 Airfoil property comparisons of optimization results	62
Figure 5.10 Angle of attack and Reynolds number regimes in optimization.	62
Figure 5.11 Opt3 wind turbine 3D geometry.	63
Figure 5.12 Risoe wind turbine 3D geometry.	63
Figure 5.13 Sectional comparisons of Risoe and Opt3 wind turbines (dimensions are in meters).	64
Figure 5.14 Performance comparisons of optimized wind turbines with Risoe wind turbine for rotational speed of 47.5 rpm.	65
Figure 5.15 Improvement in power production: percentage of Risoe wind turbine analysis result.	66
Figure 5.16 Risoe, Opt1, Opt2 and Opt3 wind turbine performance maps.	67
Figure 5.17 Risoe wind turbine performance with different blade angles.	68
Figure 5.18 Risoe power production curve for different blade angles.	69
Figure 5.19 Risoe and Opt1 comparison for different blade angles.	69
Figure 5.20 Risoe optimization results thrust comparison.	70
Figure 5.21 Optimization development in generations.	73
Figure 5.22 Comparison between initial geometry and optimization result.	74
Figure 5.23 Coefficients of DU airfoils.	74
Figure 5.24 Local Reynolds number values for design condition.	75
Figure 5.25 Performance of designed wind turbine.	75
Figure 5.26 Local angle of attack and power values in different wind speeds for designed 1 MW wind turbine.	76
Figure 5.27 Designed wind turbine performance for different blade pitch angles	77
Figure 5.28 Blade Angle (Pitch Angle) curve required for constant 1.1 MW power output.	78
Figure 5.29 Power production of designed wind turbine after pitch regulation.	78
Figure 5.30 Thrust force produced by designed wind turbine.	79
Figure 5.31 Risoe and 1MW wind turbine's coefficients comparison.	80

Figure A.1 NACA 63-2xx family airfoils	91
Figure A.2 NACA 63-4xx family airfoils	92
Figure A.3 NACA 64-4xx family airfoils	93
Figure A.4 NACA 65-4xx family airfoils	94
Figure A.5 FX-60 family airfoils	95
Figure A.6 FX-61 family airfoils	96
Figure A.7 FX-66 family airfoils	97
Figure A.8 FX S family airfoils	98
Figure A.9 DU family airfoils	100
Figure A.10FFA family airfoils	101

LIST OF ABBREVIATIONS

ϕ	Local flow angle
ϕ_P	Blade pitch angle
β	Local twist angle
α	Local angle of attack
λ	Tip speed ratio
λ_r	Local speed ratio
ρ	Density of air
w	Tangential induced velocity
a	Axial induction factor
a'	Tangential induction factor
U	Free stream velocity
A	Actuator disc area
p	Pressure
P	Power
T	Torque
r	Local blade radius
R	Blade radius
D	Turbine diameter
B	Number of blades
N	Number of blade elements
F	Prandtl tip loss factor
c	chord
l	2D lift
d	2D drag
C_l	Lift coefficient
C_d	Drag coefficient
C_P	Power coefficient
C_T	Thrust coefficient
C_Q	Torque coefficient
C_N	Normal force coefficient
C_{Tan}	Tangential coefficient
Re	Reynolds number
AR	Aspect ratio

CHAPTER 1

INTRODUCTION

World is changing. Energy and global warming are the most important problems in today's world. Fossil fuel prices are increasing day by day because of limited sources. Natural balance of earth is changing because of global warming. One of the main reasons of this change is burning too much fossil fuel. Kyoto Protocol which is an agreement to reduce the emission of CO_2 and greenhouse gases by United Nation Framework Convention on Climate Change (UNFCCC) is ratified by many countries, today [1]. Therefore, alternative energy sources are needed. These are the reasons why wind energy becomes so important. Wind source is free and clean. Wind turbine technology is growing and wind is getting to be one of the best alternative energy source, today.

1.1 Overview

Wind turbine is a machine which converts wind power to electrical energy. There are several types of wind turbines. Generally, wind turbines are divided into two groups: Vertical Axis Wind Turbines (VAWT) and Horizontal Axis Wind Turbines (HAWT). In vertical axis wind turbines, blades are rotating on a vertical axis shaft. Their generator and gearboxes are placed in the ground which is easy to access from ground and they don't need any yaw mechanism. The most common VAWT examples are Darius and Savonius type wind turbines. In horizontal axis wind turbines, turbine blades are connected to a shaft which is rotating on a horizontal axis. They are propeller type rotors which are located on the top of a tower with generators and gearboxes. HAWT are the most common wind turbine types. Most of the electricity produced today is produced by HAWT. Although VAWT wind turbines have some advantages over HAWT by means of easy operations, they cannot produce power as efficiently as HAWT.

Therefore, modern wind turbines are propeller type HAWT. In this thesis, design and optimization of modern horizontal axis wind turbines are studied. Additional information about different wind turbine concepts can be found from reference [2].



Figure 1.1: Darius type VAWT wind turbine [3].

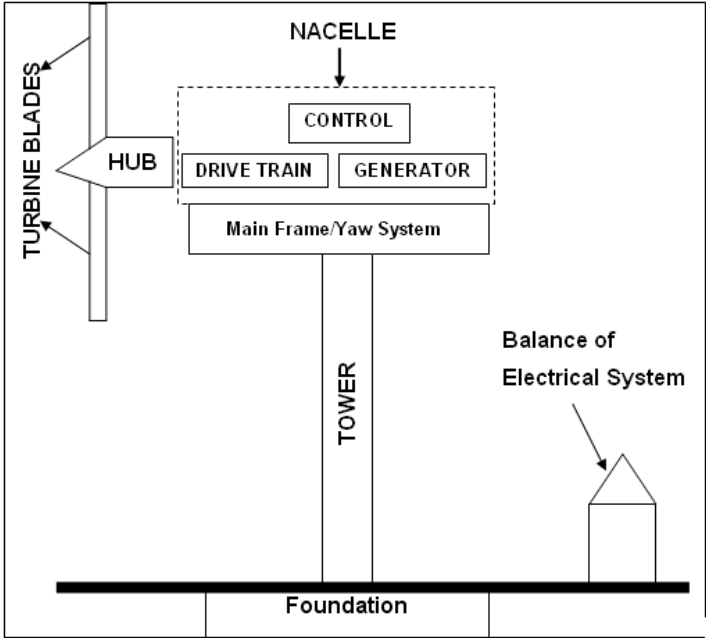


Figure 1.2: Subparts of modern wind turbines (reproduced from [4]).

Modern wind turbines have some subparts to convert wind power to electrical energy. These parts are shown in Figure 1.2. Wind turbine rotor is the main part of the wind turbine. Generally, it consists of two or three blades which are connected to the hub. Rotor and hub are connected to nacelle. Nacelle covers the internal parts: drive train, generator and control unit. Drive train part contains shafts, gearbox, mechanical brake; namely the rotating parts of wind turbine excluding the rotor. Generator and control unit are also connected to it. Power production of wind turbines are controlled aerodynamically (stall control) or by variable pitch blades (pitch control) and they operate with fixed or variable rotor speed. These decisions affect the control unit and generator types. Usually, there is a yaw system for main frame which turns the rotor to the wind direction for the best power production. This system can be designed as a free yaw system by self aligning action or active yaw by direct control. Tower and foundation carries the systems on the wind turbine. Balance of electrical systems contains cables, switchgear and transformers for electricity generation.

Wind turbines are connected to electrical networks as generators. In a site, numbers of wind turbines connected to electrical networks are called wind farms. Wind farms are located in landscape or sometimes off-shore. Figure 1.3 shows an example of off-shore wind farm.



Figure 1.3: An example of off-shore wind farm [3].

Capacity of wind turbines change. There are small scale wind turbines producing only a few watts of power whereas 5 MW huge wind turbines are installed also. In Figure 1.4 comparison of power production and dimensions of wind turbines are represented [5]. Today, wind turbine rotor diameter dimensions are compared with largest aircraft spans.

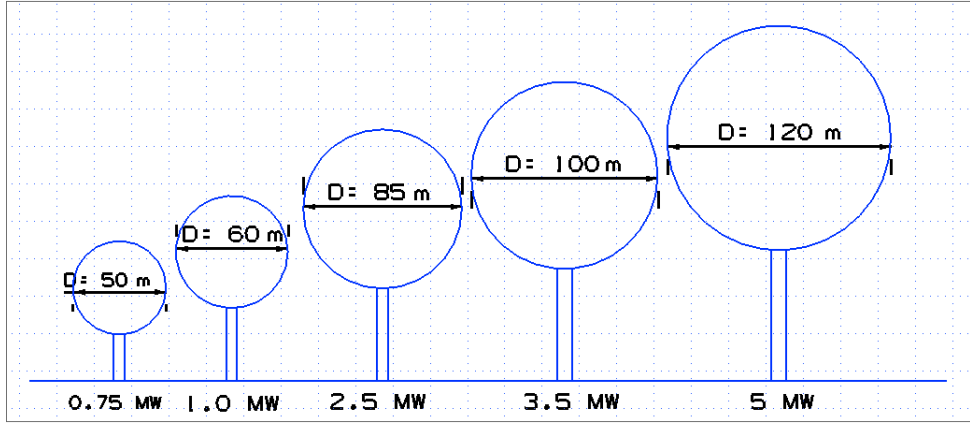


Figure 1.4: Comparison of power production and size of wind turbines.

Today, almost 100.000 MW of energy is produced from wind power [6]. The distribution of this energy to countries is shown in Table 1.1.

Table 1.1: International rankings of installed wind power capacity [6].

	Country	Starting of the year 2007	Starting of the year 2008
1	Germany	20622	22247
2	USA	11699	16971
3	Spain	11615	15145
4	India	6270	7844
5	China	2594	5906
6	Denmark	3136	3124
7	Italy	2123	2726
8	UK	1958	2425
9	France	1469	2370
10	Portugal	1716	2150
..
27	Turkey	84	192

According to Table 1.1, Turkey still needs to establish more wind farms in order to come closer to these countries by means of power production. These numbers are increasing day by day. Most of the countries are converting their energy sources from fossil fuels to wind energy. According to the statistics shown in Figure 1.5, in Denmark, more than 20 percent of the electrical energy of overall country is provided by wind power. According to reference [7], US is planning to produce 20 percent of its electricity from wind power by the year 2030. These plans and statistical information show that wind energy trend will continue to grow up in the future.

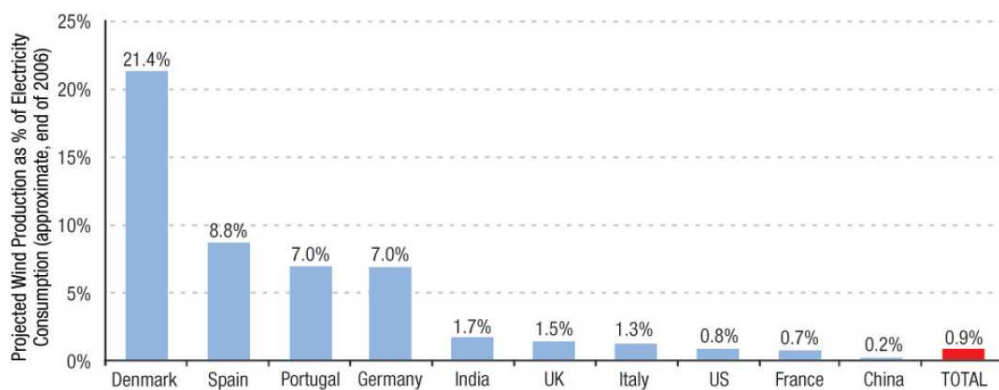


Figure 1.5: Wind power as a percentage of electricity consumption [8].

There are number of universities and research centers that are dealing with wind energy trends, technologies and future concepts. The most famous are Delft University Wind Research Institute (Netherlands), Energy Research Center of Netherlands (ECN), Risoe DTU (Denmark Technical University) National Laboratory for Sustainable Energy and National Renewable Energy Laboratory (NREL - USA). In addition to these centers, most of the countries in the world have their own wind energy associations. In Turkey, EIE (General Directorate of Electrical Power Resources Survey and Development Administration) and TUREB (Turkish Wind Energy Association) are related wind energy organizations. The technology of all wind turbines installed in Turkey today is coming from other countries [9].

1.2 Wind Turbine Design

Wind turbine design is a multidisciplinary design process and therefore, naturally, it is an optimization problem. In Figure 1.6, process of design is shown schematically.

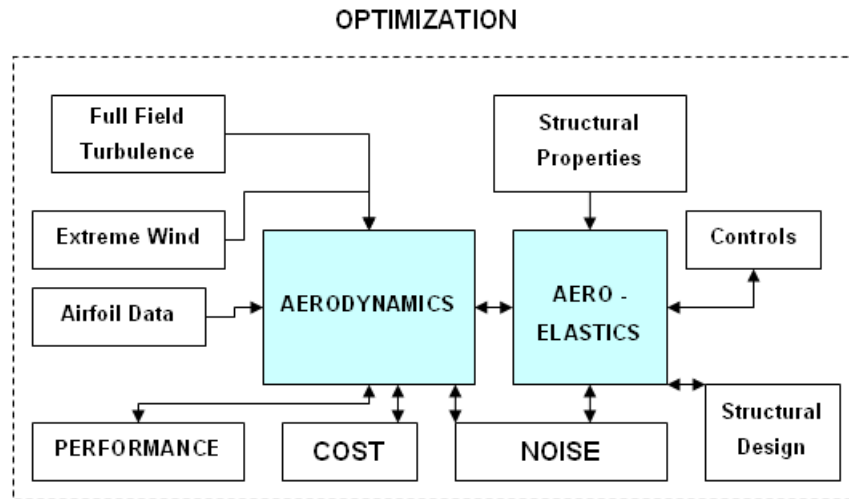


Figure 1.6: Wind turbine design process (reproduced based on the information given in reference [10]).

In order to establish an optimum system that produces as much power as possible with low cost and low noise levels, the ideal case is the optimization of this design process with all of the components included. However, this is not possible all the time. This idealized procedure needs too much time and effort to produce best wind turbine geometry by using the most accurate methods for all phases. As a result, in most of the design applications, accurate design methods are used partially [11].

Optimization of aerodynamics is the starting point of wind turbine design. Wind turbines are designed for maximum power production. In order to design a wind turbine, an analysis tool is needed for performance predictions of designed wind turbines. Almost all wind turbine design tools use Blade Element Momentum (BEM) theory for aerodynamic analysis [11]. The main reason of this is BEM theory is very fast and gives good results for steady state conditions. Although, the uncertainties of BEM method are coming from the analysis of high wind speeds, unsteady conditions and load predictions on extreme wind conditions, it is still the only tool for design [12, 13]. CFD methods need much more time for design applications;

therefore, they are used only for analysis of the specific problems with high uncertainties for BEM methods [14, 15].

Design and optimization of wind turbines are performed by several authors. In reference [16], BEM method and Genetic Algorithm is used for design of ART-2B Rotor Blades. 3 different airfoil families in NREL S-Series airfoils are used separately for design and only chord and twist is optimized. In reference [17], blade design trade-offs are studied for airfoils with different stall characteristics by using BEM method and genetic algorithm. In this study, cost is also included to the design as a constraint into optimization. Different than these approaches, design is performed by cost optimization as in reference [18], including structural constraints in reference [19] and control in reference [20]. Site specific wind turbine design studies are performed including almost all subjects in Figure 1.6 as it is described in reference [21] as a European project. This study is one of the most detailed wind turbine design process studies. The optimization is aimed to produce as much power as possible with minimum cost of energy.

1.3 Present Study

Wind turbine aerodynamic design optimization is performed in this thesis. First of all, an aerodynamic analysis tool is developed by using BEM theory which computes the performance of wind turbines according to given geometry and conditions. This part is explained in Chapter 1. The developed BEM analysis tool is validated against the field test data of three wind turbines which are NREL Phase II and III wind turbines and Risoe wind turbine [22]. The NREL wind turbines have common characteristics such that they both have the same blade radius and chord values and no taper. The only difference between them is that Phase II wind turbine does not have a twist whereas Phase III wind turbine has twist. Risoe wind turbine is a tapered and twisted wind turbine. Validations are performed for these three wind turbines and capabilities of aerodynamic analysis tool are shown.

After the validation of BEM analysis tool, wind tunnel test data of several airfoils are collected and an airfoil database is generated. This airfoil database includes C_l and C_d data of many airfoils developed or used in wind turbine applications which are found in the literature. The airfoils are stored as airfoil families in the database and they are used as families or single

airfoils during the analysis or optimization process. Airfoil database is explained in Chapter 3.

In the Chapter 4, implementation of Genetic Algorithm optimization method to the wind turbine design and optimization process is explained. An open source genetic algorithm optimization tool [23] is used for this purpose. It is combined with BEM analysis tool with some minor modifications for constraint definitions. Wind turbine blade is divided into number of sections along the blade. In the optimization process, airfoils are taken from the aerodynamic database, chord and twist distributions of the turbine blade is optimized to give the best power output for given number of blades, blade radius, wind speed and rotational speed. As a result, a novel aerodynamic design and optimization tool is developed.

Developed aerodynamic design and optimization tool is first applied to Risoe wind turbine for improved power production. It is shown that the power production may be increased by 40 to 80 percent. A novel wind turbine with 25 m blade radius is then designed for maximum power which is obtained at 1.1 MW. It should be noted that from Figure 1.4, the current commercial wind turbines that produce 1 MW power production has about 30 m radius. The design and optimization applications are described in Chapter 5. Discussion of the whole thesis is done in Chapter 6 with suggested future work.

CHAPTER 2

BLADE ELEMENT MOMENTUM THEORY

2.1 Introduction

Wind Turbine extracts kinetic energy from the wind. Kinetic energy in the wind is absorbed by wind turbine by slowing down the wind. If it is assumed that mass of the air passing through the turbine is separated from the mass that does not passing through the turbine, then the separated part of the flow field remains a long stream tube which lies upstream and downstream of the turbine.

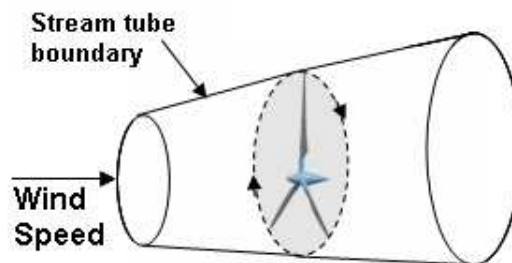


Figure 2.1: Stream tube generated through wind turbine.

While the air passes through the wind turbine, velocity of the air changes. The kinetic energy of air is absorbed by the turbine and the velocity of the air decreases following the turbine. Since mass flow rate is the same, to compensate this loss in the velocity, the stream tube extends after the turbine.

A number of steady state wind turbine performance calculation methods are derived by many

authors. The classical analysis method is developed by Betz and Glauert in 1930s [24] and [25]. In these methods, Blade Element and Momentum theories are combined into a strip theory. The theory enables the calculation of the performance characteristics of an annular section of the rotor. In this chapter, Blade Element and Momentum theories are revisited and Blade Element Momentum (BEM) theory and its application in this thesis are explained.

2.2 Actuator Disc Concept

The basic aerodynamic flow is described by actuator disc concept in the wind turbines. According to this concept, wind turbine is considered as an actuator disc. To explain the concept with momentum theory, some assumptions are made. Flow is assumed as homogenous and steady, air is assumed as incompressible. There is no frictional drag and number of blades is infinite. Also, wake is assumed as non-rotating. The static pressure far upstream and far downstream of the actuator disc is taken as equal to ambient static pressure.

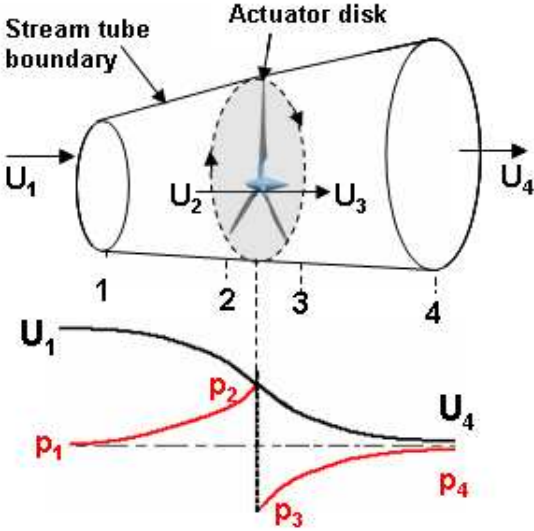


Figure 2.2: Actuator disc model of a wind turbine.

The mass of the air which passes through a given cross section of the stream tube in a unit length of time is $\rho U_1 A_1$ where ρ is air density, U_1 is air velocity which is equal to free stream velocity and A_1 is stream tube inlet area which is shown in Figure 2.2. If A_d is Actuator disk area;

$$\rho U_1 A_1 = \rho U_2 A_d = \rho U_4 A_4 \quad (2.1)$$

Actuator disc induces velocity in the stream tube. The difference between U_1 and U_2 is called the axial induced velocity. This velocity is represented in terms of freestream velocity and it is nondimensionalized with the freestream velocity:

$$\frac{U_1 - U_2}{U_1} = a \quad (2.2)$$

The nondimensional form of this induced velocity, a , is called the axial induction factor or the inflow factor. The streamwise velocity component, U_2 , is then expressed as

$$U_2 = U_1(1 - a) \quad (2.3)$$

The conservation of momentum across the actuator disk provides;

$$(p_2 - p_3)A_d = (U_1 - U_4)\rho A_d U_1(1 - a) \quad (2.4)$$

Expressing the pressure values in terms of the upstream and downstream velocities using Bernoulli's equations leads to:

$$U_4 = U_1(1 - 2a) \quad (2.5)$$

It is equivalent to:

$$U_2 = \frac{U_1 + U_4}{2} \quad (2.6)$$

The power extracted from the wind is obtained through 2.4;

$$Power = FU_d = 2\rho A_d U_1^3 a(1 - a)^2 \quad (2.7)$$

The power coefficient is defined as the ratio of power extracted to the available power:

$$\begin{aligned} \text{Power} \\ \text{Coefficient} \end{aligned} = C_P = \frac{\text{Power extracted}}{\text{Power in the wind}} = \frac{\text{Power extracted}}{\frac{1}{2}\rho U_1^3 A_d} = 4a(1 - a)^2 \quad (2.8)$$

The variation of power coefficient with respect to the induction factor, a , provides the value of the induction factor which maximizes the power:

$$\frac{dC_P}{da} = 4(1 - a)(1 - 3a) = 0 \quad (2.9)$$

Since $a = 1$ makes $C_P = 0$, the only physically acceptable solution is $a = \frac{1}{3}$. Then,

$$C_{Pmax} = \frac{16}{27} = 0.593 \quad (2.10)$$

This maximum achievable power limit is known as Betz Limit. Physically, it is not possible to have any design beyond this limit. Since, there is still no wind turbine properties taken into account until now, this limit is not related with the design of wind turbine or any geometrical properties of the wind turbine.

2.3 Angular Momentum

In the previous analysis, the flow is assumed as unidirectional. In this analysis, rotary motion of the turbine is also included in the analysis where the rotation of the wind turbine generates angular momentum which can be related to the turbine torque.

The exertion of torque on the turbine disc by the air passing through it requires an equal and opposite torque on the air. As a result of this, the air rotates in a direction opposite of the turbine. The air gains angular momentum and in the wake of the turbine disc. The air particles in the wake have a velocity that have a component in the direction which is tangential to the

rotation of turbine and a component parallel to axial freestream velocity. Then, the kinetic energy of air increases and static pressure of air in the wake decreases [26].

The air entering the actuator disc has no rotational motion at all. The flow exiting from the disc does have a rotation and the transfer of this rotational motion to the air takes place entirely across the thickness of the disc. This is shown in Figure 2.3.

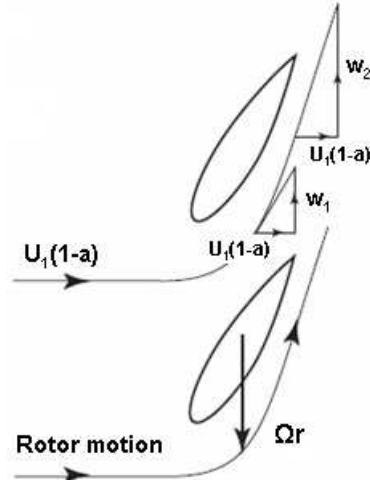


Figure 2.3: Velocity behind the turbine disc. (Reproduced from [26])

w_1 and w_2 are the tangential induced velocities which are the change in tangential velocity of air on the turbine disc and right after it, respectively. These induced velocities are nondimensionalized by the turbine rotational speed, Ωr .

$$\frac{w_1}{\Omega r} = a' \quad (2.11)$$

a' is called as tangential induction factor. From the conservation of angular momentum, w_2 is found equal to half of w_1 ([4] and [26]). Then,

$$w_1 = a' \Omega r \quad (2.12)$$

$$w_2 = 2a' \Omega r \quad (2.13)$$

If a control volume that moves with the angular velocity of the blades is used, an expression for the pressure difference across the blades can be derived. Across the disc, the angular velocity of the air relative to the blades increases from Ω to $\Omega + 2\Omega a'$. The tangential velocity is not the same in all radial positions and axial velocity is not the same in all radial positions as well. To allow both induced velocity components to vary, consider only an annular ring of the turbine disc which is of radius r and of radial width δr with area δA . The torque on the ring is equal to the rate of change of angular momentum of the air passing through the ring. Thus,

$$\begin{aligned}
 \text{torque} &= \text{rate of change of angular momentum} \\
 &= \text{mass flow rate} \times \text{change of tangential velocity} \times \text{radius} \quad (2.14) \\
 \delta Q &= \rho \delta A U_1 (1 - a) 2\Omega a' r^2
 \end{aligned}$$

Increment of the turbine shaft power output is

$$\delta P = \delta Q \Omega \quad (2.15)$$

Information about wake and detailed analysis can be found in the references [4, 26].

2.4 Blade Element Theory

The forces on the blades of a wind turbine can also be expressed as a function of lift and drag coefficients and the angle of attack. The blade is assumed to be divided into N sections which are called as blade elements. To explain Blade Element Theory, some assumptions are made. There is no aerodynamic interaction between blade elements. Spanwise velocity components on the blade are ignored. The forces on blade element are determined solely by the lift and drag characteristics of 2D airfoils of blades.

In the blade element analysis, lift and drag components are perpendicular and parallel to the relative wind speed direction. Consider a turbine with N blades of tip radius R , each with chord length c and set pitch angle β measured between the airfoil zero lift line and the plane of the disc. Chord length and pitch angle may vary along the blade span. For the angular velocity Ω and wind speed U_∞ , the total tangential velocity experienced by the element is

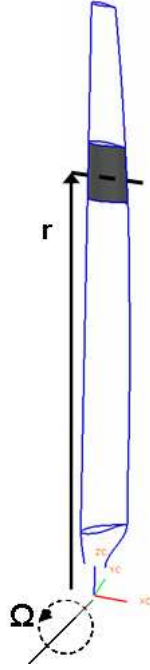


Figure 2.4: Definition of blade element used in the theory.

$(1 + a')\Omega r$ and axial velocity is $(1 - a)U_\infty$. Thus, resultant relative wind velocity at the blade element is shown in Equation 2.16.

$$W = \sqrt{U_\infty^2(1 - a)^2 + \Omega^2 r^2(1 + a')^2} \quad (2.16)$$

This relative velocity acts on the element with an angle to the plane of rotation.

From the definitions and Figure 2.5, it can be derived that

$$\tan \phi = \frac{U_\infty(1 - a)}{\Omega r(1 + a')} = \frac{(1 - a)}{(1 + a')\lambda_r} \quad (2.17)$$

The net force normal to the plane of rotation for each blade element can be written as,

$$\delta F = B(l \cos \phi + d \sin \phi)\delta r \quad (2.18)$$

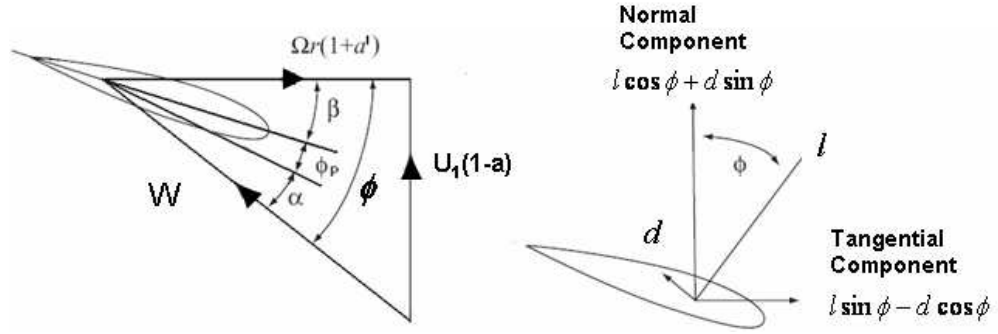


Figure 2.5: Velocities and forces acting on a blade element.

Resulting torque in the each blade element is also expressed as follows,

$$\delta Q = Br(l \cos \phi - d \cos \phi) \delta r \quad (2.19)$$

These expressions will be used for the derivation of the axial and tangential induction factors in the Blade Element Momentum theory, later.

2.4.1 Tip Losses

Because the pressure on the suction side of a blade is lower than that on the pressure side, air tends to leak around the tip from the lower to upper surface, reducing the lift and hence power production near tip. The loss is similar to the aircraft wing tip losses.

Tip loss is a 3D characteristic of the flow which can not be directly determined by the blade element or the momentum theory. Besides, there are some models generated to include the effects of tip losses into the calculations. The most acceptable and common tip loss model is developed by Prandtl [26]. According to this model, a correction factor F must be introduced into the previously discussed equations which are used to calculate the net force and torque. This factor is a function of the number of blades, the angle of relative wind, the position of the blade element and the radius of the blade.

$$f(B, \phi, r, R) \quad (2.20)$$

The final equation of the Prandtl tip loss factor is

$$F = \frac{2}{\pi} \cos^{-1} \left(\exp \left(-\frac{B R - r}{2 r \sin \phi} \right) \right) \quad (2.21)$$

2.5 Blade Element Momentum (BEM) Theory

Blade Element Momentum Theory or Strip Theory basically aims to model the axial and tangential induction factors by equating the force and torque relations derived from each blade element and momentum theories.

The total force acting on the annular radius is calculated by both blade element theory and momentum theory independently. By equating the force relations in two theories, which are Equation 2.7 and Equation 2.18 with Prandtl tip loss correction; axial induction factor can be derived.

$$2\rho\delta AFU_1^2 a(1-a) = B(l \cos \phi + d \sin \phi)\delta r \quad (2.22)$$

$$\delta A = r\delta r \quad (2.23)$$

$$l = C_l \frac{1}{2} \rho W^2 c \quad (2.24)$$

$$d = C_d \frac{1}{2} \rho W^2 c \quad (2.25)$$

$$C_N = C_l \cos \phi + C_d \sin \phi \quad (2.26)$$

$$\sigma' = \frac{Bc}{2\pi r} : \text{Local Solidity} \quad (2.27)$$

$$a = \frac{1}{\frac{4F \sin^2 \phi}{\sigma' C_N} + 1} \quad (2.28)$$

After that, equating the rate of change of momentum in the annular disc by using Equation 2.14 and Equation 2.19, tangential induction factor is calculated.

$$2\rho\delta AFU_1^2 a(1-a)2\Omega a' r^2 = Br(l \cos \phi + d \sin \phi)\delta r \quad (2.29)$$

$$C_{Tan} = C_l \sin \phi - C_d \cos \phi \quad (2.30)$$

$$a' = \frac{1}{\frac{4F \sin \phi \cos \phi}{\sigma' C_{Tan}} - 1} \quad (2.31)$$

The combination of these theories aim to predict induced velocities by predicting induction factors. Once induced velocities are modeled accurately, then, any wind turbine can be analyzed for power and thrust outputs.

2.6 Modifications to BEM Theory

There are some assumptions in BEM theory coming from both Momentum and Blade Element theories. With these assumptions, 3D characteristics of the flow, turbulence, separation or losses are not included in the theory. The assumptions do good work when the wind turbine is operating in such conditions where 3D characteristics are not very important. However, this is not always the case. Therefore, some modifications are applied to the theory.

Separation of the flow at the tip of the turbine disc causes low static pressure downstream of the turbine. Also, high static pressure is created on the turbine disc stagnation point. This difference between pressures creates high thrust values on the turbine disc. This thrust value is not predicted by BEM theory. In Figure 2.6, this phenomenon is shown. This is likely to be seen when the induction factors are high and the turbulence in the flow is getting more important. Regarding this difference between physics of the flow, two turbine states are identified for wind turbines. Windmill state or lightly loaded state which is when the flow field is not dominated by turbulence. Turbulent wake state or highly loaded state which is when the flow is turbulent and momentum theory is no longer valid.

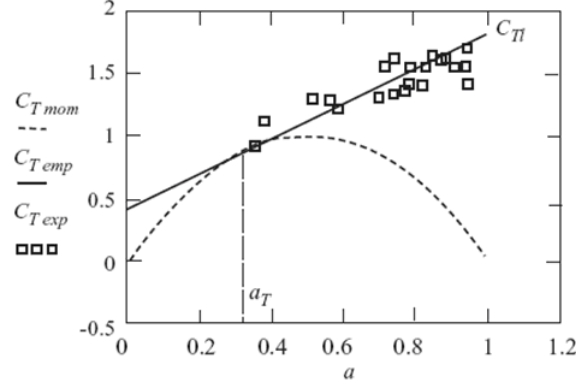


Figure 2.6: Experimental and predicted C_T values [26].

This phenomenon is included in the Blade Element Momentum Theory with different c_T and/or a prediction models. Glauert has developed a correction for this phenomenon by using experimental measurements of helicopter rotors. This model is developed for correction to thrust coefficient of entire rotor. However, it is used to correct local thrust coefficients while using BEM theory. Glauert corrections are related to the tip loss model. When the losses near the tip are high, the induced velocities are large; therefore, the possibility of turbulent wake near tip increases. Thus for each element, the total induced velocity calculation must use a combination of the tip-loss and Glauert corrections. In the reference [27], Glauert empirical relation with a modification by tip loss factor is explained. The model is;

$$C_T = \frac{8}{9} + \left(4F - \frac{40}{9}\right)a + \left(\frac{50}{9} - 4F\right)a^2 \quad (2.32)$$

or

$$a = \frac{18F - 20 - 3\sqrt{C_T(50 - 36F) + 12F(3F - 4)}}{30F - 50} \quad (2.33)$$

As shown in the Figure 2.6 the slope and value of BEM result and Glauert correction should be the same for a value of induction factor to prevent the numerical instability. Therefore, Glauert correction is applied after a limit which includes the tip loss correction and c_T value.

This correction is also used in the tool which is developed for analyzing wind turbines by BEM theory. The details of the code and methodology are explained in the next section.

2.7 Method Used In the Thesis

Wind turbine performance analysis with BEM theory is the prediction of induction factors, angle of attacks and thrust for each blade element separately. To do this, induction factors are needed to be calculated first which is an iterative process. Similar procedure which is in reference [27] is used for this purpose. To initialize the axial induction factor, Equations 2.16 and 2.28 are used assuming;

$$\sin \phi \approx \phi \text{ (}\phi \text{ is small)} \quad (2.34)$$

$$F = 1, C_d = 0, a' = 0 \quad (2.35)$$

$$C_l = 2\pi\alpha \quad (2.36)$$

Then, axial induction is found as;

$$a = \frac{1}{4} \left[2 + \pi\lambda_r\sigma' - \sqrt{4 - 4\pi\lambda_r\sigma' + \pi\lambda_r^2\sigma'(8\beta + \pi\sigma')} \right] \quad (2.37)$$

Instead of using an initial value for axial induction factor, it may also be taken as zero initially. This would not change the result. The benefit of using an initially predicted axial induction factor is decreasing the number of steps for iterative induction factors prediction.

After initialization, next step is to calculate the inflow angle by using induction factors calculated.

$$\tan \phi = \frac{U_\infty(1-a)}{\Omega r(1-a')} \quad (2.38)$$

β information comes with the wind turbine geometry information. Therefore, the only unknown angle is the angle of attack which is calculated from

$$\alpha = \phi - \beta \quad (2.39)$$

The next step is to calculate the thrust coefficient and tip loss factor from another form of Equation 2.18.

$$C_T = \frac{\sigma' (1 - a)^2 (C_l \cos \phi + C_d \sin \phi)}{\sin^2 \phi} \quad (2.40)$$

Equation 2.21 is used for the tip loss calculation.

$$F = \frac{2}{\pi} \cos^{-1} \left(\exp \left(-\frac{B}{2} \frac{R - r}{r \sin \phi} \right) \right) \quad (2.41)$$

Once the thrust coefficient and tip loss factor is calculated, the axial induction is calculated. If $C_T > 0.96F$, then the blade is highly loaded and modified Glauert correction is applied.

$$a = \frac{18F - 20 - 3 \sqrt{C_T(50 - 36F) + 12F(3F - 4)}}{30F - 50} \quad (2.42)$$

Otherwise, the blade is lightly loaded and standard BEM theory is used (Equation 2.28). Tangential induction factor is calculated directly from BEM theory (Equation 2.31). This calculation procedure is an iterative process which is described in Figure 2.7 below. Loop ends when the desired accuracy is achieved in induction factors and the procedure is applied for each blade element. Once the induction factors are calculated, thrust and torque of each blade element are found from the equations below which are rewritten from Equation 2.18 and Equation 2.19.

$$dT = B \frac{1}{2} \rho V_{tot}^2 C_N c dr \quad (2.43)$$

$$dQ = B \frac{1}{2} \rho V_{tot}^2 C_{T_{an}} c dr \quad (2.44)$$

The overall turbine thrust and torque parameters are calculated by integrating the Equation 2.43 and Equation 2.44 along the turbine span. Power is also calculated from Equation 2.15.

During the iteration process, lift and drag coefficients are given as input to the program. For each blade element, airfoil information is required with chord and twist values. Lift and drag coefficients have to be given according different to angle of attack values. Details of airfoil information used in the BEM analysis and in optimization process are given in Chapter 3. The iteration and power calculation procedure explained here is coded by using FORTRAN90 programming language. BEM analysis tool predicts the performance of wind turbines according to the given geometrical variables which are shown in Figure 2.7 as inputs box. This tool is also used for calculating wind turbine power production during the optimization loop. BEM analysis tool is validated with the experimental data obtained from literature which is explained in the next section.

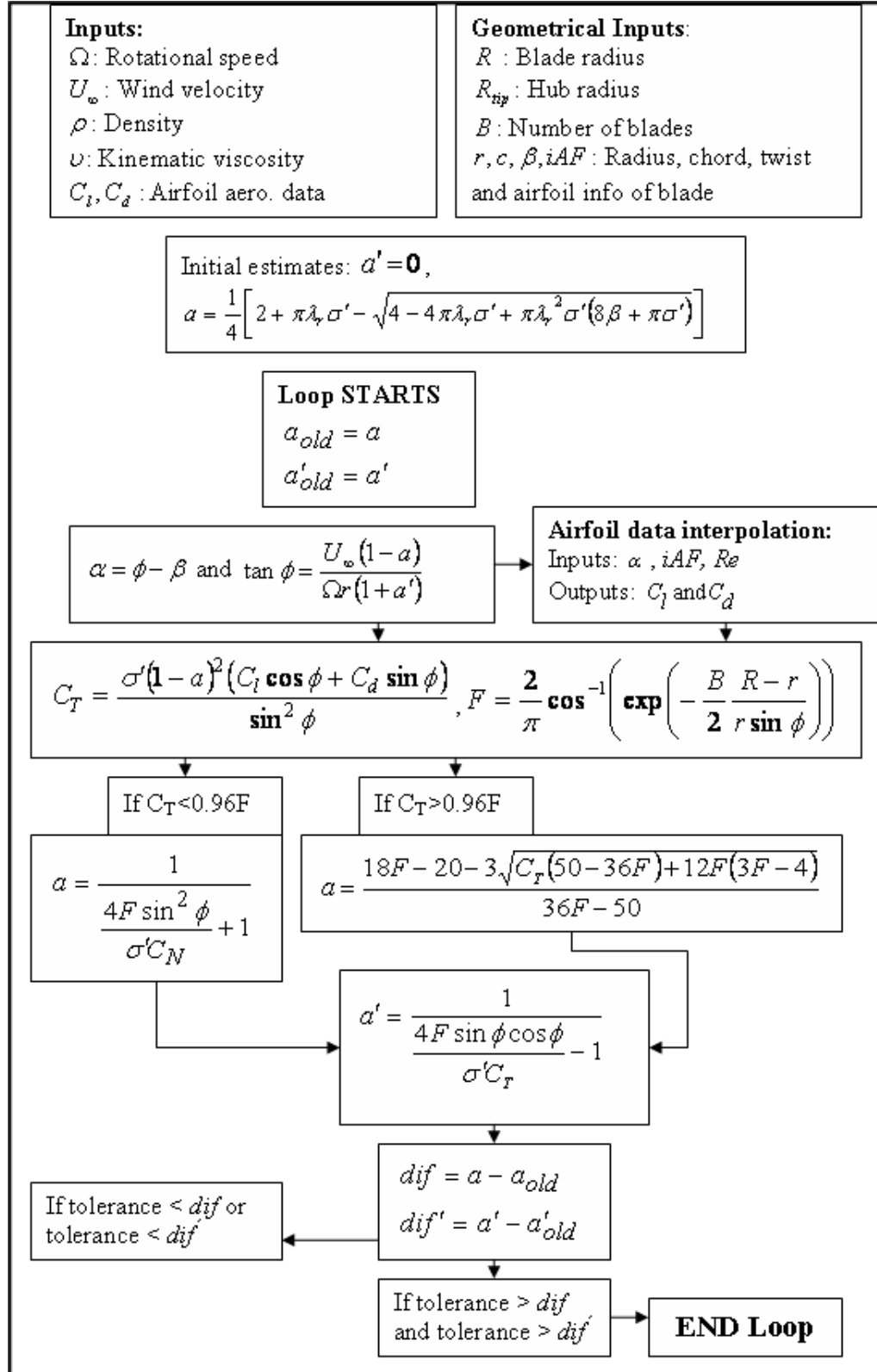


Figure 2.7: Induction factor calculation: Iteration procedure.

2.8 Validation of BEM Analysis Tool

Before the implementation of BEM analysis tool to the optimization process, some validations are performed in order to understand the capability and the limits of the theory. Validation is performed for three different wind turbines that have experimental results in reference [22].

In the analysis, the number of blade elements is chosen according to the given geometrical data for each wind turbine. In the NREL (National Renewable Energy Laboratory) Phase II and Phase III wind turbines, 18 blade element geometries are specified whereas in Risoe (National Laboratory for Sustainable Energy) wind turbine only 9 blade element geometries are given in the reference. The differences between experimental data and analysis results which may result from selection of the number of blade elements are also explained in Risoe wind turbine application section.

In the all cases, BEM analysis tool is used for two purposes. One purpose is to show the standard BEM analysis which the calculation procedure includes both C_l and C_d coefficients. Other purpose is to show C_d effect in the calculations, thus, C_d is taken to be zero everywhere in the analysis results named "no- C_d ". These two analyses results are compared by means of drag coefficient effect. Despite the fact that power losses in the wind turbines coming from the drag force are not very important in power production; it becomes an important issue when the wind speeds are getting higher. Therefore, BEM analysis tool is also evaluated from this point of view.

2.8.1 NREL Untwisted and Untapered Wind Turbine

Tests done with NREL untwisted and untapered wind turbine is called Phase II experiments and the turbine is called Phase II turbine. The turbine is developed in NREL for testing purposes. General characteristics of the turbine are explained in the Table 2.1 and geometrical properties are shown in Figure 2.8.

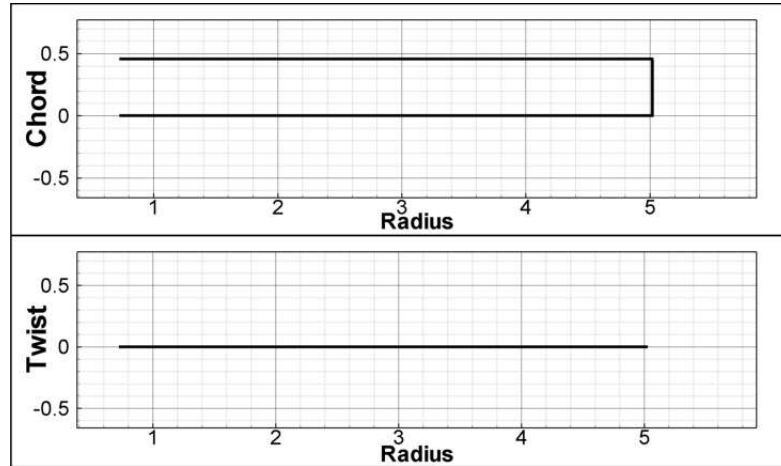


Figure 2.8: Geometry information of NREL Phase II wind turbine.

Table 2.1: NREL Phase II wind turbine general characteristics

Number of Blades	3
Turbine diameter	10.06 m
Rotational Speed	71.3 rpm
Cut-in wind speed	6 m/s
Control	Stall Control
Rated power	19.8 kW
Root extension	0.723 m
Blade set angle	12 degrees
Twist	None
Chord	0.4572 m @ all span locations
Airfoil	S809

In the NREL experiments, S809 airfoil is used for all stations on the blade span. This airfoil is designed for specifically for wind turbine applications by NREL. C_l and C_d coefficients of this airfoil are obtained from reference [22] for different angle of attack values. These coefficients are also shown in Figure 2.9.

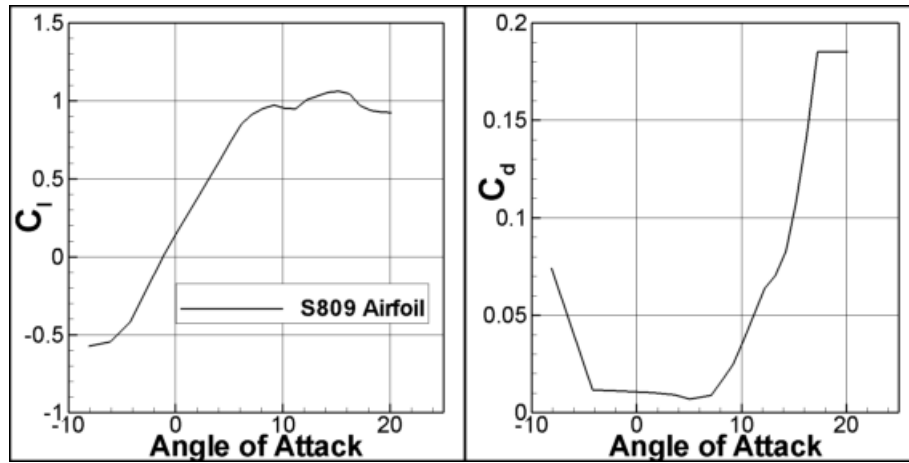


Figure 2.9: S809 airfoil C_l and C_d coefficients.

Phase II wind turbine is analyzed with BEM analysis tool. For different wind speeds, power production of the wind turbine is calculated. Two different analysis results are compared with test results in Figure 2.10. In the analysis, 18 blade elements are used and analyses are also performed without considering C_d contribution to the power production.

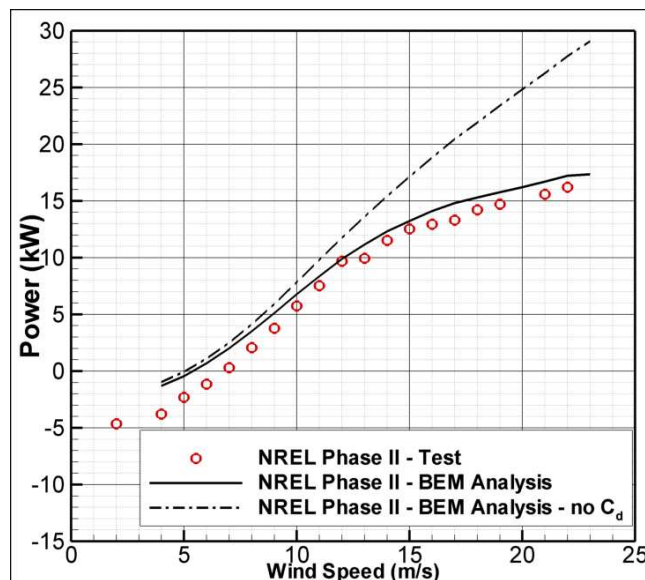


Figure 2.10: NREL Phase II wind turbine test and analysis comparison.

BEM analysis tool predicted NREL Phase II wind turbine performance well as shown in Figure 2.10. There is only a delta difference between analysis and test results for all wind speeds. In the analysis without considering C_d contribution to the power predicted, the turbine performance well for low speed regions which are the wind speeds below 10 m/s. For high wind speeds where the turbine is loaded and the local angles are high, C_d contribution to power becomes more important. For wind speeds higher than 10 m/s, analysis without C_d are over predicting the power production.

2.8.2 NREL Twisted and Untapered Wind Turbine

NREL experiment with twisted and untapered wind turbine is called Phase III experiments and the wind turbine is called Phase III wind turbine. This wind turbine is designed for testing purposes as Phase II wind turbine. Phase III wind turbine has similar characteristics with Phase II wind turbine which is tabulated in Table 2.2. Geometrical information of the turbine is shown in Figure 2.11.

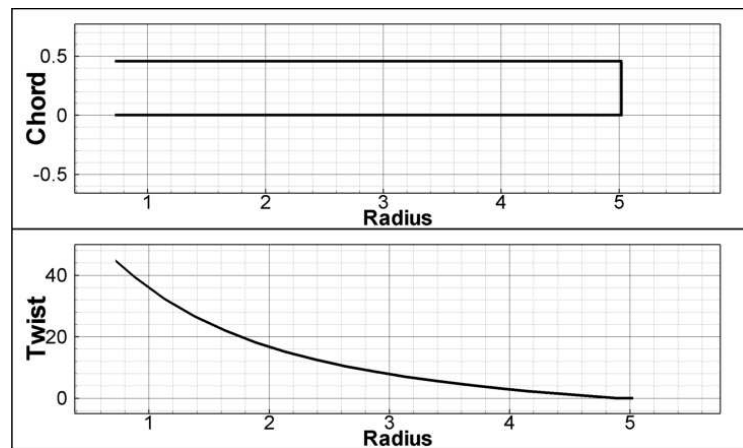


Figure 2.11: Geometry information of NREL Phase III wind turbine.

Table 2.2: NREL Phase III wind turbine general characteristics

Number of Blades	3
Turbine diameter	10.06 m
Rotational Speed	71.3 rpm
Cut-in wind speed	6 m/s
Control	Stall Control
Rated power	19.8 kW
Root extension	0.723 m
Blade set angle	3 degrees
Twist	44 degrees (max.)
Chord	0.4572 m @ all span locations
Airfoil	S809

The airfoil used in the Phase III wind turbine is the same as the Phase II wind turbine. Airfoil coefficients for S809 airfoil are shown in Figure 2.9 in the Phase II application.

Phase III wind turbine BEM analyses are compared with the test data in Figure 2.12. As in Phase II, 18 blade elements are used in this analysis.

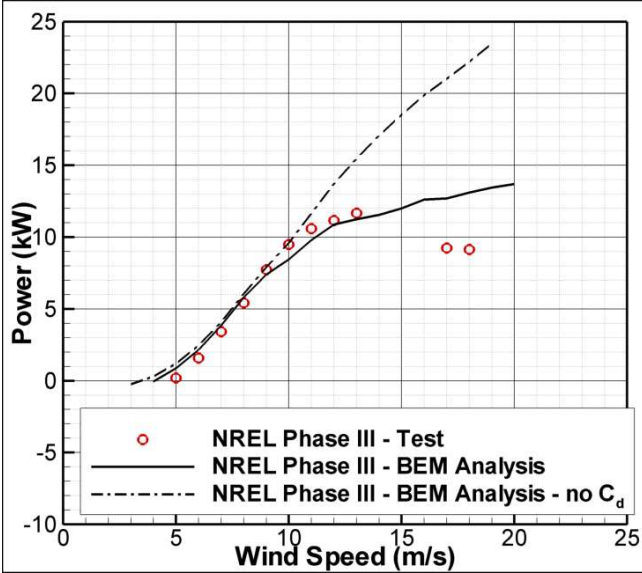


Figure 2.12: NREL Phase III wind turbine test and analysis comparison.

BEM analysis results are close to test data for low wind speeds which is shown in Figure 2.12. However, BEM analysis tool overpredicts the results beyond the turbine stall wind speed, where the power production no longer increase by further increasing speed. This mismatch may be related with high twist angles of Phase III wind turbine. Because of the high twist angles, when the turbine operates in high wind speeds, the performance prediction is poor. The local angle of attack values are higher which decreases the reliability of airfoil C_l and C_d coefficients. In Figure 2.13, the local angle of attack distribution of Phase III wind turbine is compared with Phase II wind turbine local angle of attack distribution for 15 m/s wind speed.

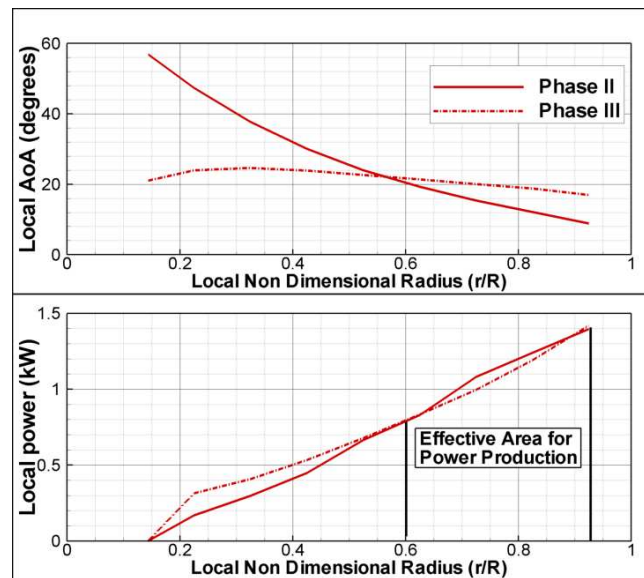


Figure 2.13: Local angle of attack and power comparisons of NREL Phase II and Phase III wind turbines for 15 m/s wind speed.

If the effective area for power production is defined as the area under the local power curve where almost 75-80 percent of power is produced, it is near tip regions as it is shown in Figure 2.13. In the untwisted Phase II blade, local angle of attack values are below the airfoil stall. However, in the Phase III twisted blades, these angles are higher than the stall angles. Therefore, reliability of airfoil C_l and C_d coefficients are decreasing in this area for high wind speeds. This brings the mismatch from experimental value. Moreover, for these highly loaded regions, induction factors are corrected in BEM method. From this validation case it can also be concluded that accuracy of BEM method is decreasing for high wind speeds when the turbine is highly twisted and local angle of attack values are beyond the stall values. Very

high local angle of attack values are seen in Phase II wind turbine root section. Although the root sections are not effective in power production, they produce some power. Airfoil data are extrapolated for this region without considering complicated flowfield in this area. Therefore, this can be considered as one of the reasons for the shift in Phase II analysis results from the experimental test data. Airfoil data extrapolation method for high angle of attack values will be explained in Chapter 3.

2.8.3 Risoe Wind Turbine

The last application is Risoe wind turbine. This turbine has twisted and tapered blades. General characteristics of Risoe wind turbine is shown in Table 2.3 and geometrical characteristics are shown in Figure 2.14.

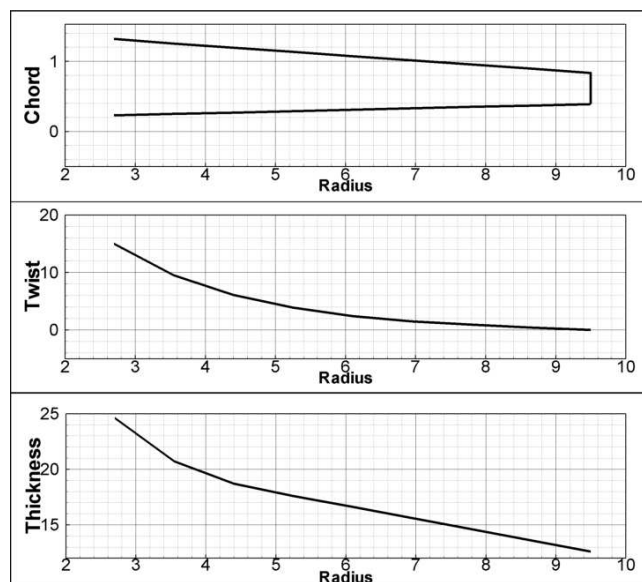


Figure 2.14: Geometry information of Risoe wind turbine.

Table 2.3: Risoe wind turbine general characteristics

Number of Blades	3
Turbine diameter	19.0 m
Rotational Speed	35.6 and 47.5 rpm
Cut-in wind speed	4 m/s
Control	Stall Control
Rated power	100 kW
Root extension	2.3 m
Blade set angle	1.8 degrees
Twist	15 degrees (max.)
Root Chord	1.09 m
Tip Chord	0.45 m
Airfoil	NACA 63-2xx Series

In Risoe wind turbine, NACA 63-2xx series airfoils are used. C_l and C_d coefficients of these airfoils for different angle of attack values are obtained from reference [22]. In the Figure 2.15, coefficients of NACA 63-2xx airfoils are shown for different thickness values.

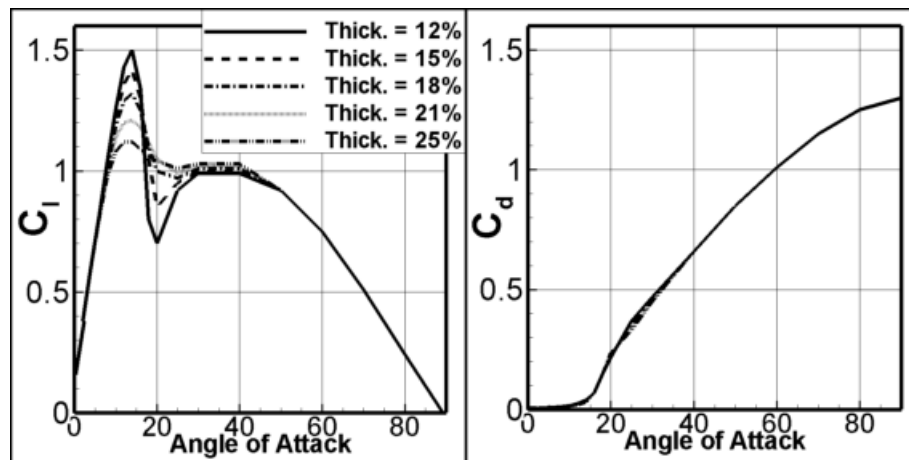


Figure 2.15: C_l and C_d coefficients of NACA 63-2xx airfoils.

Risoe wind turbine is analyzed with 9 blade element sections. Comparison with field test data is shown in Figure 2.16. BEM analysis tool power predictions are quite close to the experimental data of the wind turbine. When C_d is not included in power calculations, the accuracy of the tool is decreasing.

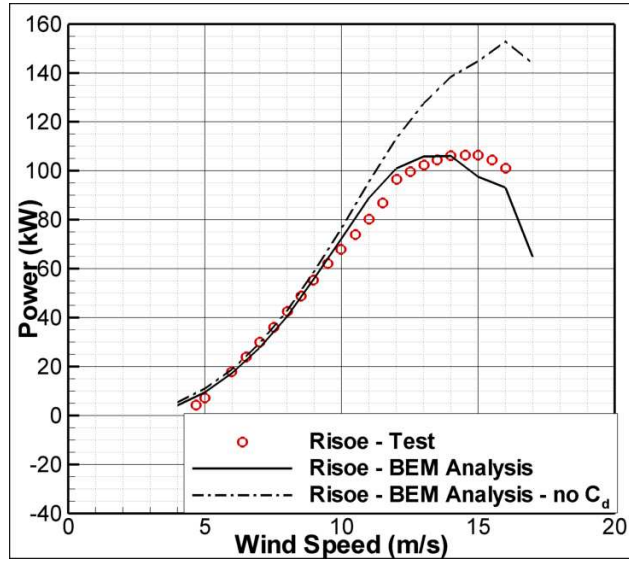


Figure 2.16: Riso wind turbine test and analysis comparison.

In Riso wind turbine BEM analysis, only 9 blade element sections are used since the turbine blade geometry is given for 9 stations in reference [22]. To show the difference between test data and analysis result originated from number of blade elements, BEM analysis for 50 blade elements are also performed. The distribution of these 50 blade elements are shown in Figure 2.17. Blade elements are clustered in the tip regions since tip sections' power production contribution is higher.

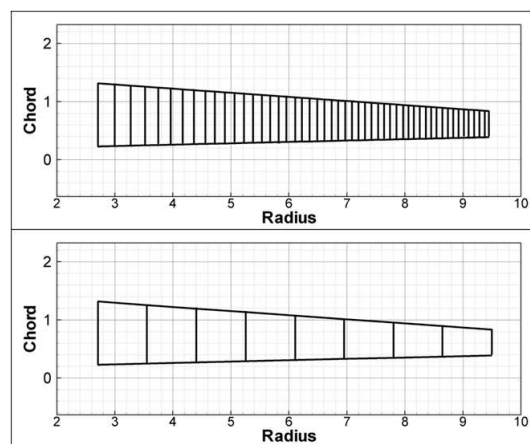


Figure 2.17: Blade elements used in Riso wind turbine analysis.

BEM analyses for 50 blade elements are compared with 9 blade element results and Risoe test data in Figure 2.18. The results are closer to the test data when number of blades are 50 as expected. However, the accuracy is not improving so much. The main reason of this is coming from the airfoil information. When the number of blade elements are increasing, 2D airfoil coefficients have to be interpolated correctly in order to improve accuracy of results. Thickness interpolation on airfoil coefficients always carry an order of error. In this analysis, information is coming from only 5 airfoils but distributed to 50 sections. Therefore, increasing the number of blade elements does not increasing the accuracy of analysis as much.

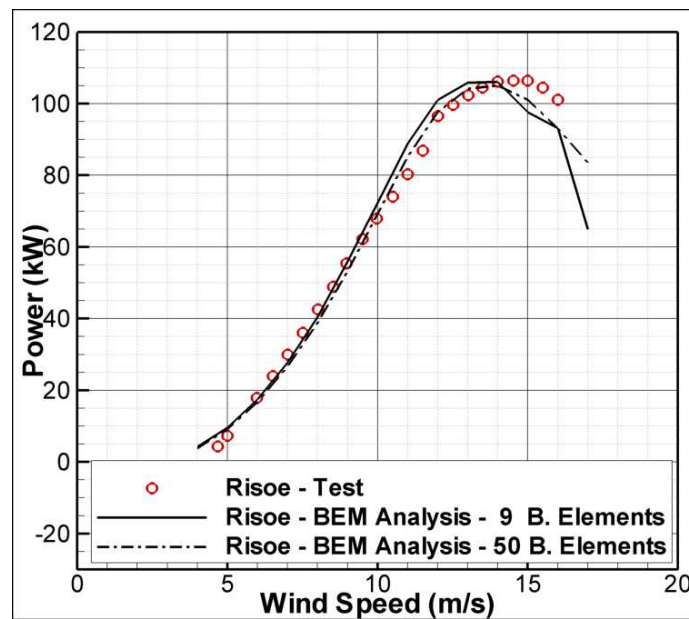


Figure 2.18: Risoe wind turbine BEM analyses with different number of blade elements.

CHAPTER 3

AIRFOILS IN WIND TURBINE APPLICATIONS

3.1 Introduction

Airfoils generate the aerodynamic forces on a wind turbine blade. Power of a wind turbine is related to aerodynamical and geometrical properties of its airfoils. Airfoil properties such as aerodynamic forces which are lift and drag produced by airfoils of a wind turbine blade has to be known in order to achieve desired performance. In this chapter, main characteristics and properties of airfoils will be revisited.

3.2 Airfoil Terminology and Airfoil Classification

Geometrical parameters defining an airfoil are shown in Figure 3.1 below.

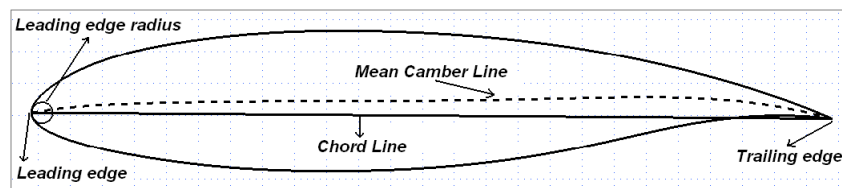


Figure 3.1: Basic airfoil properties.

Most of the time, dimensions related with airfoils are given as referenced to the chord length. Thickness of an airfoil is usually represented with maximum thickness percentage of the airfoil related to chord. Camber of an airfoil also has a similar definition: it is represented by

maximum camber percentage related to chord.

From structural point of view, thickness and camber distribution is very important. Airfoils may have the same thickness or camber values but different distributions. This is shown in Figure 3.2. Both airfoils have similar thickness and camber values. However, since the distributions are different, these airfoils can not be used at the same time for the same wind turbine blade. Therefore, different airfoils have to have some common characteristics in order to be used together on a wind turbine blade.

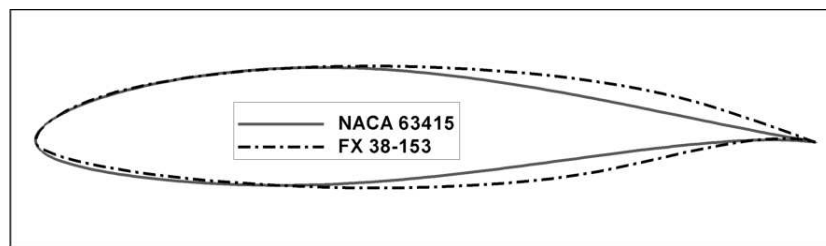


Figure 3.2: An example for different thickness distributions in two airfoils.

Airfoils that have similar thickness or camber characteristics are produced for this purpose. These airfoils are called airfoil families or airfoil series. Most famous airfoil families are produced by NACA. The examples of NACA airfoil families which are used also in wind turbine applications are NACA 63, NACA 64 and NACA 65 airfoil families. In addition to NACA airfoils, there are several airfoil families developed by European and US research institutes for wind turbine applications. For example, Risoe-A1, A2 or Risoe-B1 airfoil families which are designed by Risoe National Laboratory in Denmark. Other famous airfoil families are developed by Delft University in Netherlands which are called as DU airfoil families. An example of DU airfoil families is shown in Figure 3.3. NREL (National Renewable Energy Laboratory) in US also developed airfoil families which are called as NREL S-series airfoils. There are several other airfoils developed and used in wind turbine applications. In almost all of the airfoil families produced for wind turbines, structural concerns are included in airfoil design [28, 29, 30].

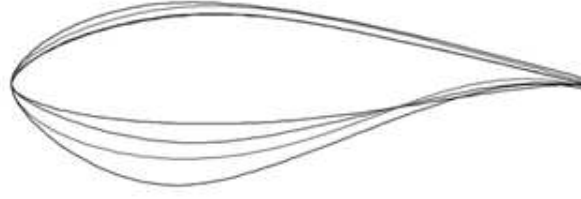


Figure 3.3: DU airfoil family designed for a 55 m diameter wind turbine[31].

3.3 Aerodynamics of Airfoils

Flow over an airfoil creates distributed force on the airfoil. When the flow passes over the upper or convex side of the airfoil, flow velocity increases which decreases the pressure acting on the surface. On the other hand, flow velocity decreases when it is passing on the lower (generally concave) surface of airfoil and as a result, pressure on this surface increases. Moreover, friction between air and airfoil surface exists and air flow velocity decreases when it reaches to airfoil surface. These pressure differences and friction create a net force and moment on the airfoil.

The net force acting on an airfoil is divided into two components as lift force and drag force. Lift force is the component of the net force on an airfoil perpendicular to flow direction. Drag force is the component of the net force on an airfoil parallel to flow direction. Moment which is acting on quarter chord is called as pitching moment. These forces and pitching moment calculations are illustrated in Equation 3.1.

$$\begin{aligned}
 \text{Lift} &= l = C_l \frac{1}{2} \rho U^2 c \\
 \text{Drag} &= d = C_d \frac{1}{2} \rho U^2 c \\
 \text{Moment} &= m = C_m \frac{1}{2} \rho U^2 cr
 \end{aligned} \tag{3.1}$$

In this equation, C_l is airfoil lift coefficient, C_d is airfoil drag coefficient, C_m is airfoil moment coefficient, c is the chord length.

Flow passing on the surface of an airfoil is not always the same. Related to the effects such as velocity, temperature, air ambient pressure, viscosity, the length of airfoil etc., flow has different characteristics. As a result, forces and moments on an airfoil are different. Most of these effects are represented by a nondimensional number which is called as Reynolds

Number. Reynolds number is the ratio of the inertia forces over viscous forces. Reynolds number is calculated with Equation 3.2.

$$Re = \frac{UL}{\nu} = \frac{\rho UL}{\mu} = \frac{\text{Inertia forces}}{\text{Viscous forces}} \quad (3.2)$$

In this formulation, U and L are velocity and reference length, ρ is fluid density, μ is dynamic viscosity and ν is kinematic viscosity. Reynolds number basically represents character of the flow and it has direct effects on the force coefficients.

In aircraft applications, Reynolds numbers are usually high, much more than a few millions. However, in wind turbine applications Reynolds numbers are usually low (except huge wind turbines), less than a million or only a few millions, since the wind velocities are very low. This means that airfoils designed for high Reynolds numbers may not be suitable for low Reynolds number applications. In order to design a wind turbine, real characteristics of the airfoil has to be known and decision should be done by considering these effects.

3.4 Airfoil Database

In the BEM analysis and optimization performed in this thesis, airfoil force coefficient information from different airfoils is needed. In the optimization studies, different airfoils and airfoil families are included into the optimization process. An airfoil database is set up for this purpose. This airfoil database consists of many airfoils or airfoil families designed for wind turbines or used in wind turbine applications [32, 33, 34, 35, 36, 37]. In the database, lift and drag coefficients for a range of angle of attack values and for different Reynolds numbers are used. One property of this database is that the only force coefficients produced in wind tunnel tests are used for each airfoil. The main goal of this criterion is to perform BEM theory analysis more accurately. By keeping 2D section data accuracy of a wind turbine blade as close to real as possible, wind turbine performances are predicted as accurate as possible. The applications of the BEM method with this concept is shown during the validation of BEM analysis code in Chapter 2.

There are two groups in the database. First group consists of airfoils belongs to an airfoil family. There are single airfoils not belong to any airfoil family but still kept in the database

for single airfoil applications along a wind turbine blade. Main properties of airfoils used in the database are shown in Appendix A. 11 airfoil families found in the literature are used in the database. These families are shown in Table 3.1.

Table 3.1: Airfoil families used in airfoil database

Name of Family	Number of Airfoils in the Family	Thickness Range (percent of chord)	Re Number Range
NACA 63-2xx	3	15 to 21	1.0E6 to 9.0E6
NACA 63-4xx	4	15 to 30	1.0E6 to 9.0E6
NACA 64-4xx	2	15 to 21	3.0E6 to 9.0E6
NACA 65-4xx	2	15 to 21	3.0E6 to 9.0E6
Risoe A1	3	18 to 24	1.6E6
FX-61	4	14.7 to 18.4	1.0E6 to 3.0E6
DU	2	21 to 25	1.0E6
FFA-W3	3	21 to 30	1.4E6 to 1.8E6
FX-60	3	12.6 to 17.7	1.0E6 to 3.0E6
FX S	2	15.8 to 19.6	1.0E6 to 3.0E6
FX-66	4	16.1 to 19.6	1.0E6 to 3.0E6

3.5 Airfoil C_l and C_d Data Interpolation and Extrapolation

Airfoil database includes C_l and C_d data of many airfoils for various Reynolds number data. To apply this airfoil information to the iteration procedure in BEM analysis code, an interpolation method is chosen. 3D surface fitting method is used which is included in FORTRAN90 libraries. With this method, airfoil coefficients are stored as surfaces according to changing angle of attack and Reynolds number. Interpolation examples are shown in Figures 3.4 and 3.5. In Figure 3.4, angle of attack values are interpolated whereas in Figure 3.5, interpolation is performed for different Reynold number regimes.

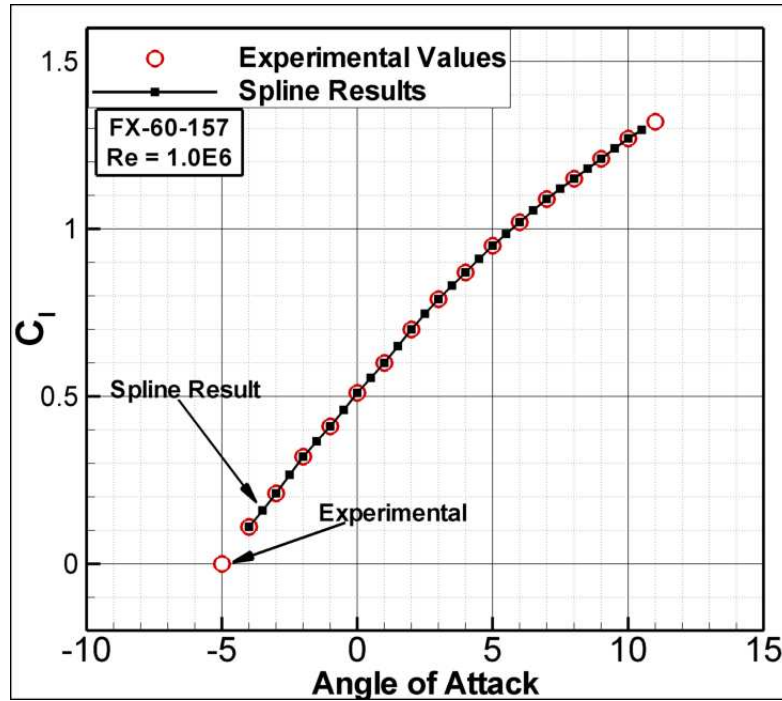


Figure 3.4: Airfoil data interpolation for angle of attack results compared with originals.

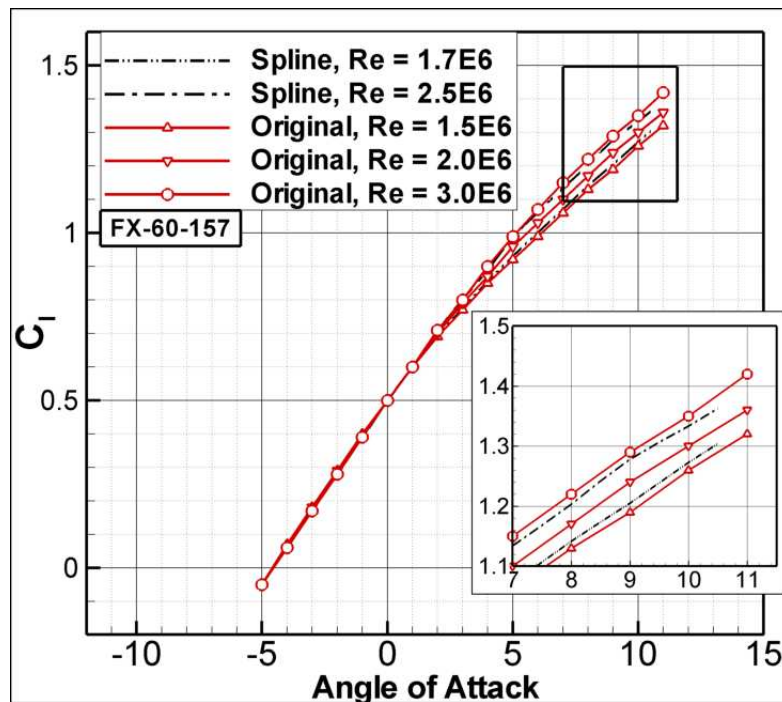


Figure 3.5: Airfoil data interpolation for Reynolds number results compared with originals.

Wind turbines are operating at very high angle of attack regimes. Some of the wind turbine airfoils have test results for high angle of attacks. But, most of the airfoil data have to be extrapolated for very high angle of attack values between -180 to +180 degrees to cover the all angle of attack regimes. For this purpose, a preprocessing tool, AirfoilPrep is used which is developed in NREL [38]. This tool takes airfoil information for limited angle of attack range and extrapolates the data between -180 and +180 degrees of angle of attack. The tool is developed for aerodynamic analysis tools of NREL; WT Perf [39] and AeroDyn [40] which also need extrapolated airfoil information for their analysis. The extrapolation of airfoil data is done by Viterna's method in AirfoilPrep v2.2 [41]. Viterna's method is simply a kind of correlation between the post-stall characteristics of wind turbine the airfoils and Aspect Ratio of wind turbine for which the post stall characteristics of airfoils are close to experimental data. A series of tests are performed for this purpose and explained in the reference [41].

In the Figure 3.6 extrapolated airfoil data by using AirfoilPrep v2.2 are shown and compared with original limited angle of attack values. Before a new airfoil is added to the airfoil database, its coefficients have to be pre-processed with AirfoilPrep for high angles of attack values. Then, BEM analysis code is able to analyze wind turbines in very high and low angles of attack within the limits of this extrapolation accuracy.

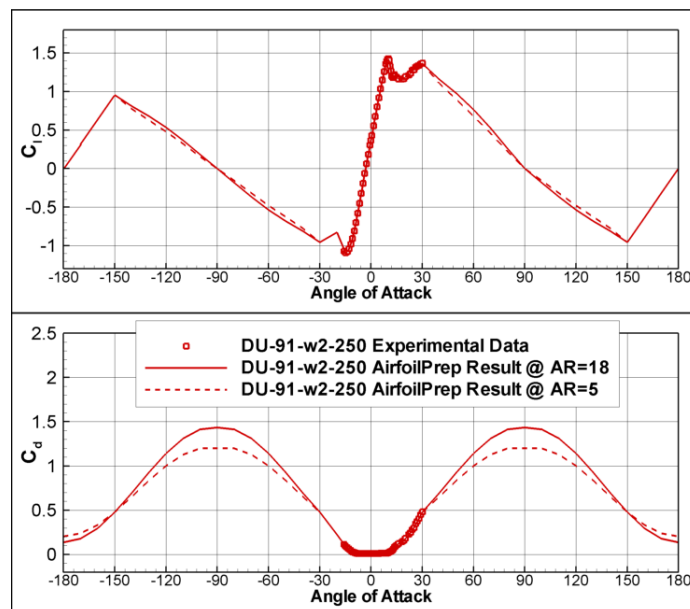


Figure 3.6: Airfoil data interpolation for Reynolds number results compared with originals.

CHAPTER 4

GENETIC ALGORITHM AND ITS IMPLEMENTATION

4.1 Introduction

Wind turbine optimization is a combination of many different disciplines including aerodynamics, structures, electrical systems and production and maintenance costs. Aerodynamical concerns are in the first place of these disciplines. Therefore, optimization starts with aerodynamics. More power with similar blade geometry can be obtained by optimizing wind turbine geometrical properties for maximum power output. Genetic Algorithm optimization is a very efficient method which is suitable especially for parametrical studies. Combination of BEM analysis code with the genetic algorithm optimization method is developed for wind turbine optimization purposes. Methods and implementation are explained in this chapter.

4.2 Genetic Algorithm Overview

A genetic algorithm is a heuristic search inspired by biological evolution. It is a part of evolutionary computing which is a rapidly growing area of artificial intelligence [42]. Genetic algorithm is inspired by Darwin's theory about evolution. Darwin's evolution theory states that good characteristics which are directly related to the survival of a member in a population will dominate in the population where bad characteristics will die off. Simple genetic algorithm optimization involves generation of a "population" of possible solutions, evaluation of the solutions according to a fitness function, selection of a set of fit "parent" solutions, and finally reproduction of those parents to generate a new population of possible solution. Population is governed by natural selection with crossover, reproduction and mutation operations.

Since the terminology used in the Genetic Algorithms embedded in biology, it is common to discuss "parents", "population", and so on. Some examples of this terminology:

Individual - Any possible solution

Population - Group of all individual

Chromosome - Blueprint of an individual

Genome - Collection of all chromosomes for an individual

Steps in a basic genetic algorithm are explained below:

Representation and Fitness: The solution representation used is a fixed-length string of units (bits, real numbers, letters, etc.). Each string must represent a possible solution. The fitness function defines the shape of the fitness. The fitness function is the essence of the problem. It provides the means by which the quality of a solution may be assessed and probability of that solution will reproduce.

Generation and initial population: The initial population is generated as if each string represents a potential solution (impossible solutions are excluded).

Selection of solutions: A fitness based selection method is used to choose the solutions which will produce next generation. The selection method is biased towards individuals of higher fitness, in order that better genetic material can persist in the population, and be improved upon through reproduction.

Reproduction: Reproduction consists of two parts: crossover and mutation.

1- **Crossover:** Crossover is the basic method of recombining genetic material from two parents. Crossover commonly involves randomly selecting some number of crossover points and exchanging those alleles which lie between the points.

2- **Mutation:** Mutation is the disruption of material after crossover. By introducing random variations into the child population, one can ensure that the diversity of the population remains large, and the ability to explore the landscape is retained.

Genetic algorithm optimization is applied to many engineering problems [11, 12, 13, 14 and 15]. Wind turbine optimization problem is also very suitable for genetic algorithm application.

Wind turbine can be divided into several parameters by using blade element concept; all parameters can be coded by genetic algorithm and optimized accordingly.

4.3 Implementation of GA to Wind Turbine Optimization Problem

For the genetic algorithm optimization, an open source FORTRAN77 code written by David L. Carroll is used [23]. This code is used as core of the wind turbine optimization problem by making some minor modifications for constraint definitions which are also explained in this section.

The optimization code itself needs some inputs. These are related with the efficiency of Genetic Algorithm and they are used as they are proposed by author. Fitness function in the optimization code is replaced with BEM analysis code which is developed for this study. Each member produced in every generation is analyzed with BEM analysis tool for power output. When a member has a high power production, its optimization variables are kept for next generations for better power production. Schematic representation of genetic algorithm optimization of wind turbine for best power output is in the Figure 4.1.

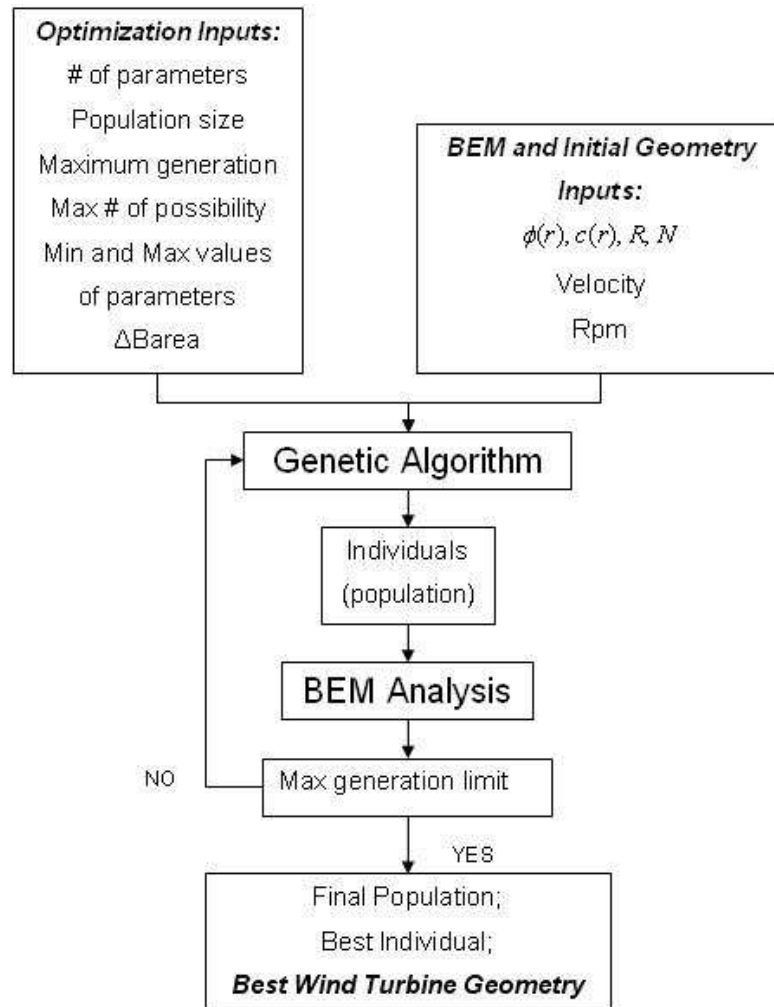


Figure 4.1: Wind turbine genetic algorithm optimization process chart.

Wind turbine optimization is performed by optimizing the parameters which are used to define a wind turbine blade in BEM analysis code. These are turbine diameter, number of blades, chord, twist distributions and airfoils. For this study, optimization parameters are chosen as chord, twist and airfoil sections for each blade element where diameter and number of blades are kept constant. In the optimization, twist and chord values are limited with predefined upper and lower values. However, airfoils are picked from an airfoil database which is explained in Chapter 3. Optimization is performed for a chosen operating point which is turbine rpm and wind speed. As a result, genetic algorithm searches for best chord and twist distributions with best airfoils to give highest power output for the given operating condition.

4.4 Wind Turbine Optimization

Wind turbine optimization starts with the selection of blade elements along the blade span. The more blade elements are used, the more accurate results are obtained from BEM analysis code as it is explained in Chapter 2. However, when the number of blade elements is high, time required for optimization process is high, too. For example, if 50 number of sections are used in the optimization, accuracy would be increased by 3-4 percent compared to 8 sections, but optimization time would be about 6 times longer than the case when 8 number of sections are used in the optimization. Therefore, limited number of blade elements is chosen for the optimization. Radial locations of each blade elements are also kept constant during optimization. For each blade element, 2 parameters are being optimized: chord and twist. As a result, there are $2 \times$ (number of blade elements) parameters coming from the blade elements. In addition to these, airfoil families are also involved in the optimization as a parameter. Totally, $2 \times$ (number of blade elements) + 1 (airfoil family) parameters are optimized. Overall optimization parameters are shown on a wind turbine in Figure 4.2 schematically. These parameters are updated for each generation during the optimization in order to reach the optimum geometry.

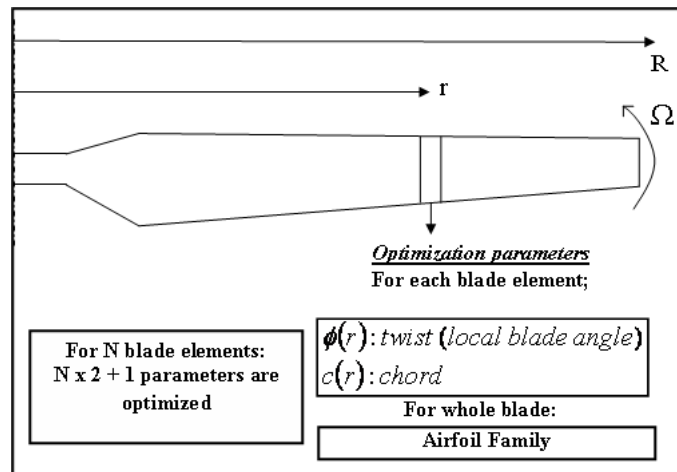


Figure 4.2: Wind turbine geometrical representation for the optimization process.

In the optimization, some constraints are introduced to the optimization parameters. These constraints are required in order to prevent wind turbine to become an improper geometry. In BEM method, blade elements are decoupled by assumption. This does not create big problems for basic wind turbine performance analysis applications. However, in the optimization, blade elements have to be related or connected somehow, in order to create more realistic wind turbine geometries. The optimization parameters and related constraints are explained in the next sections.

4.4.1 Chord Optimization

Chord distribution has a direct effect to power generated by wind turbine. For each blade element, chord is defined as an optimization parameter. Chord distribution varies along a turbine blade. These variations and typical chord distributions used in the real wind turbine applications are shown in Figure 4.3. Optimization code searches best chord values for each blade element to give maximum power output for a given operating condition.

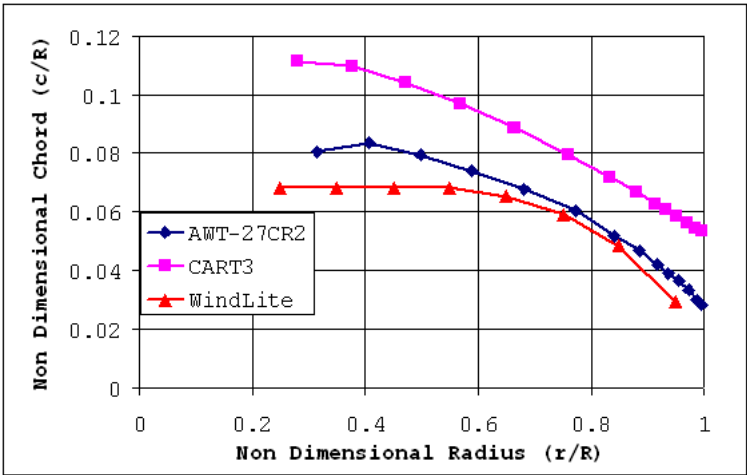


Figure 4.3: Typical chord distributions of wind turbines [39]

For each blade element, upper and lower limits for chord values are defined. Chord values are defined in this limit. A possible chord value for a blade element is then defined as;

$$c(r) = c_{min}(r) + \frac{c_{max}(r) - c_{min}(r)}{2^{N_{ch}} - 1} g_{ch}(r) \quad (4.1)$$

$$g_{ch}(r) \in [0; 2^{N_{ch}} - 1] \quad (4.2)$$

N_{ch} is the number of bits that chord is defined. In the wind turbine blades, chords are decreasing from root to tip. This is also added to the optimization as a constraint as;

$$c(r) < c(r + 1) \text{ for each blade element} \quad (4.3)$$

Individuals verifying the criteria in Equation 4.3 are taken into account, others are not. Applying these two constraints prevent the blade shape from improper geometries. Chord values have tendency to increase and reach the upper chord limits. Also, if planform area changes much during the optimization, resultant blade geometries are not comparable among themselves, anymore. To handle this problem, the blade planform area constraint is defined.

$$Barea = \sum_{r=0,R} \frac{1}{2} (c(r) + c(r + 1)) \Delta r \quad (4.4)$$

$$Barea_{min} < Barea < Barea_{max} \quad (4.5)$$

Individuals have to satisfy this constraint in the optimization. Chord distribution is produced within these limitations and maximizes power production with proper blade geometry.

4.4.2 Twist Optimization

Twist angle is another important parameter used in this optimization study. It is also called as local blade angle which decides the local angle of attack values. Local force and moment values are calculated from the angle of attack values as explained in the BEM theory. Therefore, twist distribution is very sensitive to the design condition of the turbine. Some twist distribution examples are shown in the Figure 4.4. As in the chord, an upper and lower limit is defined

for twist of each blade element. Genetic Algorithm searches for the best twist distribution to give the best power output for a given operating condition.

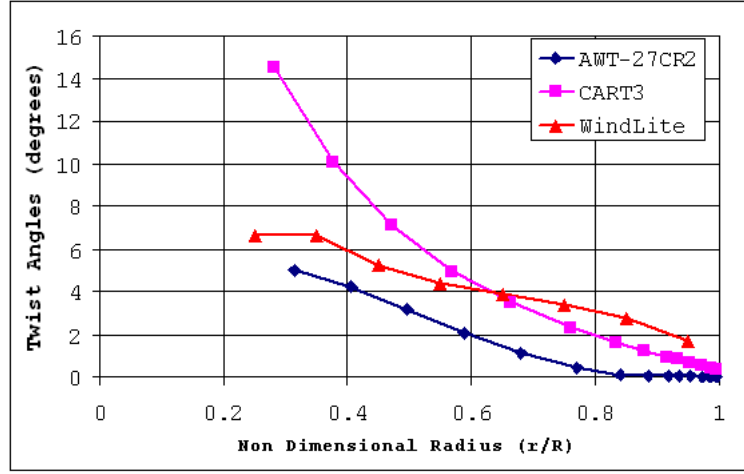


Figure 4.4: Twist distribution examples of wind turbines [39].

If there is no upper limit, twist angle tends to increase. To prevent twist to increase improperly, an upper limit constraint is applied to the optimization separately for each blade element. If value of twist is defined with N_{tw} bits, then,

$$\phi(r) = \phi_{min}(r) + \frac{\phi_{max}(r) - \phi_{min}(r)}{2^{N_{tw}} - 1} g_{tw}(r) \quad (4.6)$$

$$g_{tw}(r) \in [0; 2^{N_{tw}} - 1] \quad (4.7)$$

In addition to this, twist angles have to be located as decreasing from root to tip. This is applied as a second constraint to the optimization. Only individuals verifying the criteria in Equation 4.8 are taken.

$$\phi(r) < \phi(r + 1) \text{ for each blade element} \quad (4.8)$$

4.4.3 Airfoils

Airfoils are other important properties of wind turbine performance. An airfoil database is set up for optimization process. There is no direct constraint for airfoils in the optimization. Geometrical constraints and structural limitations in airfoil selection are described in Chapter 3. To prevent improper geometries may occur related to the arbitrary selection of airfoils for each blade element, airfoil families are used in the database. Optimization chooses airfoil family for each individual. Before the optimization, every member in the family should be assigned to blade elements, properly. By this way, thickness distribution of blade can be adjusted as increasing from blade tip to hub which is an important structural concern. This is explained with an example in Figure 4.5. There are 5 airfoils in the NACA 63-4xx family. These 5 airfoils are assigned along the blade for certain percentage of the blade span. During the optimization, blade elements that have local radius values stay in this percentages are assigned with that airfoil. Thickness distribution has to be continuous in the real applications. The smoothed version of thickness distribution is also shown in Figure 4.6.

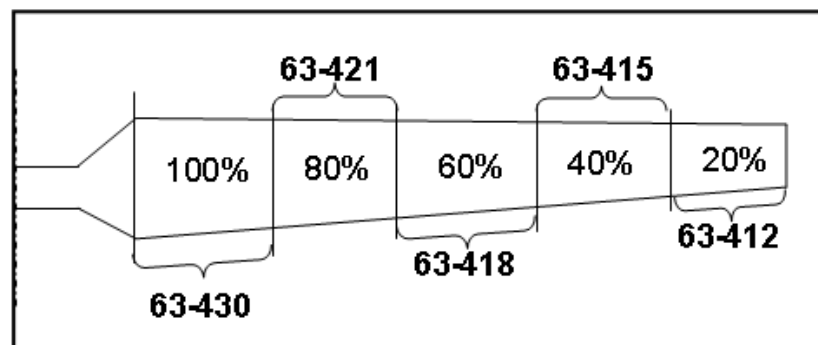


Figure 4.5: Airfoil definition example of blade elements for 63-4xx family

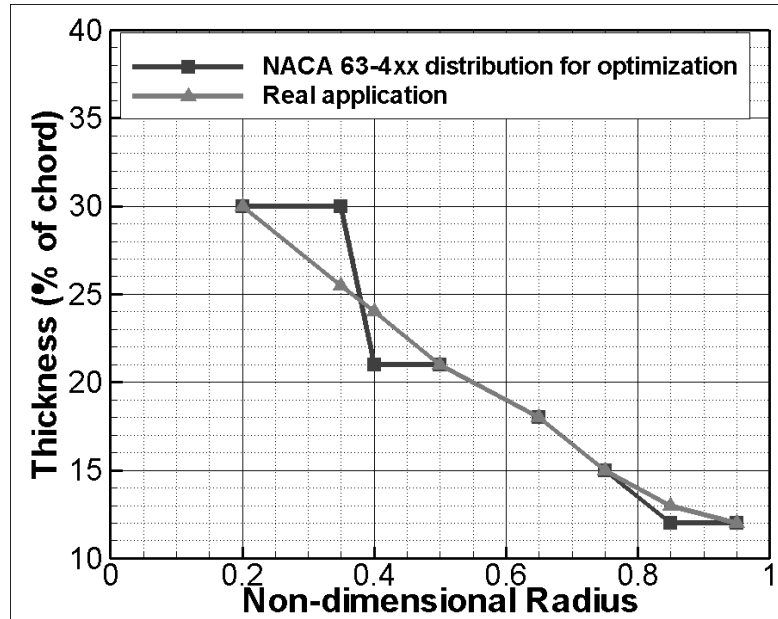


Figure 4.6: Thickness distribution of NACA 63-4xx family to 8 blade elements: for optimization problems and real application

Airfoil database contains also airfoils which do not belong to any family. Using all airfoils in the database including family members, an alternative optimization approach is also developed. According to this approach, same airfoil is used for all blade elements. Again, number of optimization parameters are $2 \times (\text{number of blade elements}) + 1$, but this time (+1) stands for single airfoil instead of airfoil family. Optimization result is the new wind turbine geometry with only one airfoil everywhere.

4.4.4 Operating Conditions

Wind turbine operating condition is referred as to be design condition of wind turbine for this thesis. Operating condition of a wind turbine is defined by wind speeds and rpm. These parameters are related to two main characteristics. One of them, wind speed, is related to yearly mean wind speed of the area where the wind turbine is designed to. The other one, rpm is more related to electrical and mechanical properties of wind turbine.

Every land on earth has different wind characteristics. A lot of measurements are performed for long time periods on windy areas to determine yearly wind distributions for energy production. These measurements are vital for wind industry to describe the variation in wind

speeds. When a wind turbine producer designs a wind turbine, these measurements are used to reach the best possible power production on that area. Wind turbine investors estimate their income from electricity generation by the wind measurements information. Wind distribution on a typical site is represented by Weibull distribution. Weibull distribution shows change in power density which is watts per square meter with change in velocity in a specified area for a specified period of time. A Weibull distribution is shown in Figure 4.7. This graph shows probability of power produced per square meter of an area for a time period. The area under the curve is exactly equal to one when the probability that wind will be blowing at some wind speeds including zero is 100 percent. In this example, if the measurements are performed for a year and the results are represented for that year, then, speed of 6.6 m/s which is signed with a vertical line shows that half of the year the wind will be blowing under 6.6 m/s and other half is more than 6.6 m/s. Design wind speed for a wind turbine is selected by using this Weibull distribution of the site that turbine is designed for.

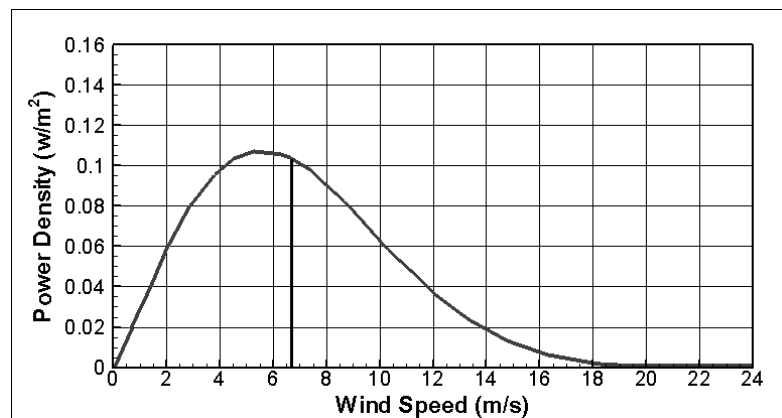


Figure 4.7: An example of Weibull distribution

The other parameter in operating condition of a wind turbine is rotational speed. Wind turbines are classified as variable and fixed speed wind turbines according to their rotational speed characteristics. Difference between these two turbines is coming from their generators. Variable speed wind turbines use variable frequency alternator. Fixed speed generators use induction generator. In the variable speed wind turbines, when the wind blows, the turbine turns faster and produces more energy. This type is not very common since the application is not very easy. In the fixed speed wind turbines, the turbine starts to rotate when it reaches to

its fixed rpm value. When the wind blows faster, it tries to rotate the turbine faster. Since rpm is fixed, extra energy is collected as electrical energy. Most of the wind turbines used now are fixed speed wind turbines. Therefore, all the wind turbines will have fixed rotational speed used this thesis.

In addition to these, the easiest way to choose operating condition is searching for the previous wind turbines that have similar geometrical properties such as diameter and number of blades. They can be used as a starting point for initial selection of operating point.

Once proper airfoil information and the operating conditions are chosen with suitable constraint definitions, optimization of a wind turbine and even a design optimization can be performed by using Genetic Algorithm and BEM based wind turbine optimization method which are explained until now. In the next chapter, optimization applications are shown.

CHAPTER 5

OPTIMIZATION APPLICATIONS

5.1 Introduction

BEM analysis code and Genetic Algorithm optimization method is applied to optimization of Risoe wind turbine which is used in Chapter 2 as a validation case of BEM analysis code. In order to study how the optimization method improves a wind turbine power performance, a real wind turbine is chosen. Design and off-design performance of each wind turbine are produced and compared with Risoe wind turbine. In addition to these, a design optimization case is studied for chosen radius and operating conditions. During the design, similar procedures are followed which are applied to Risoe wind turbine optimization case.

5.2 Risoe Wind Turbine Optimization

Risoe wind turbine is chosen as the baseline wind turbine for this optimization case. Mechanical and geometrical parameters of Risoe wind turbine is given in Chapter 2. From wind turbine test data, the maximum power is reached at wind speed of 14.5 m/s. This value is taken as optimization point for optimization work. Also, rotational speed of the turbine is defined as 47.5 rpm. This value is used as rotational speed value in the optimization cases. 8 blade element sections are used for optimization. All of the constraints are defined referencing the Risoe wind turbine parameters in order to see how a small geometrical modification affects the power performance.

5.2.1 Constraints of Optimization

The reason of constraint definitions in the wind turbine optimization is explained in Chapter 4. There are specific constraints defined for Risoe wind turbine optimization problem which are the same as in Chapter 4. Since Risoe wind turbine geometry is the baseline for optimization, upper and lower limits of chord and twist values are defined according to Risoe parameters as well as blade area. Upper and lower chord limits are defined as in the Figure 5.1.

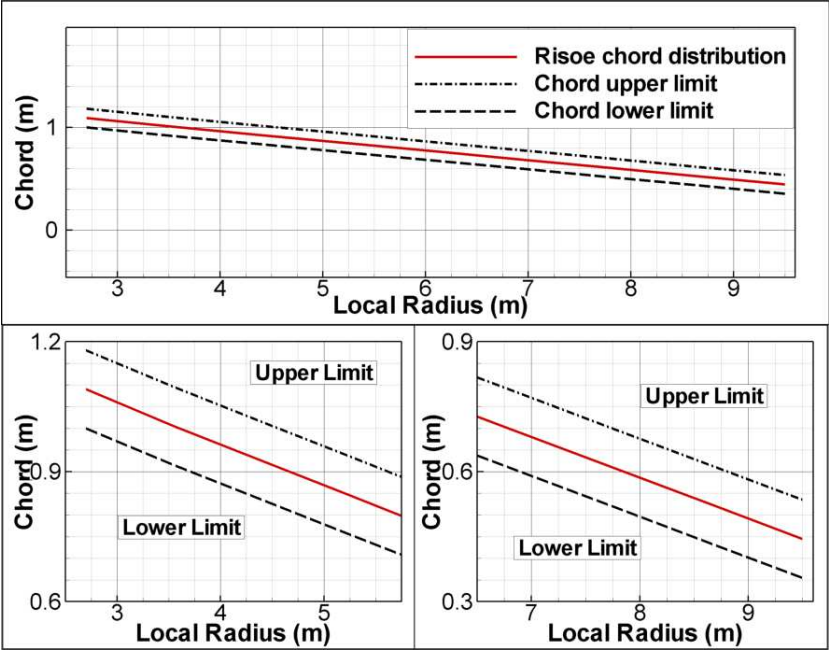


Figure 5.1: Risoe wind turbine optimization; chord upper and lower limits definitions.

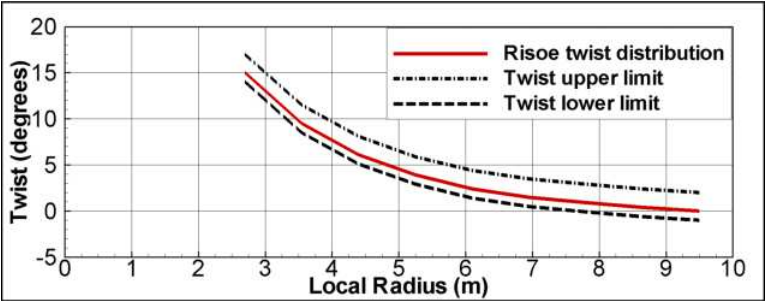


Figure 5.2: Risoe wind turbine optimization; twist upper and lower limits definitions.

Twist angles are also limited and upper and lower limits are shown in Figure 5.2.

Airfoil families used in optimization are shown in Appendix 2. In the appendix also distribution of the airfoil members of the family to the blade element sections are included. The blade planform area is limited to ± 5 percent of its original value. If an individual exceeds these limits, it is not taken to the optimization. The summary of the optimization constraints with optimization inputs and operating condition is shown in Table 5.1.

Table 5.1: Risoe wind turbine optimization parameters summary

Number of Blade Elements	8
Upper Lower chord limit	Risoe chord dist. 0.1 m
Upper Lower twist limit	Risoe twist dist. +2.0, -1.0
Blade planform area limited in	10%
Wind Speed	14.5 m/s
Rotational Speed	47.5 rpm
Generation no in optimization	300
Child no in population	20

Risoe wind turbine is optimized by applying three different strategies during optimization. These three methods are named as Opt1, Opt2 and Opt3. In Opt1, only chord and twist parameters are optimized by keeping the airfoils as originals. In Opt2, airfoil families are included in the optimization as well as chord and twist parameters. In Opt3, chord and twist is optimized with single airfoil selection for all blade elements. To summarize the 3 different optimization approach, Table 5.2 is referred. In the table, properties of Opt1, Opt2 and Opt3 are revisited.

Table 5.2: Optimization cases used in Risoe wind turbine optimization.

<i>Optimization Case</i>	<i>Chord</i>	<i>Twist</i>	<i>Airfoil</i>
Opt1	For all blade elements	For all blade elements	-
Opt2	For all blade elements	For all blade elements	Airfoil Family
Opt3	For all blade elements	For all blade elements	Single Airfoil

5.2.2 Generation

Number of generation used in both 3 optimization is 300. Evolution of the optimization is shown in Figure 5.3.

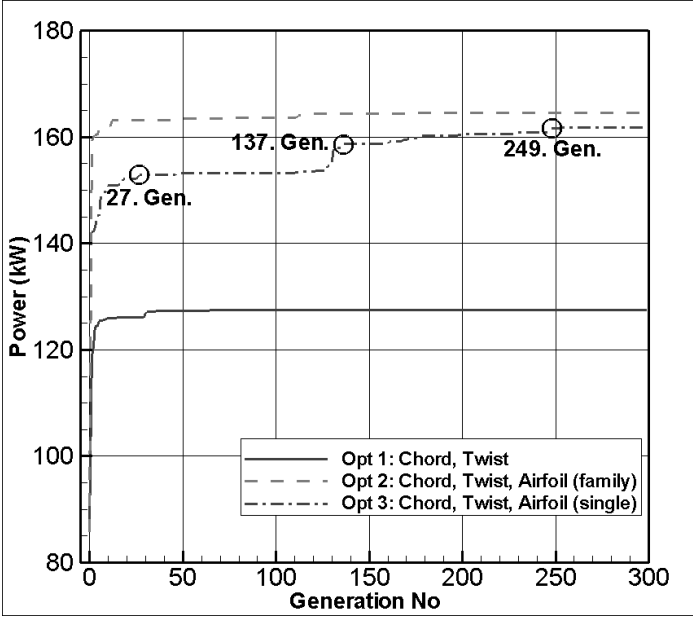


Figure 5.3: Evolution of optimization for each generation.

In Figure 5.3, how power generation increased can also be observed. In the very first generation, power production is nearly 90 kW. However, at the end of optimization, it is increased almost 80 percent reaching to almost 160 kW. Detailed comments about power generation as a result of optimization are explained in the results section. Before these comments, optimization process and decision for best wind turbine in populations are explained in this section.

In Figures 5.4, populations in the last generation are shown for each optimization case. Best wind turbine geometries for each optimization case are the children which produce maximum power and signed with circle in related figures.

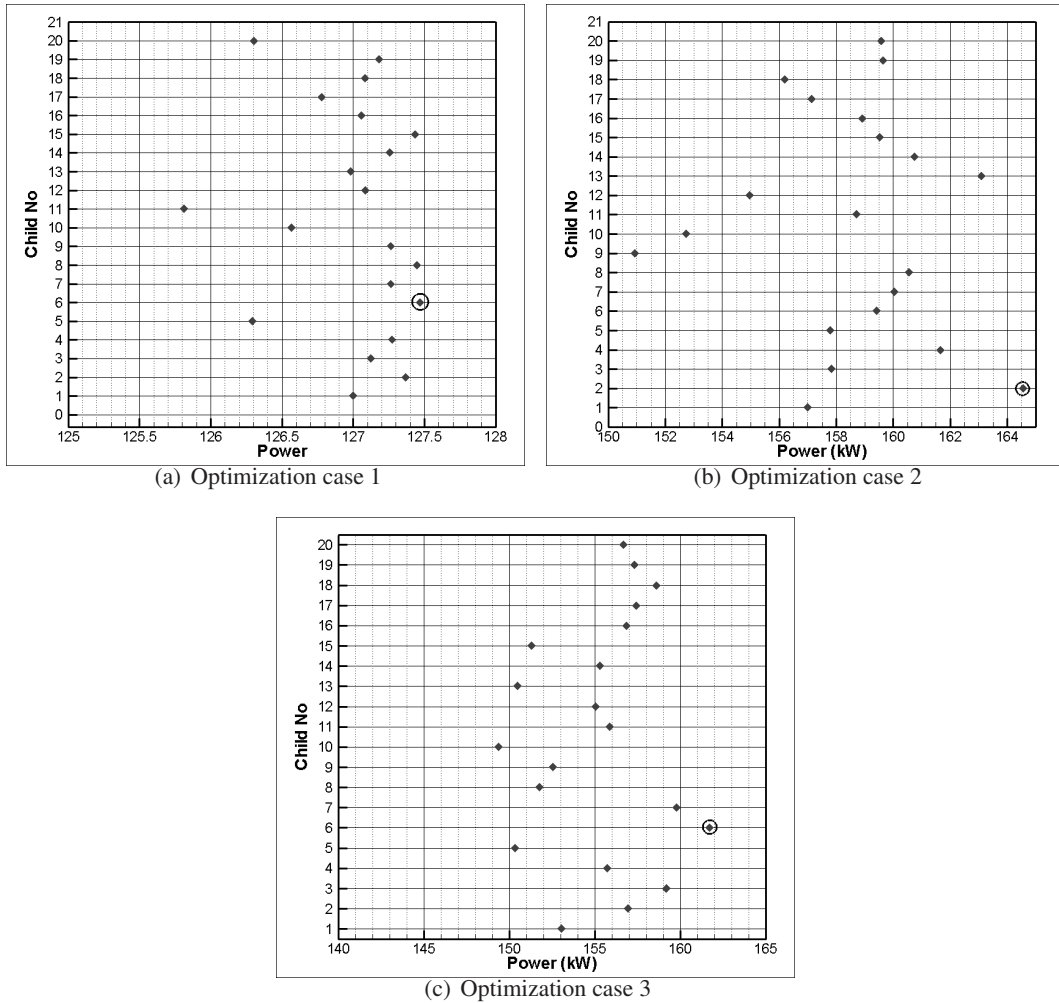


Figure 5.4: Best wind turbine in the population of last generation of various optimization cases Opt1 (a), Opt2 (b) and Opt3 (c)

5.2.3 Generation Steps

To understand what is happening inside the generations, development of Opt3 best wind turbine generation is explained here. In order to reach the best wind turbine geometry, geometrical parameters are changing from one generation to another. Therefore, middle steps which are taken from Opt3 optimization case are shown. The reason of the selection of Opt3 is that the sharpest peaks in power production are seen in Opt3 in Figure 5.3. In Figure 5.5, generation numbers investigated are signed with circle.

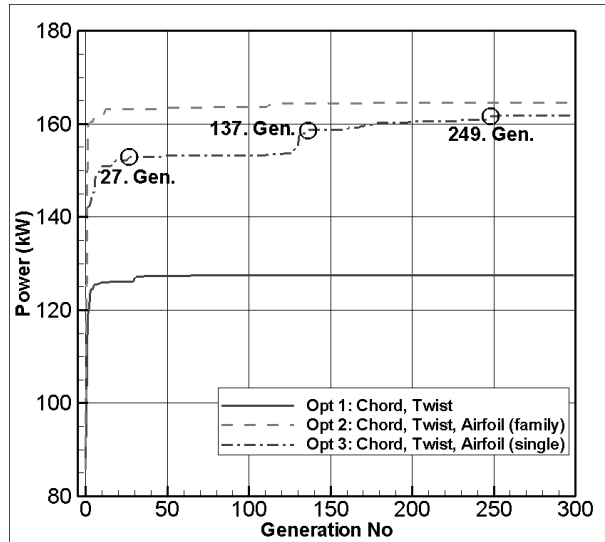


Figure 5.5: Investigated generation steps in Opt3.

In the generation numbers 27 and 137 represents certain jumps to a better power production level during the development of generations. 249th generation represents an individual with maximum power production very close to best wind turbine geometry. Their geometries are compared with each other. In Figure 5.6, changes in chord parameters are compared within themselves and Opt3 result.

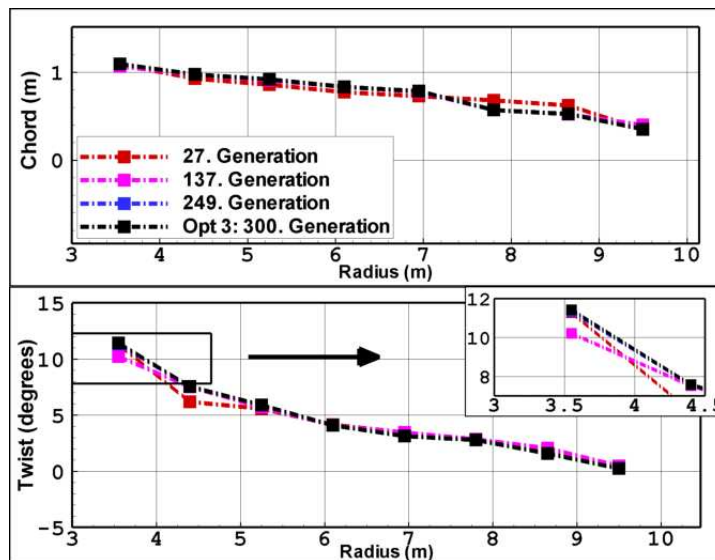


Figure 5.6: Generation in chord and twist parameters for Opt3.

For 27th and 137th generations, the chord distribution is different than the previous ones. The jumps in the power are coming from these geometry differences as expected. However, passing from 137th to 249th generation, chord is not changing much except tip and hub sections. This is the reason of small difference between 137th and 249th in power production. In addition to this, difference between 249th and 300th generations is not visible. This is consistent with power production difference between 249th and 300th generations: there is almost no difference between the power produced by 249th and 300th generation. Another important conclusion coming from this is that there is no need to go further from 300th generation because there is not much difference between 249th and 300th or even 137th and 300th generations.

Twist parameters are also compared in Figure 5.6. Similar statements can be concluded from twist parameters comparisons. Difference between 27th generation and base geometry is clear in the Figure 5.6. Also, it is observed that because of the twist difference between 27 and 137th generations, power production is changing. 249th and 300th generations have again almost the same twist distributions. As in the chord parameters comparisons, there is no need to increase the number of generations. In 300th generation, wind turbine reaches its final geometry.

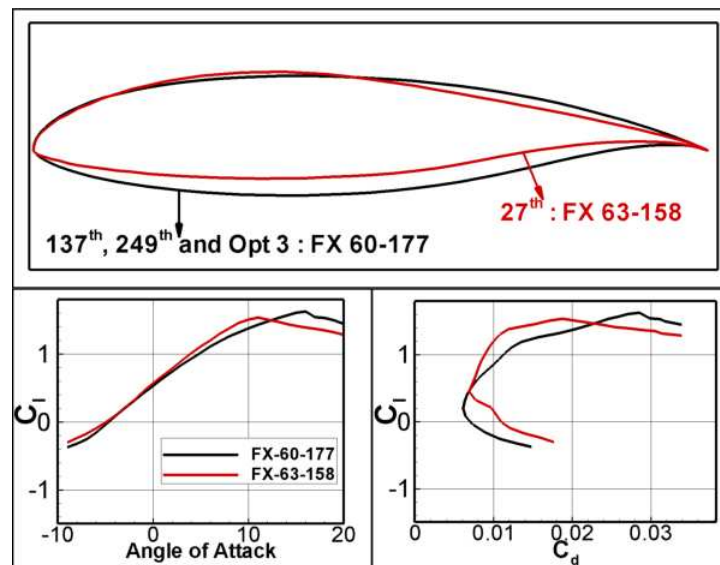


Figure 5.7: Generation in airfoils for Opt3 and 2D C_l and C_d comparisons.

In Figure 5.7, development in airfoil parameter is shown. Since Opt3 includes only single airfoil for all blade sections, there is only a few airfoils which are compared with each other. In 27th generation, FX 63-158 is selected. After that generation, airfoil parameter is converged faster than other parameters. In 137th, 249th and 300th generations the same FX 66-177 airfoil is selected. In the Figure 5.7 also 2D performance characteristics of airfoils are compared. In the optimization, FX 60-177 airfoil is chosen as the best airfoil for this operating condition.

5.2.4 Optimization Results

Geometrical results of the three optimization cases are compared with original Risoe wind turbine. In Figure 5.8, differences in chord and twist distributions at different optimization approaches are emphasized.

Figure 5.8 shows that how a wind turbine chord and twist distribution may change according to different optimization concepts. Optimization with a single airfoil for all blade elements, which is Opt3, increases chord values in the root and decreases them near tip sections. However, in Opt2, when airfoil family is used, chord values are almost remain the same with baseline wind turbine geometry until middle sections and they increase again until the tip section, but in the tip, chord values are again decreasing. When no airfoil parameter is introduced to optimization which is the case in Opt1, chord values are increased as much as they can, except again tip section. In all optimization cases, twist angles are increased by changing twist distribution along blade. In Opt1 and Opt3 twist angles are almost keep the same values with Risoe wind turbine. In Opt2, Instead of small twist angles in tip section, root section angle is small compared to other optimization cases. There is no general trend in twist distributions but the only result is the increase in twist angles.

In Figure 5.9, Opt2 and Opt3 airfoils are compared with original Risoe wind turbine airfoils. NACA 65-4xx family airfoils have more cambered shapes than NACA 63-2xx family. Also, FX-60-177 airfoil has more camber than NACA 63-2xx family airfoils. Moreover, FX-60-177 airfoil lift production capability is high when it is compared with other airfoils in the Figure 5.9. Both, NACA 63-2xx and 65-4xx family have less lift production capability and close to each other. The difference between these families comes from the difference in maximum lift angles and drag coefficients. NACA 65-4xx family produces less drag than NACA 63-2xx family. To explain the airfoil selection, local angle of attack values and local Reynolds

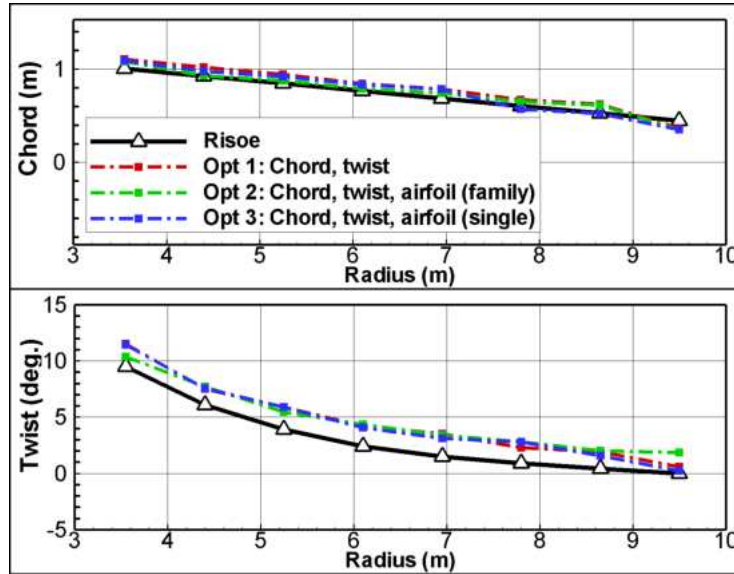


Figure 5.8: Chord and twist distribution comparisons of optimization results with Risoe wind turbine.

number values along the blade of each wind turbine in optimization case is shown in Figure 5.10. Risoe, Opt2 and Opt3 wind turbines have similar angle of attack distributions whereas Opt1 has less angle of attack values from them. Reynolds numbers of all wind turbines are between $1.0E6$ and $2.0E6$ which are inside the limits of the airfoil database.

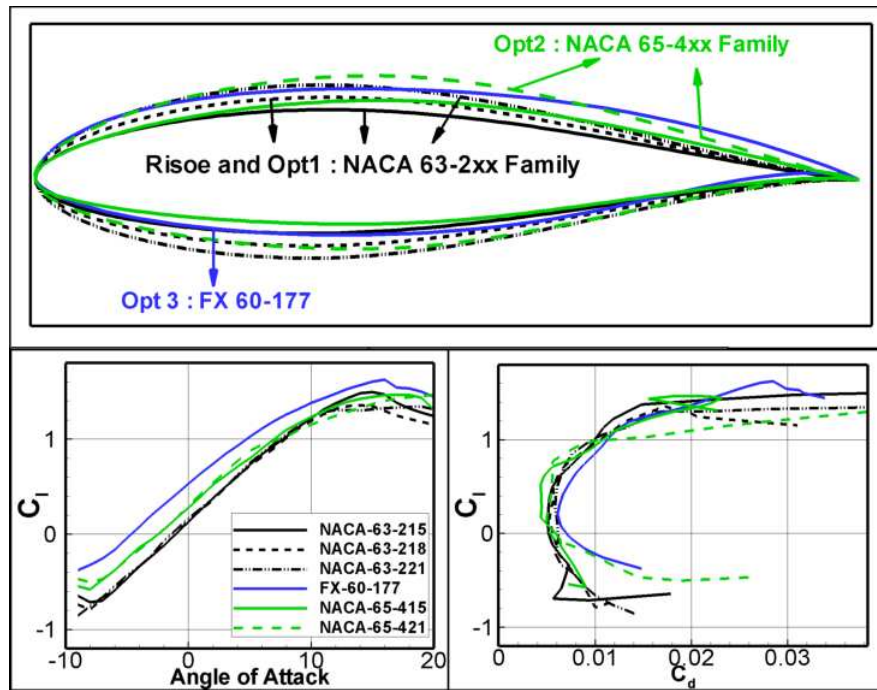


Figure 5.9: Airfoil property comparisons of optimization results

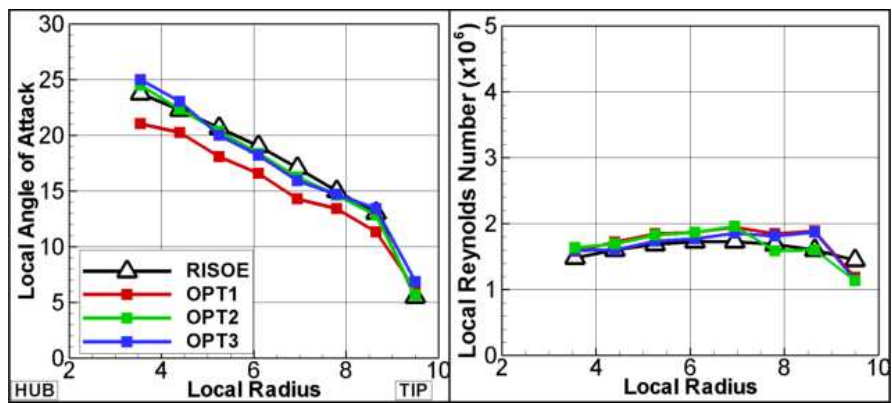


Figure 5.10: Angle of attack and Reynolds number regimes in optimization.

Risoe and Opt3 wind turbine 3D geometries are produced by using a CAD program. In Figure 5.11 and 5.12, both wind turbines are shown. Root chords are greater in Opt3 wind turbine whereas tip chords are smaller than Risoe wind turbine. From this figure, there is no information about local differences between chord and twist values.

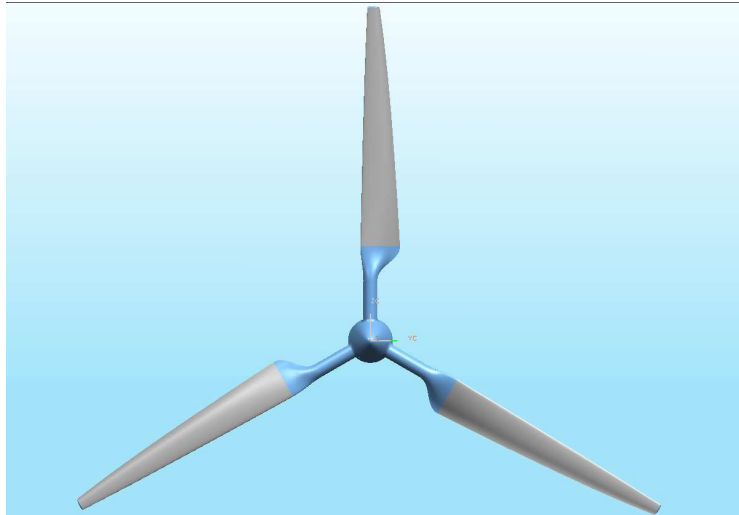


Figure 5.11: Opt3 wind turbine 3D geometry.

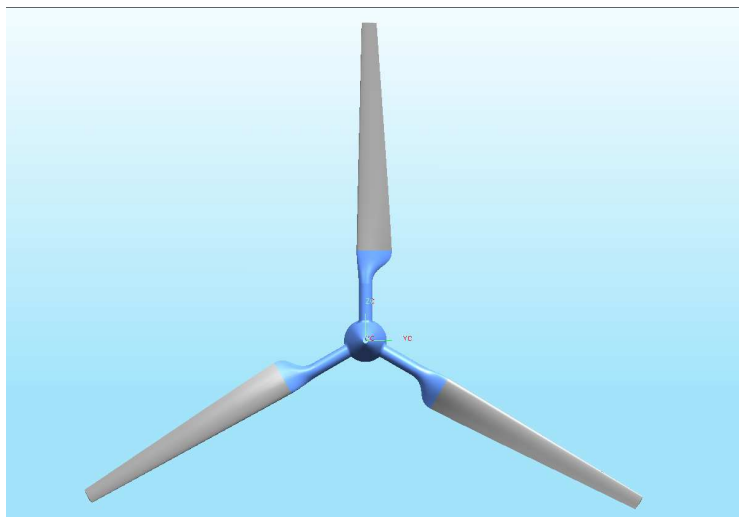


Figure 5.12: Risoe wind turbine 3D geometry.

In Figure 5.13, sectional comparisons are done between Risoe wind turbine and Opt3 wind turbine. Twist angle differences are also shown. From the section comparisons, airfoil differences become visible. Only a few degrees twist and about 10 cm chord modifications may bring a very high power production improvement with airfoil modifications. Improvements as a result of optimization will be explained in the next chapter.

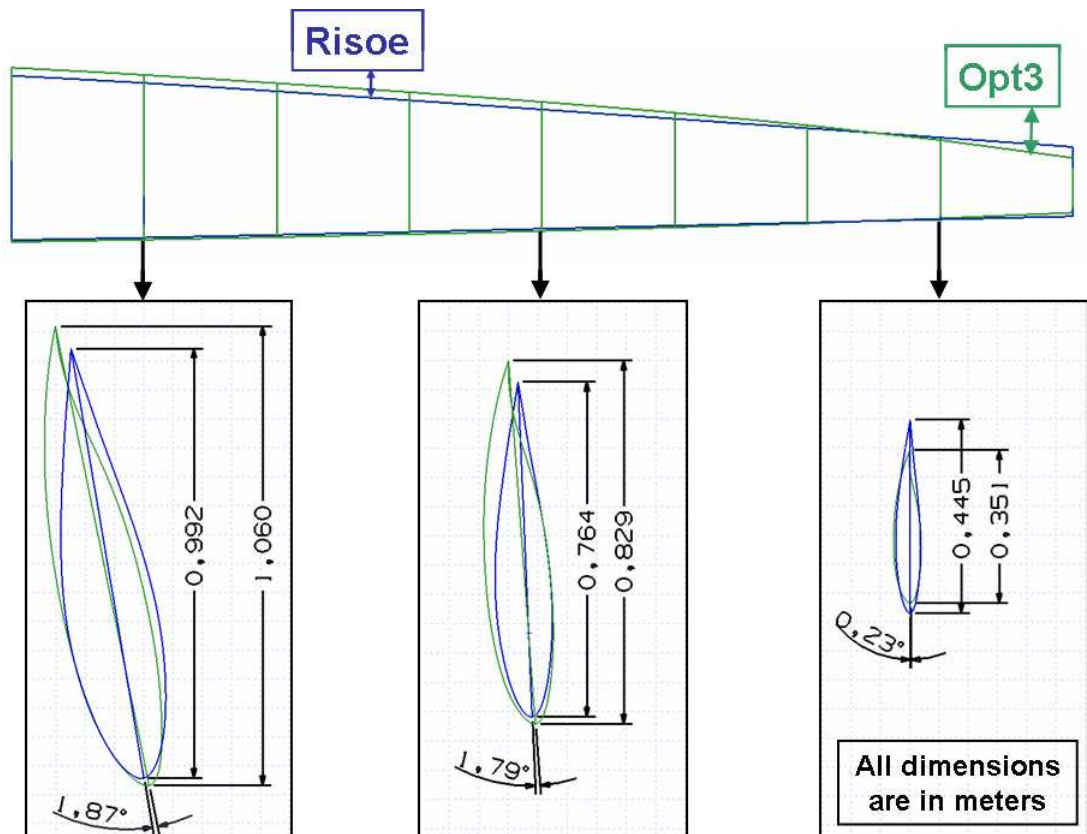


Figure 5.13: Sectional comparisons of Risoe and Opt3 wind turbines (dimensions are in meters).

5.2.5 Performance of Wind Turbines

Figure 5.3 shows the improvement in power production. This increase is shown only for a single operating point: wind speed of 14.5 m/s and rotational speed of 47.5 rpm. Performances of Opt1, Opt2 and Opt3 wind turbines can also be compared in off-design conditions. In Figure 5.14, their performances for different wind speeds are compared with Risoe wind turbine.

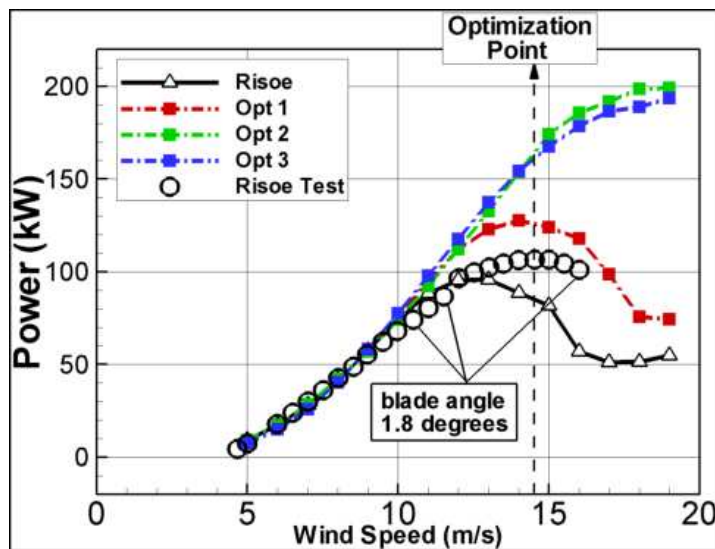


Figure 5.14: Performance comparisons of optimized wind turbines with Risoe wind turbine for rotational speed of 47.5 rpm.

Power production performance of Risoe wind turbine is improved as a result of three optimization cases. Even the airfoils are kept same, it is possible to improve the performance with some modifications to chord and twist values. This is the result of Opt1. Optimizing chord and twist values and replacing the original NACA 63-2xx airfoil family with NACA65-4xx airfoil family, power production capability improvement is quite successful. Opt3, which is the optimization with single airfoil along blade element, has best performance for low wind speeds. After about 14.0 m/s, Opt2 has the best performance. In any case, Opt2 and Opt3 performances are very close to each other. In Figure 5.15, percentage improvements are also represented. Improvements are calculated according to the Risoe wind turbine analysis result with zero blade angle. Except Opt1 and Opt2 power performance improved for all wind

speeds. Until wind speed of 8m/s, Opt3 has worse performance than Risoe. After that speed, Opt3 produce more power. In high wind speeds, Opt2 and Opt3 are 2 times more productive than Risoe.

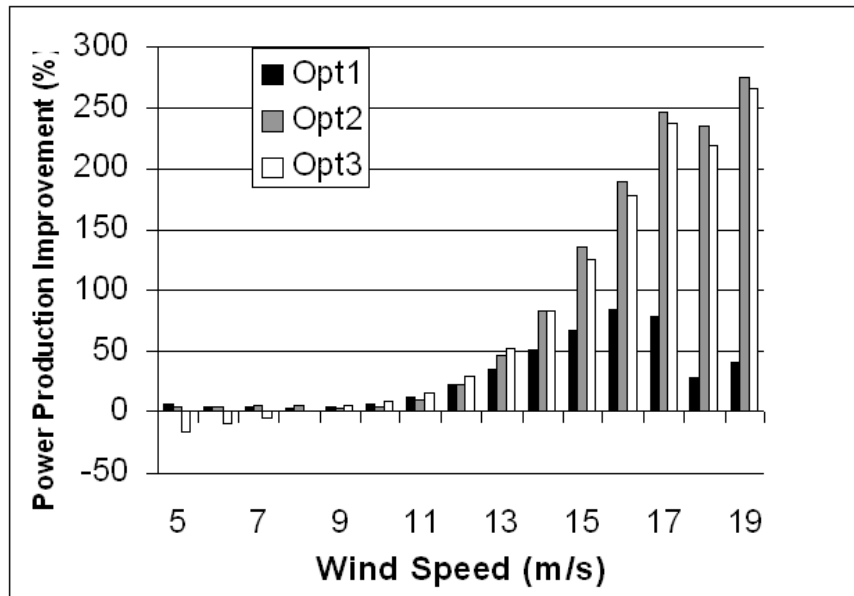


Figure 5.15: Improvement in power production: percentage of Risoe wind turbine analysis result.

The reason of that much improvement in a Risoe wind turbine lies into the fact that this wind turbine is an experimental wind turbine and designed to stall at some wind speed. Optimization results enable the designed wind turbines to stall at higher wind speeds. Therefore, in the high wind speeds, optimization results are much more productive than Risoe wind turbine.

Figure 5.14 is not a complete performance graph for these wind turbines. The analyses are performed only for rotational speed of 47.5 rpm. In order to find full performances of the turbines also for other rotational speeds, performance maps can be very useful. Risoe wind turbine performance map is shown in Figure 5.16. In this figure, operating condition and optimization point of this wind turbine is also shown. Since rotational speed is increasing, power production is increasing and stall wind speed is also increasing. For each rotational speed, there is a stall character of this turbine. Similar stall character is kept in all rotational speeds.

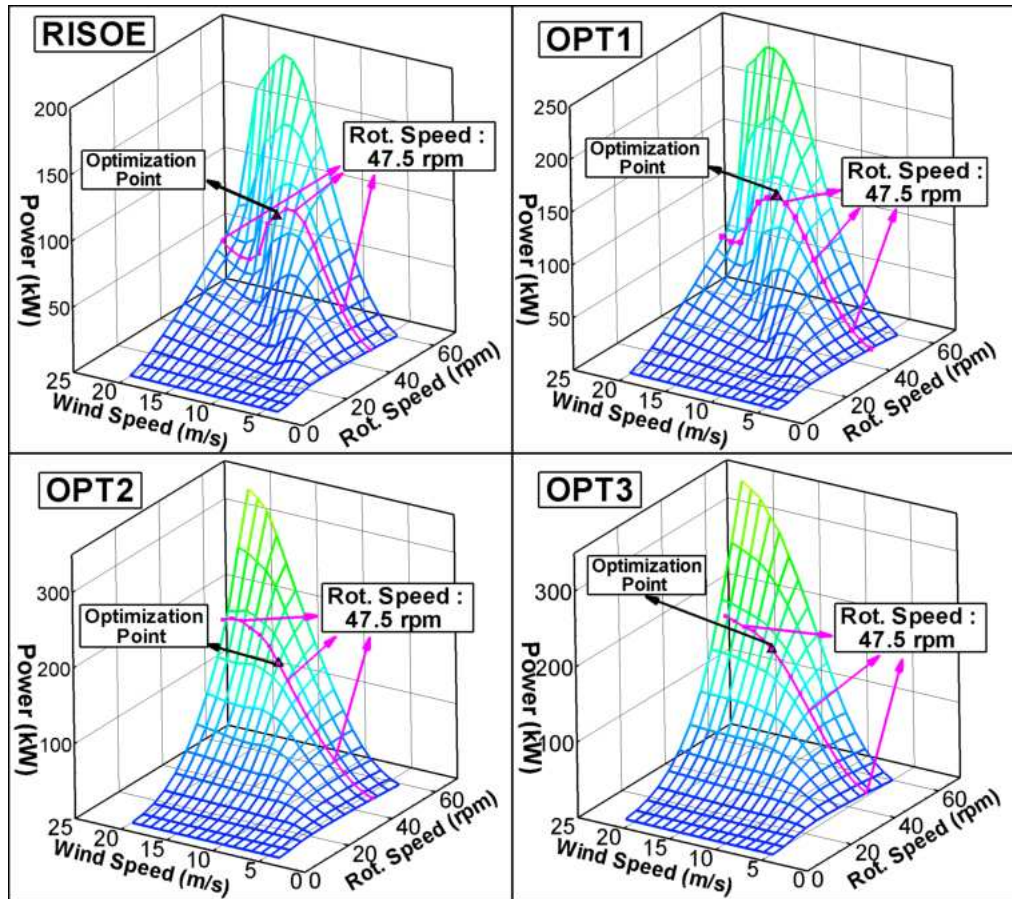


Figure 5.16: Riso,Opt1, Opt2 and Opt3 wind turbine performance maps.

In Figure 5.16, optimized wind turbine performances are compared with Riso wind turbine. Opt1 has similar character with Riso wind turbine since their airfoils are the same. However, Opt1 produces more power than Riso wind turbine. This improvement is seen in all rpm values in the map. The optimization point and normal operating condition is shown in the figure also. Opt2 wind turbine map shows that stall of this wind turbine is not very sharp. There is stall on constant rpm curves but the turbine does not lose power production capability much. Optimization point marked on its operating condition is also far from stall point. Opt3 performance map is a smooth one. Opt3 wind turbine keeps producing power, while the wind speed is increasing. As in the Opt2, optimization point is not the stall point. Performance maps of wind turbines help to explain rpm-velocity relation related to power production capability. Sometimes, wind turbines are installed with blade angles to produce more power for certain conditions in certain sites. In order to show wind turbine performances according to different blade pitch angle values, blade pitch angle, velocity and power curves are collected in graph

below.

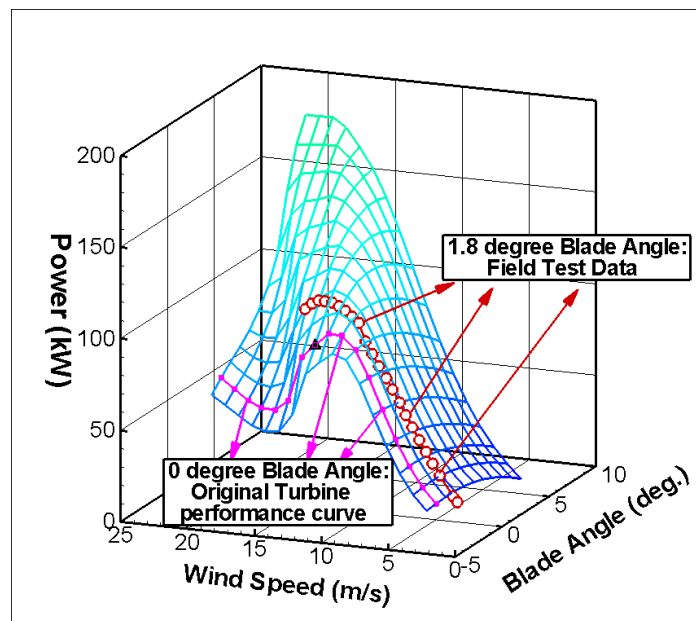


Figure 5.17: Risoe wind turbine performance with different blade angles.

In Figure 5.17, Risoe wind turbine power production capability is shown for its normal operating condition rotational speed of 47.5 rpm. It improves with more blade pitch angle for high wind speeds. On the contrary, it decreases in low wind speeds. To produce more power on high speeds, one may consider the reduction in power production in low speeds. This decision is done for each site uniquely. Every location has its unique wind characteristics and wind topology. Weibull distribution of wind speeds is very helpful for this kind of decisions. It is explained in Chapter 4. Decrease in power production with blade angles are shown in Figure 5.18 for Risoe wind turbine.

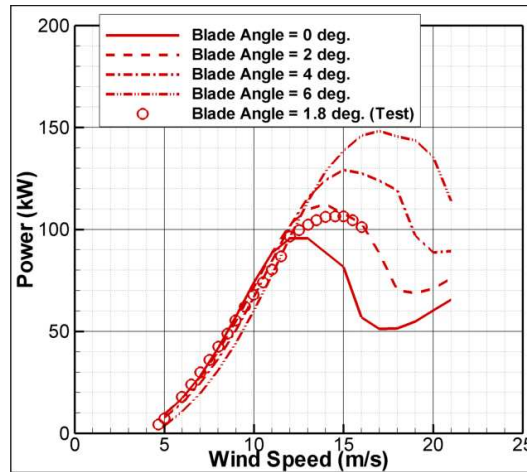


Figure 5.18: Riso power production curve for different blade angles.

To produce more power in high wind speeds without decreasing performance in low speeds, site specific optimization is the most efficient way. Consider Riso wind turbine with 0 degrees blade pitch angle and Opt1 wind turbine. To produce same amount of power in 15 m/s wind speed, Riso wind turbine needs 4 degrees of blade pitch angle. In Figure 5.18, Riso wind turbine with 4 degrees blade pitch angle is compared with Opt1 wind turbine. To produce more power in 15 m/s wind speed, Riso power production is reduced in low wind speeds. However, in Opt1 wind turbine, which is a small modification to Riso, this loss in power production is prevented.

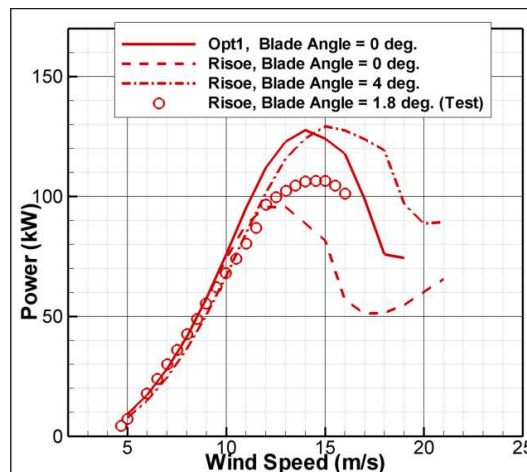


Figure 5.19: Riso and Opt1 comparison for different blade angles.

5.2.6 Thrust Force

Thrust force is found as the only disadvantage of this power production improvement, aerodynamically. Thrust is produced in the parallel direction to the wind. It pushes wind turbine to move with the wind and this creates bending moments in the tower. Therefore, towers which carry the wind turbine should be strongly attached to the ground to resist this force. Thrust productions are compared in Figure 5.20.

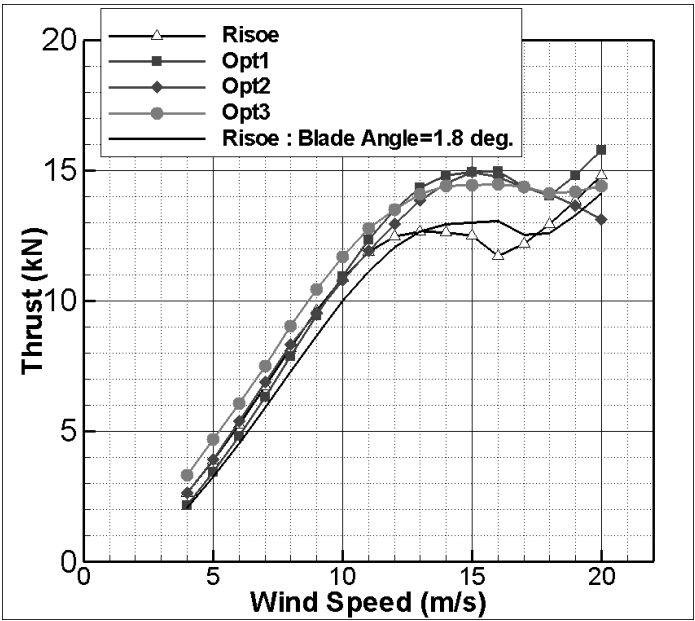


Figure 5.20: Risoe optimization results thrust comparison.

Risoe, Opt1 and Opt2 thrust forces are close to each other until 11 m/s. After that wind speed, Risoe thrust force is not increasing much, but, optimization results have more thrust value. Risoe has at most 13 kN thrust whereas optimized wind turbines reach 15 kN thrust value. Moreover, Risoe wind turbine with 1.8 degree blade angle which has test data is also analyzed and thrust force is shown in Figure 5.20. Blade angle decreased the thrust production for low speeds by increasing thrust for high speeds.

Risoe wind turbine optimization produce three optimized wind turbines. They improved the power performance in high and low wind speeds. However, generated thrust is also increased. These forces may not be an important concern for small wind turbines. For large scale wind

turbines that have 50 m radius and offshore wind turbines where the nearest ground to fix the tower is very far from sea level, thrust force becomes an important parameter. More detailed investigations and studies have to be done for large scale wind turbines for this purpose.

5.3 Design Optimization

Design optimization application is performed for a 1MW wind turbine. Initially, information about other commercial wind turbines that produce 1MW power is obtained for initial selection of blade radius, number of blades and operating point (optimization condition). Provided information from competitors is shown in Table 5.3.

According to Table 5.3, some design parameters are chosen. Since all of the wind turbines have 3 blades, number of blade is chosen as 3. Although the radius of competitors' wind turbine blades are close to 30 m, in this design application radius value is taken as 25 m to force the optimization process for the production of as much power as possible with 25 m radius wind turbine. Power control is chosen as pitch control since power production of most of the competitor wind turbines are controlled by blade pitch angle. In the pitch controlled wind turbines, power production kept constant by modifying the pitch angle of the blades for different wind speeds. Wind speed for optimization is taken as 12 m/s. This speed is lowest nominal wind speed in the Table 5.3. For rotational speed, instead of deciding from competitors' rotational speed ranges, a regulation about noise is considered. According to this regulation, tip speeds are limited to about 65 m/s in the wind farms located near habitants [26]. Assuming that the designed wind turbine will not be too close to habitants, 66.5 m/s for tip speed is taken and that makes the corresponding rotational speed, 25 rpm. In summary, chosen parameters for optimization are shown in Table 5.3.

Table 5.3: Competitor study for 1MW wind turbine design optimization

	<u>DeWind</u> D6	<u>Enercon</u> E44	<u>Fuhrlander</u> 1000Plus	<u>Gamesa</u> G52	<u>Made</u> AE61	<u>Nordex</u> N60-1	<u>Vestas</u> V52
Rated Power	1000kW	900kW	1000kW	850kW	1350kW	1300kW	850kW
Number of Blades	3	3	3	3	3	3	3
Radius	31 m	22 m	29 m	26 m	30.5 m	30 m	26 m
Power Control	pitch	pitch	pitch	pitch	stall	stall	pitch
Cut-in Wind Speed	2.5 m/s	2 m/s	3 m/s	4 m/s	3.5 m/s	3-4 m/s	4 m/s
Nominal Wind Speed	12 m/s	16 m/s	14 m/s	13 m/s	15 m/s	15 m/s	16 m/s
Cut-out Wind Speed	23 m/s	28 m/s	(no info)	25 m/s	25 m/s	25 m/s	25 m/s
Rot. Speed	20 rpm	12 - 34 rpm (variable)	(no info)	14 - 30 rpm (variable)	18 rpm	19 rpm	14 - 31 rpm (variable)
Hub Height	60 m	55 m	54 m	55 m	60 m	60 m	55 m
Tip Speed (m/s)*	68.174	79.946	-	84.859	61.890	62.154	85.905

Table 5.4: Chosen parameters for optimization

Number of Blades	3
Blade Radius	25 m
Power Control	pitch
Optimization wind speed	12 m/s
Rotational Speed	25 rpm

For the initial wind turbine geometry, a non-tapered and non-twisted wind turbine is given to the optimization. Optimization is performed with airfoil families which is similar to Opt2 strategy in the Risoe wind turbine optimization application and 10 blade elements are used which means $10 \times 2 + 1 = 21$ parameters are optimized. Airfoil families used in this design optimization and their radial distribution is given in Appendix A.1.

Optimization generation is shown in Figure 5.21. Different than previous optimization applications, much more number of generations is needed for design optimization with less number of children for each generation.

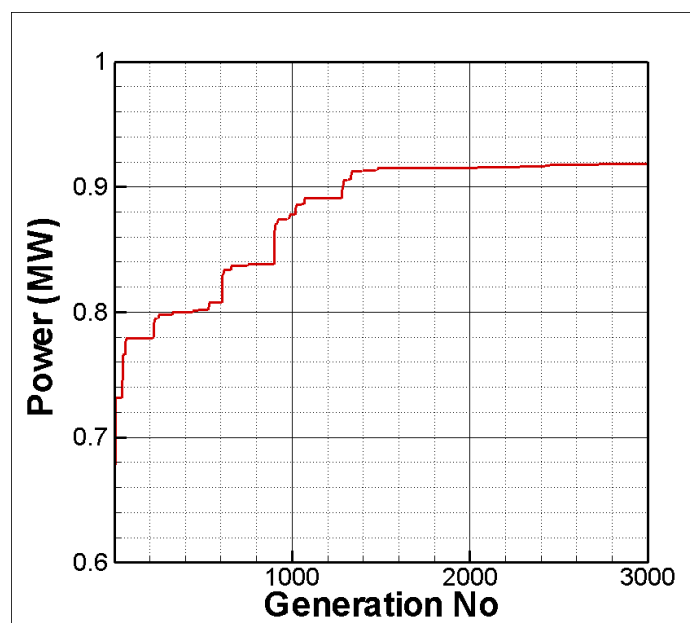


Figure 5.21: Optimization development in generations.

As a result of optimization, twisted and tapered wind turbine geometry with DU airfoil family is obtained. The comparison between the base geometry and optimization result is compared in Figure 5.22.

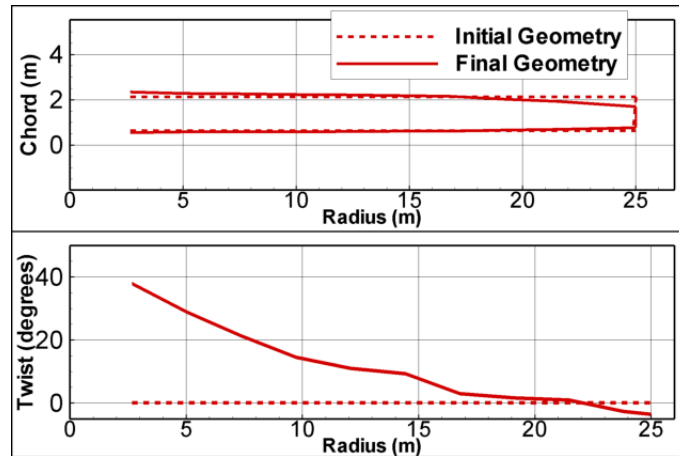


Figure 5.22: Comparison between initial geometry and optimization result.

C_l and C_d data of DU airfoils are given in the Figure 5.23. These airfoils have almost constant drag coefficient values between -0.5 and 1.4 lift coefficient values. DU airfoil data used in the aerodynamic database is obtained only for $1.0E6$ Re Number. In the Figure 5.24, Reynolds number change along the span of the designed wind turbine blade is shown. In the root sections, Re numbers are close to $1.0E6$ however, in the middle and tip sections, Reynolds numbers are sometimes higher than $4.0E6$. Higher lift but also higher drag values than $1.0E6$ Reynolds number data is normally expected for this range. In the design and analysis, it is assumed that this difference will be small and it is ignored and obtained data is used without any Reynolds number correction.

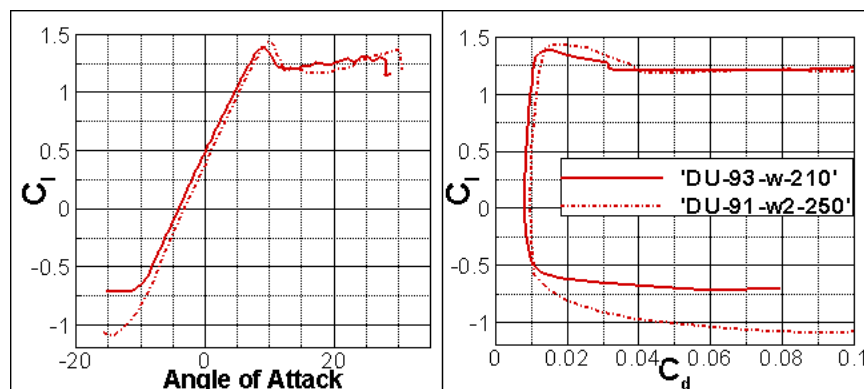


Figure 5.23: Coefficients of DU airfoils.

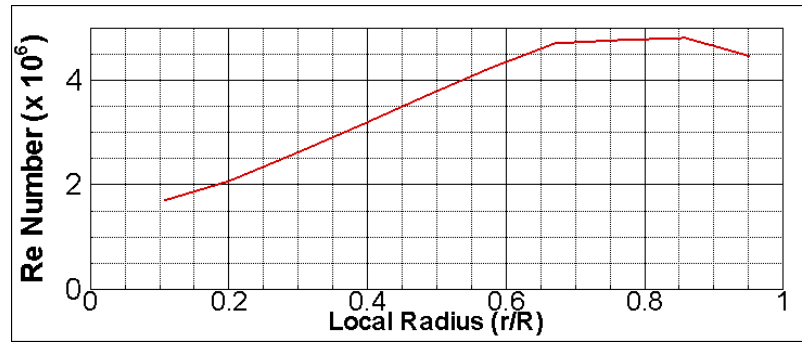


Figure 5.24: Local Reynolds number values for design condition.

Designed wind turbine is also analyzed for off-design conditions. Off-design performance of the wind turbine is shown in Figure 5.25. However, the turbine can not reach 1MW power generation at the design condition (12 m/s), it is able to reach 1MW power production in 12.5 m/s.

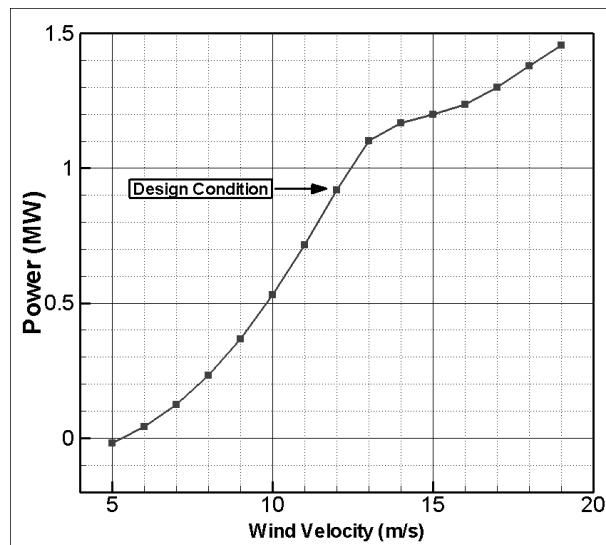


Figure 5.25: Performance of designed wind turbine.

Designed wind turbine has highly twisted blades. According to Chapter 2 which is the NREL Phase III validation case which has highly twisted blades, there is a difference between the BEM analysis code results and experimental data for high speeds. Therefore, detailed study is required for the designed 1MW wind turbine analysis results.

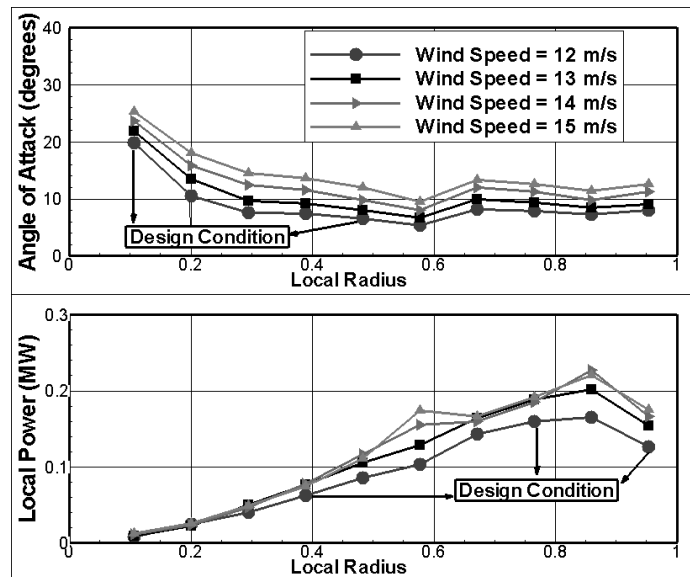


Figure 5.26: Local angle of attack and power values in different wind speeds for designed 1 MW wind turbine.

In order to investigate the BEM analysis results of designed 1MW wind turbine, angle of attack distribution along the span of turbine blade for different wind speeds are shown in 5.26. In the same Figure also, local power values for each blade elements are shown to realize the effective area for power production. The effective area for power production can be taken as after the 0.6 radius. For the design condition which is the wind speed of 12 m/s and also for 13 m/s, local angles of attack values are lower than 10 degrees in effective area. According to the Figure 5.23, these local angle of attack values are below the stall region of selected airfoils. Below the local stall range, BEM analysis code performance predictions are close to experimental data as it is explained in validation sections in Chapter 2. As a result, in the design condition for 1 MW wind turbine and for 13 m/s wind speed, BEM analysis code predictions can be considered as still reliable. After these speeds, local angles of attack values are in the stall limits or exceed the limits, therefore BEM analysis code predictions starts to loose its reliability.

In the beginning of this design optimization, the turbine is selected as a pitch regulated turbine. This is actually a very suitable decision for this design application, since BEM analysis code predictions after 13 m/s wind speeds may not be reliable as slower wind speeds. Since the limit of the reliable predictions is 13 m/s, 1.1 MW wind power is selected as limit power which is produced by the wind turbine. This value will be fixed by blade pitch angle change

for corresponding wind speeds. In order to find the required blade pitch angles to produce constant 1.1 MW power, some analysis are performed for different blade angles. The results are shown in Figure 5.27.

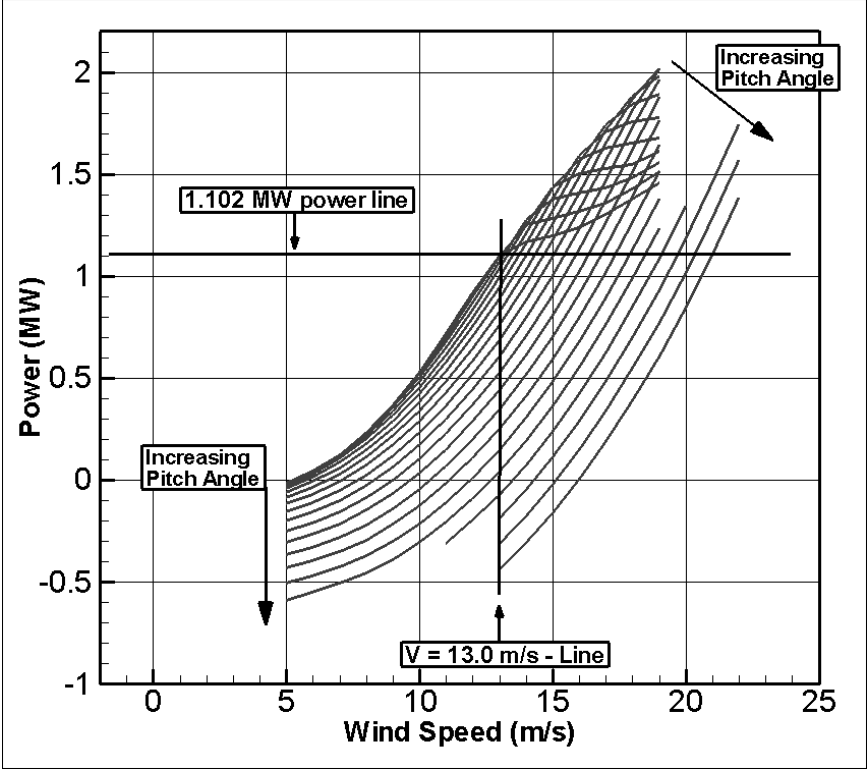


Figure 5.27: Designed wind turbine performance for different blade pitch angles

In the Figure 5.27, constant 1.1 MW wind power line is shown. The wind speed values which are the intersection of each blade angle curve with this line are found in this graph. This means that when the wind is blowing with one of these speeds which is faster than 13 m/s, required blade angle is the angle that this speed is found from. The resultant blade angle trend is shown in Figure 5.28.

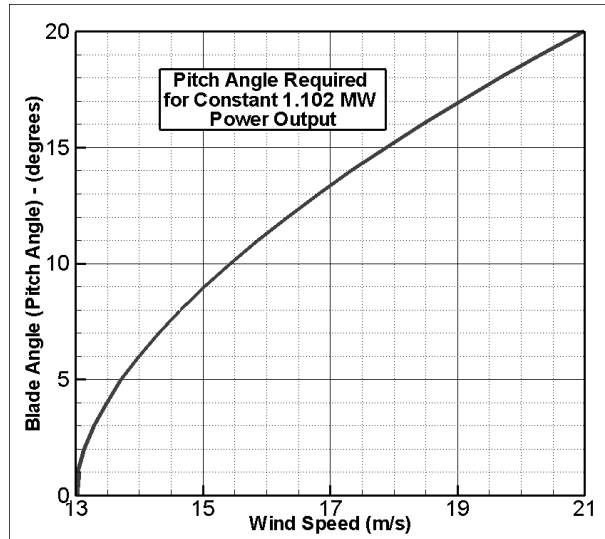


Figure 5.28: Blade Angle (Pitch Angle) curve required for constant 1.1 MW power output.

If a sensor installed on wind turbine to sense instantaneous wind speed and a mechanism changes the pitch angle of blades to corresponding angle shown in Figure 5.28, wind turbine produce 1.1 MW wind power for the wind speeds higher than 13 m/s. Power curve after pitch regulation is shown in Figure 5.29. In the figure, power curves with pitch regulation and without regulation are compared.

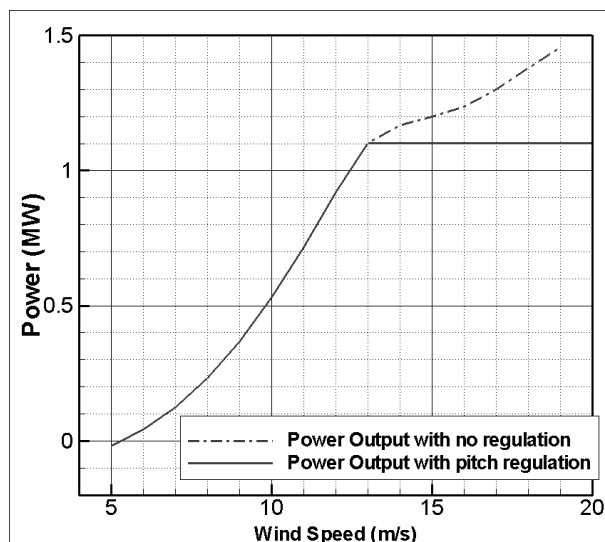


Figure 5.29: Power production of designed wind turbine after pitch regulation.

As a result of power production, thrust is also produced. Thrust curve of the designed wind turbine is shown in Figure . In the figure, thrust produced by the turbine with and without pitch regulation is also compared. After 13 m/s which is the speed that the pitch of the turbine starts to change according to wind speed, thrust produced by the wind turbine is decreasing. Therefore, it can be stated that low thrust force is caused by pitch control.

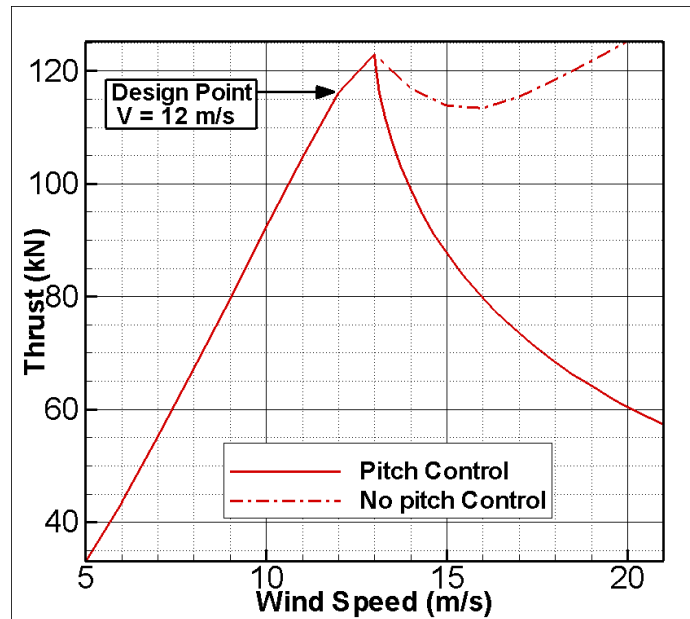


Figure 5.30: Thrust force produced by designed wind turbine.

Since there is no other wind turbine geometry found available in the literature to compare the results of thrust production, non dimensional thrust and power values of this wind turbine is compared with Risoe wind turbine. This comparison is shown in Figure 5.31. Designed 1.1 MW wind turbine has higher power production than Risoe wind turbine; however its power coefficient is lower than Risoe. If power coefficient is considered to be as power efficiency, Risoe wind turbine is more efficient than 1.1 MW wind turbine. Moreover, 1.1 MW wind turbine has higher C_T values. For pitch controlled turbine, this difference is getting decreasing which is the benefit of pitch control on thrust. The difference of thrust coefficients between Risoe and 1MW wind turbine may be indicating that more detailed thrust analysis of designed wind turbine should be done for possible effects on tower and foundation design.

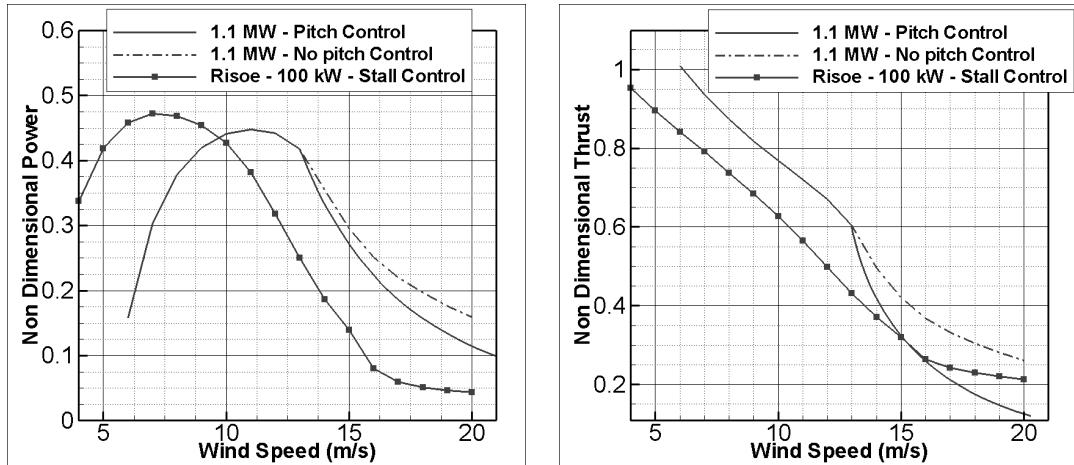


Figure 5.31: Riso and 1MW wind turbine's coefficients comparison.

A design optimization study of 1.1 MW wind turbine is performed here. 1.1 MW power is produced with 25 m blade radius, which is shorter than other commercial wind turbines that produce 1 MW power. Control by pitch angle is also shown and pitch angle range is calculated. Thrust generation is compared with Riso wind turbine. Considering that airfoil information for limited Reynolds number range and uncertainties of BEM analysis code for highly twisted turbines, more detailed analysis preferably with Navies Stokes methods are required.

CHAPTER 6

CONCLUSION

In this study, aerodynamic design and optimization of horizontal axis wind turbines are done by using BEM theory and Genetic Algorithm. Different optimization strategies are applied to a wind turbine which has experimental data to compare with. A design optimization is performed to achieve 1 MW power production.

BEM analysis tool is developed for this thesis. The code is validated against three different wind turbine data. In the NREL Phase II validation case where the blade has no twist or taper, BEM analysis tool results are successful. In the NREL Phase III validation case where the blade has high twist but no taper, BEM analysis tool results are successful until a wind speed. After that speed, there is a difference between the test result and BEM analysis results. The reason of this difference is found as high local twist angles of wind turbine. High twist angles of the turbine blade create high local angle of attack values and complex flow phenomena where the BEM theory assumptions are no longer valid. In the Risoe test case where the blade has taper and twist, BEM analysis tool again successfully predict the performance of the wind turbine for low and moderate wind speeds. As a result, the tool developed for this thesis successfully performs for low and moderate wind speeds where BEM theory assumptions are valid. However, for high wind speeds more accurate flow analyses with Navier Stokes solvers are needed to improve the predictions at these speeds.

An aerodynamic database is created by collecting several airfoils from the literature which are designed or used in wind turbine applications. All of the airfoils used in the thesis have wind tunnel test data and most of the airfoils have data for different Reynolds numbers. In the database, interpolation and extrapolation is also applied to C_l and C_d data of airfoils while they are used in BEM analysis code for higher angle of attack regimes. The airfoils that have

common geometrical characteristics are grouped and kept as airfoil families in the database.

Genetic Algorithm optimization method is selected for optimization applications. BEM analysis code is used as fitness function in the optimization. Twist and chord distributions of each blade element are optimized for best power output for given blade radius, number of blades, wind speed and rotational speed. In the optimization, optimum airfoil family is also selected from airfoil database during the optimization.

The developed tool is applied to optimization of Risoe wind turbine which is also used as a validation case for BEM analysis tool. Various strategies are followed for this application. In the first strategy, only chord and twist distributions are optimized by keeping the airfoils as they are in the Risoe wind turbine. About 40 percent improvement is achieved as a result of optimization. In the second strategy, airfoil families are also included into the optimization with chord and twist distributions. Optimized turbine performance is higher than 80 percent compared to Risoe wind turbine. Stall speed of the turbine is also improved and more power is produced for off design conditions. In the third strategy, single airfoil is used along the blade span in the optimization with chord and twist distributions. Result of this optimization is also found close to previous optimization strategy. Power production of the turbine is again improved about 80 percent. As a result of this optimization application, aerodynamic design and optimization tool developed for this thesis has improved the power production of an existing wind turbine significantly.

A wind turbine design is performed with the developed tool for selected 25 m blade radius to maximize the power production with this radius. 1.1 MW power is produced as a result of design optimization. Other commercial wind turbines that produce 1MW power have about 30 m blade radius. In this design, more power is produced with 5 m less blade radius. Also, this power is produced also in less wind speeds than competitors.

To sum up, developed aerodynamic design and optimization tool is performed successfully for both design and optimization of wind turbines. It is possible to design more powerful wind turbines. Also, improvements in power production of any present wind turbine are also possible. However, the tool needs further improvements for higher wind speeds. Then this tool will be an ideal design tool.

6.1 Future Work

Some future works are suggested after this study mainly for analysis of design and optimization applications. These are listed below:

- Designed and optimized wind turbines can be analyzed with Navier Stokes analysis tools for better predictions of higher wind speeds.
- Airfoil data used in the airfoil database can be extended by including data for lower and higher Reynolds numbers. Also, more airfoils can also be added to database.
- BEM analysis tool can be improved for analyzing wind speeds that are not parallel to wind turbine rotation axis (i.e. yaw and cone angles) and also for unsteady conditions.
- Turbulence in the site where the wind turbine is designed for can be given as input to the program and design and optimization can be done specific to a site.

REFERENCES

- [1] Kyoto Protocol website “<http://unfccc.int/kyoto-protocol/items/2830.php>”, as accurate of August 2008.
- [2] Eriksson S., Bernhoff H., Leijon M., “*Evaluation of Different Turbine Concepts for Wind Power*”, Renewable and Sustainable Energy Reviews, 24 May 2006.
- [3] Risoe, “*Guidelines or Design of Wind Turbines*”, Det Norske Veritas (DNV) and Wind Energy Department, Riso National Laboratory (Risoe), 2002.
- [4] J. F. Manwell, J. G. McGowan, A. L. Rogers “*Wing Energy, Theory, Design and Applications*”, Contract NAS2-11665, Muadyne Report 83-2-3, John Wiley and Sons, 2006.
- [5] Case van Dam, “*Airfoilss for Structures - Passive and Active Load Control for Wind Turbine Blades*”, Sandia National Laboratories, 2004 Wind Turbine Blade Workshop
- [6] Wind Power Monthly, Windicator, “<http://www.windpower-monthly.com/WPM:WINDICATOR>”, as accurate of August 2008.
- [7] DOE (US Department of Energy) News, “<http://www.doe.gov/news/6253.htm>”, as accurate of August 14, 2008.
- [8] Clean Energy Presentation File “<http://www.utahcleanenergy.org/documents/Flowers-11-30-2007-UT-Update-PUC.ppt>”, as accurate of August 2008.
- [9] TUREB, ”Rüzgar Enerjisi Sektör Raporu”, “<http://www.ruzgarenerjisibirligi.org.tr/guncel/Rapor02.06.pdf>”, as accurate of August 2008.
- [10] Laird D., “*Blade Design Codes*”, Sandia National Laboratories, 2004 Wind Turbine Blade Workshop
- [11] Molenaar D. P., Dijkstra S., “*State-of-the-art Wind Turbine Design Codes: Main Features Overview for Cost-Effective Generation*”, Contract NAS2-11665, Muadyne Report 83-2-3, John Wiley and Sons, 2006.
- [12] Snel H., “*Review of Aerodynamics for Wind Turbines*”, Wind Energy, Vol. 6, pp 203-211, 2003.
- [13] Schepers J. G., Heijdra J., et all, “*Verification of European Wind Turbine Design Codes, VEWTC; Final Report*”, ECN-C-01-055, May 2002.
- [14] Schreck S., “*Turbine Aerodynamics and Modeling Uncertainties*”, Sandia National Laboratories, 2004 Wind Turbine Blade Workshop.
- [15] Benjanirat S., “*Computational Studies of Horizontal Axis Wind Turbines in High Wind Speed Condition Using Advanced Turbulence Models*”, Doctor of Philosophy Thesis, Georgia Institute of Technology, December 2006.

- [16] Griffin D. A., “*NREL Advanced Research (ART) Aerodynamic Design of ART-2B Rotor Blades*”, NREL/SR-500-28473, August 2000.
- [17] Giguere P., Selig M. S., Tangler J. L., “*Blade Design Trade-Offs Using Low-Lift Airfoils for Stall-Regulated HAWTs*”, NREL/CP-500-26091, April 1999.
- [18] Diveux T., Sebastian P., Bernard D., Puiggali J. R., Grandidier J. Y., “*Horizontal Axis Wind Turbine Systems: Optimization Using Genetic Algorithms*”, Wind Energy, Vol.4, pp. 151-171, 2001.
- [19] Jureczko M., Pawlak M., Mezyk A., “*Optimization of Wind Turbine Blades*”, Journal of Material Processing Technology, 167, pp. 463-471, 2005.
- [20] Molenaar D. P., “*Cost Effective Design and Operation of Variable Speed Wind Turbines*”, Doctor of Philosophy Thesis, Technical University of Delft, 2003.
- [21] Fuglsang P., Bak C., et all, “*Site Specific Design Optimization of Wind Turbines*”, Wind Energy, Vol. 5, pp. 261-279, 2002.
- [22] J. G. Schepers et all, “*Final Report of IEA Annex XVIII: Enhanced Field Rotor Aerodynamics Database*”, Technical Report ECN-C-02-016, Energy Research Centre of Netherlands, February 2002.
- [23] Carroll D., “Genetic Algorithm Optimization Code by FORTRAN77” “<http://www.cuaerospace.com/carroll/ga.html>”, as accurate of July 2007.
- [24] Betz, “*A. Windenergie und Ihre Ausnutzung durch Windmüllern*”, Gottingen, Germany, 1926.
- [25] Glauert H., “*Airplane Propellers : Aerodynamic Theory*”,(ed. W. F. Durand), Springer Verlag, Berlin (reprinted by Peter Smith, Gloucester, MA, 1976).
- [26] Burton T., Sharpe D., Jenkins N., Bossanyi E., “*Wind Energy Handbook*”, John Wiley and Sons, 2001.
- [27] Moriarty P. J., Hansen C. A., “*AeroDyn Theory Manual*”, NREL EL/-500-36881, December 2005.
- [28] Sandia Reports, “*Innovative Design Approaches for Large Wind Turbine Blades*”, Sandia National Laboratories, SAND2003-0723, 2003.
- [29] Giguere P., Selig M. S. and Tangler J. L. , “*Blade Design Trade-Offs Using Low-Lift Airfoils for Stall-Regulated HAWTs*”, NREL/CP-500-26091, 1999.
- [30] Dahl K. S., Fuglsang P., “*Design of the Wind Turbine Airfoil Family Riso-A-XX*”, Riso-R-1024(EN), December 1998.
- [31] Timmer W.A., van Rooij R. P. J. O. M., “*Summary of Delft University Wind Turbine Dedicated Airfoils*”, AIAA-2003-0352, 2003.
- [32] Miley S. J., “*A Catalog of Low Reynolds Number Airfoil Data for Wind Turbine Applications*”, RFP-3387 VC-60, Rockwell International, February 1982.
- [33] Bertagnolio F., Sorensen N., Johansen J., Fuglsang P., “*Wind Turbine Airfoil Catalogue*”, Riso-R-1280, 2001.

- [34] Selig M., McGranahan B. D., “*Wind Tunnel Aerodynamic Tests of Six Airfoils for Use on Small Wind Turbines*”, NREL/SR-500-34515, 2004.
- [35] Timmer W. A., van Rooij R. P. J. O. M., “*Summary of The Delft University Wind Turbine Dedicated Airfoils*”, AIAA-2003-0352, 2003.
- [36] Fuglsang P., Dahl K. S., Antoniou I., “*Wind Tunnel Tests of the Riso-A1-18, Riso-A1-21 and Riso-A1-24 Airfoils*”, Riso-R-1112, 1999.
- [37] Bak C., Fuglsang P., Johansen J., Antoniou I., “*Wind Tunnel Tests of the NACA 63-415 and a modified NACA 63-415 Airfoil*”, Riso-R-1193, 2000.
- [38] Hansen C., ”NWTC Design Codes (AirfoilPrep)”, “<http://wind.nrel.gov/designcodes/preprocessors/airfoilprep/>”, last modified 16-January-2007; accessed August-2007.
- [39] Buhl M., ”NWTC Design Codes (WT-Perf)”, “<http://wind.nrel.gov/designcodes/simulators/wtperf/>”, last modified 14-July-2008, accessed July-2008.
- [40] Laino D. J., ”NWTC Design Codes (Aerodyn)” “<http://wind.nrel.gov/designcodes/simulators/aerodyn/>”, last modified 05-July-2005; accessed March-2007.
- [41] Viterna L. A., Janetzke D. C., “*Theoretical and Experimental Power From Large Horizontal Axis Wind Turbines*”, NASA TM-82944, 1982.
- [42] Goldberg D. E., “*Genetic Algorithms in Search, Optimization and Machine Learning*”, NASA TM-82944, Kluwer Academic Publishers, Boston, MA, 1989.

APPENDIX A

AIRFOIL SPECIFICATIONS

A.1 AIRFOILS USED IN THE AIRFOIL DATABASE

Table A.1: Airfoils used in the database.

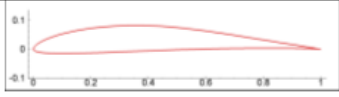
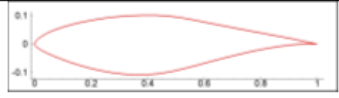
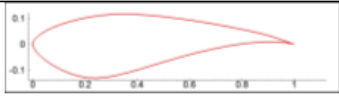
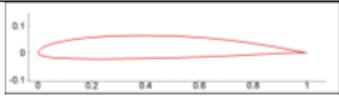
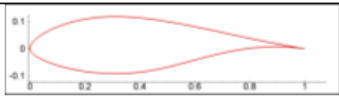
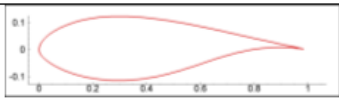
	Name	Airfoil	thickness (chord %)	Test Re Number ($\times 10^6$)
1	Riso-A1-18		18	1.6
2	Riso-A1-21		21	1.6
3	Riso-A1-24		24	1.6
4	E387		9.07	0.1 - 0.5
5	S809		21	1.0
6	S814		24	1.0
7	SD2030		8.56	0.1 - 0.5
8	FFA-W3-211		21	1.8
9	FFA-W3-241		24	1.5

Table A.1: Continued.

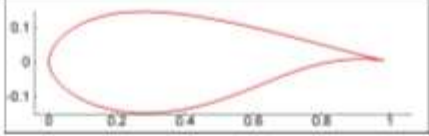
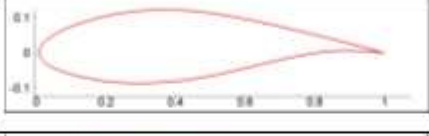

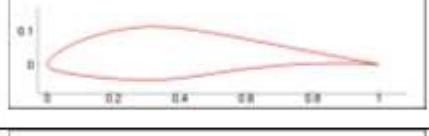
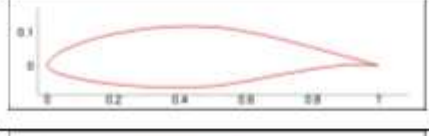
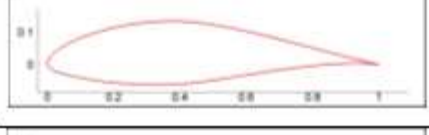
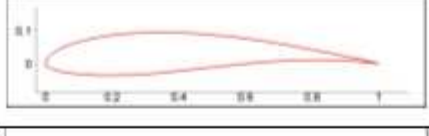
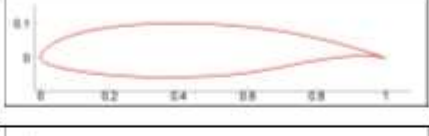
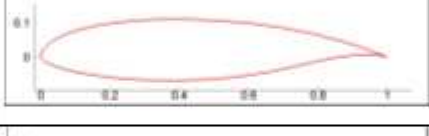
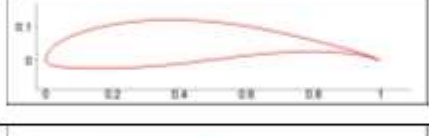
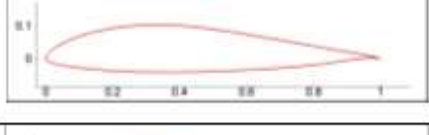
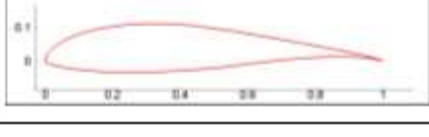
10	FFA-W3-301		30	1.5
11	DU 93-W-210		21	1
12	DU 91-W2-250		25	1
13	FX S 02/1-158		15.8	1.5 - 3.0
14	FX S 03-182		18.2	2.0 - 3.0
15	FX S 02-196		19.6	1.5 - 3.0
16	FX 60-126/1		12.6	0.7 - 2.0
17	FX 60-157		15.7	1.0 - 3.0
18	FX 60-177		17.7	1.0 - 3.0
19	FX 63-137		13.66	0.1 - 0.5
20	FX 63-143		14.3	1.0 - 3.0
21	FX 63-145		14.5	1.5 - 3.0

Table A.1: Continued.

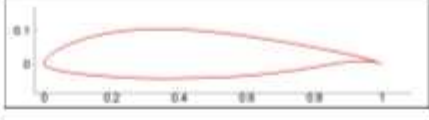
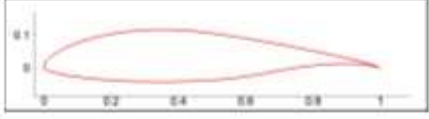
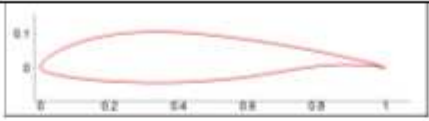
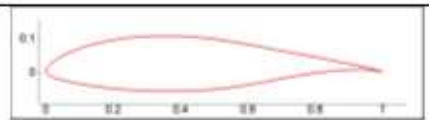
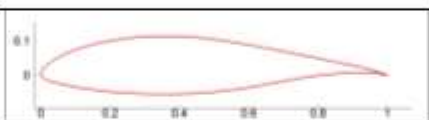




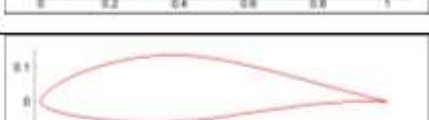

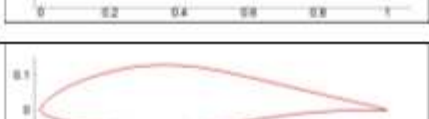

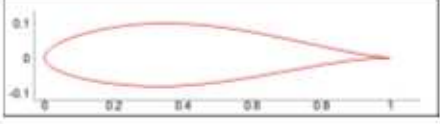
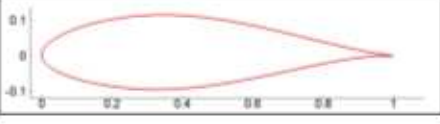

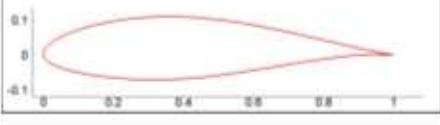
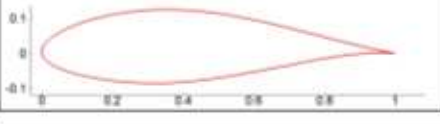
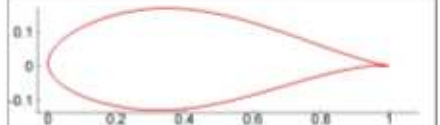
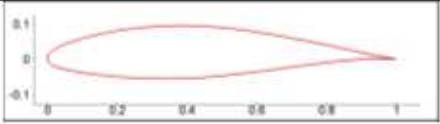
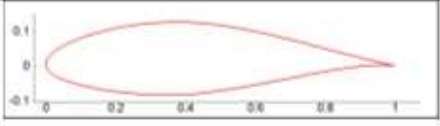

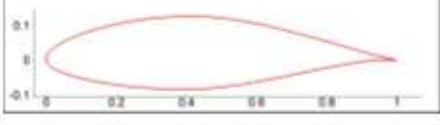
22	FX 63-147		14.7	1.0 - 3.0
23	FX 63-158		15.8	1.5 - 3.0
24	FX-61-147		14.7	1.0 - 3.0
25	FX 61-163		16.3	1.0 - 3.0
26	FX 61-168		16.8	1.0 - 3.0
27	FX 61-184		18.4	1.0 - 3.0
28	FX 38-153		15.5	1.0 - 3.0
29	FX 66-s-161		16.1	1.0 - 3.0
30	FX 66-s-196		19.6	1.0 - 3.0
31	FX66-S196- V1		19	1.5
32	FX 66-17A- 175		17.5	1.0 - 3.0
33	FX 66-17All- 182		18.2	1.0 - 3.0

Table A.1: Continued.

34	Naca 63-215		15	3.0 - 9.0
35	Naca 63-218		18	3.0 - 9.0
36	Naca 63-221		21	3.0 - 9.0
37	Naca 63-415		15	1.6 - 9.0
38	Naca 63-418		18	3.0 - 9.0
39	Naca 63-421		21	3.0 - 9.0
40	Naca 63-430		30	1.5
41	Naca 64-415		15	3.0 - 9.0
42	Naca 64-421		21	3.0 - 9.0
43	Naca 65-415		15	3.0 - 9.0
44	Naca 65-421		21	3.0 - 9.0

A.2 AIRFOIL FAMILIES USED IN THE OPTIMIZATION

A.2.1 NACA 63-2xx Family

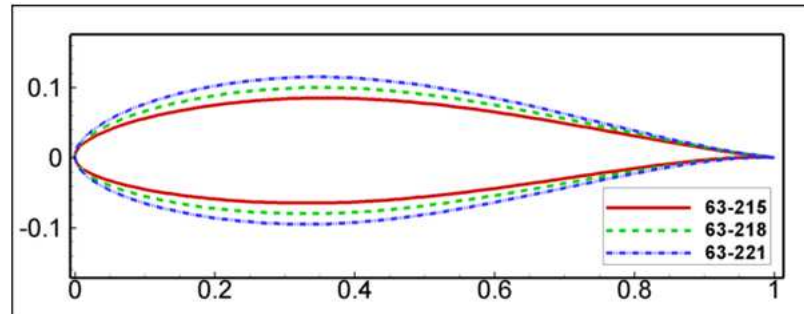


Figure A.1: NACA 63-2xx family airfoils

Table A.2: NACA 63-2xx family airfoil distribution along blade span (r/R)

NACA-63-2xx Family		
Local Radius	Thickness	Airfoil
0.30	21	63-221
0.60	18	63-218
0.90	15	63-215

A.2.2 NACA 63-4xx Family

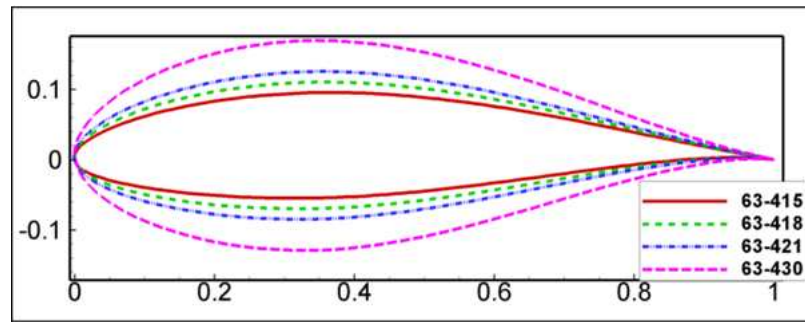


Figure A.2: NACA 63-4xx family airfoils

Table A.3: NACA 63-4xx family airfoil distribution along blade span (r/R)

NACA-63-4xx Family		
Local Radius	Thickness	Airfoil
0.20	30	63-430
0.45	21	63-421
0.70	18	63-418
0.95	15	63-415

A.2.3 NACA 64-4xx Family

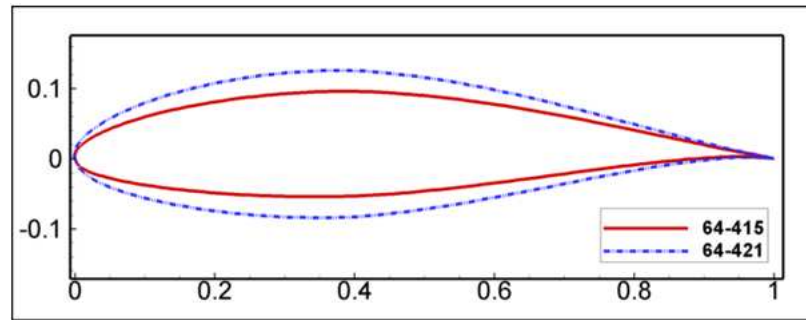


Figure A.3: NACA 64-4xx family airfoils

Table A.4: NACA 64-4xx family airfoil distribution along blade span (r/R)

NACA-64-4xx Family		
Local Radius	Thickness	Airfoil
0.40	21	64-421
0.90	15	64-415

A.2.4 NACA 65-4xx Family

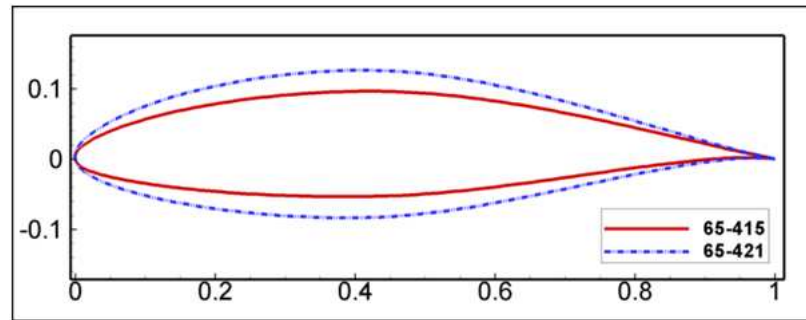


Figure A.4: NACA 65-4xx family airfoils

Table A.5: NACA 65-4xx family airfoil distribution along blade span (r/R)

NACA-65-4xx Family		
Local Radius	Thickness	Airfoil
0.40	21	65-421
0.90	15	65-415

A.2.5 FX-60 Family

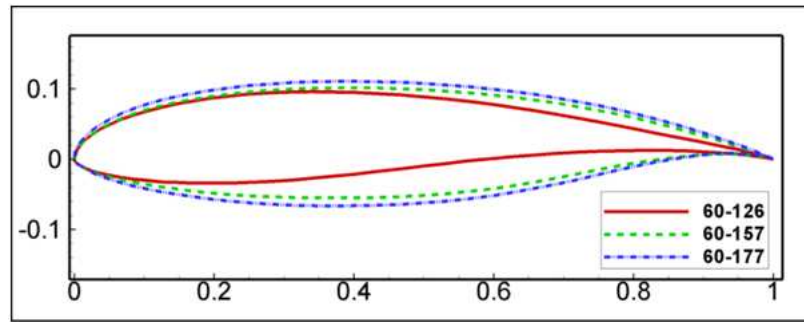


Figure A.5: FX-60 family airfoils

Table A.6: FX-60 family airfoil distribution along blade span (r/R)

FX-60 Family		
Local Radius	Thickness	Airfoil
0.30	17.7	60-177
0.60	15.7	60-157
0.90	12.6	60-126

A.2.6 FX-61 Family

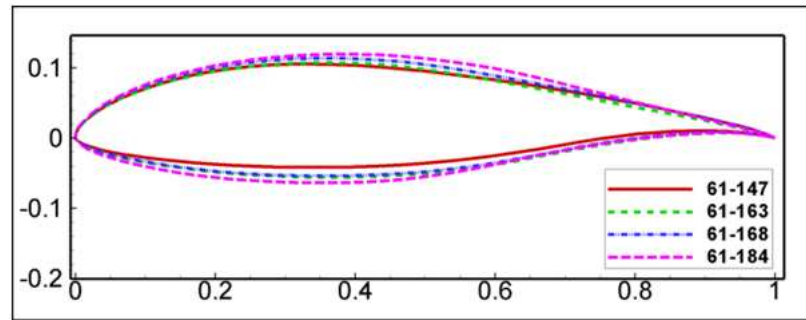


Figure A.6: FX-61 family airfoils

Table A.7: FX-61 family airfoil distribution along blade span (r/R)

FX-61 Family		
Local Radius	Thickness	Airfoil
0.20	18.4	61-184
0.45	16.8	61-168
0.70	16.3	61-163
0.95	14.7	61-147

A.2.7 FX-66 Family

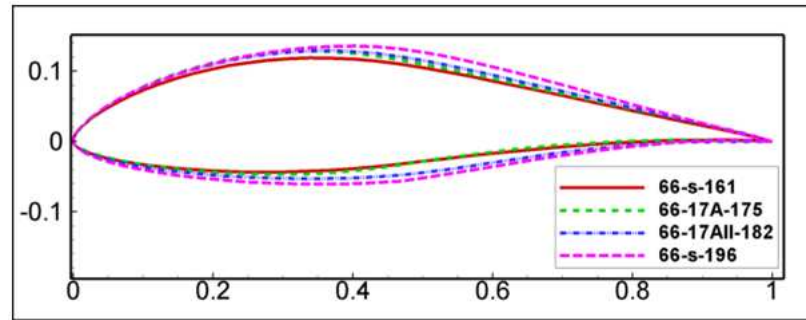


Figure A.7: FX-66 family airfoils

Table A.8: FX-66 family airfoil distribution along blade span (r/R)

FX-66 Family		
Local Radius	Thickness	Airfoil
0.20	19.6	66-s-196
0.45	18.2	66-17AII-182
0.70	17.5	66-17A-175
0.95	16.1	66-s-161

A.2.8 FX S Family

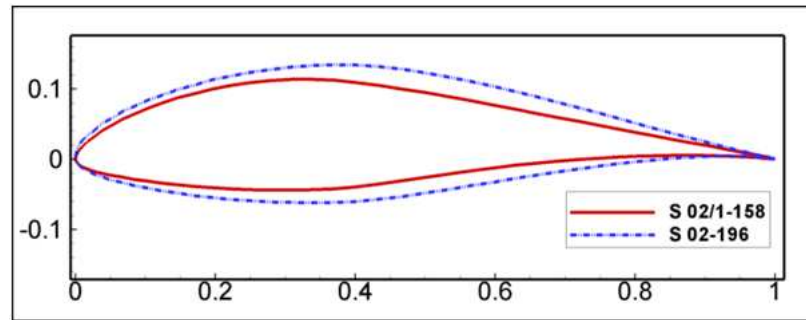


Figure A.8: FX S family airfoils

Table A.9: FX S family airfoil distribution along blade span (r/R)

FX S Family		
Local Radius	Thickness	Airfoil
0.40	19.6	S 02-196
0.90	15.8	S 02/1-158

A.2.9 Risoe-A1 Family

The coordinates of these airfoils are not publicly available.

Table A.10: Risoe-A1 family airfoil distribution along blade span (r/R)

Risoe-A1 Family		
Local Radius	Thickness	Airfoil
0.30	24	Riso-A1-24
0.60	21	Riso-A1-21
0.90	18	Riso-A1-18

A.2.10 DU Family

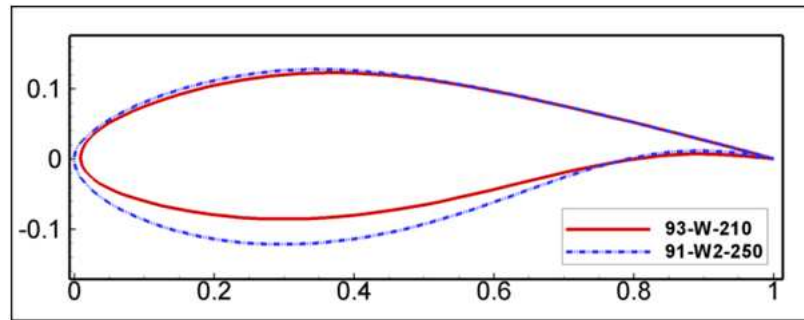


Figure A.9: DU family airfoils

Table A.11: DU family airfoil distribution along blade span (r/R)

DU Family		
Local Radius	Thickness	Airfoil
0.40	25	91-W2-250
0.90	21	91-W2-210

A.2.11 FFA Family

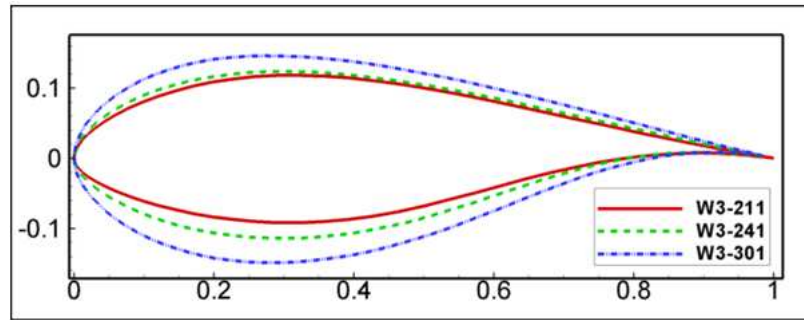


Figure A.10: FFA family airfoils

Table A.12: FFA family airfoil distribution along blade span (r/R)

FFA Family		
Local Radius	Thickness	Airfoil
0.30	30	W3-301
0.60	24	W3-241
0.90	21	W3-211